



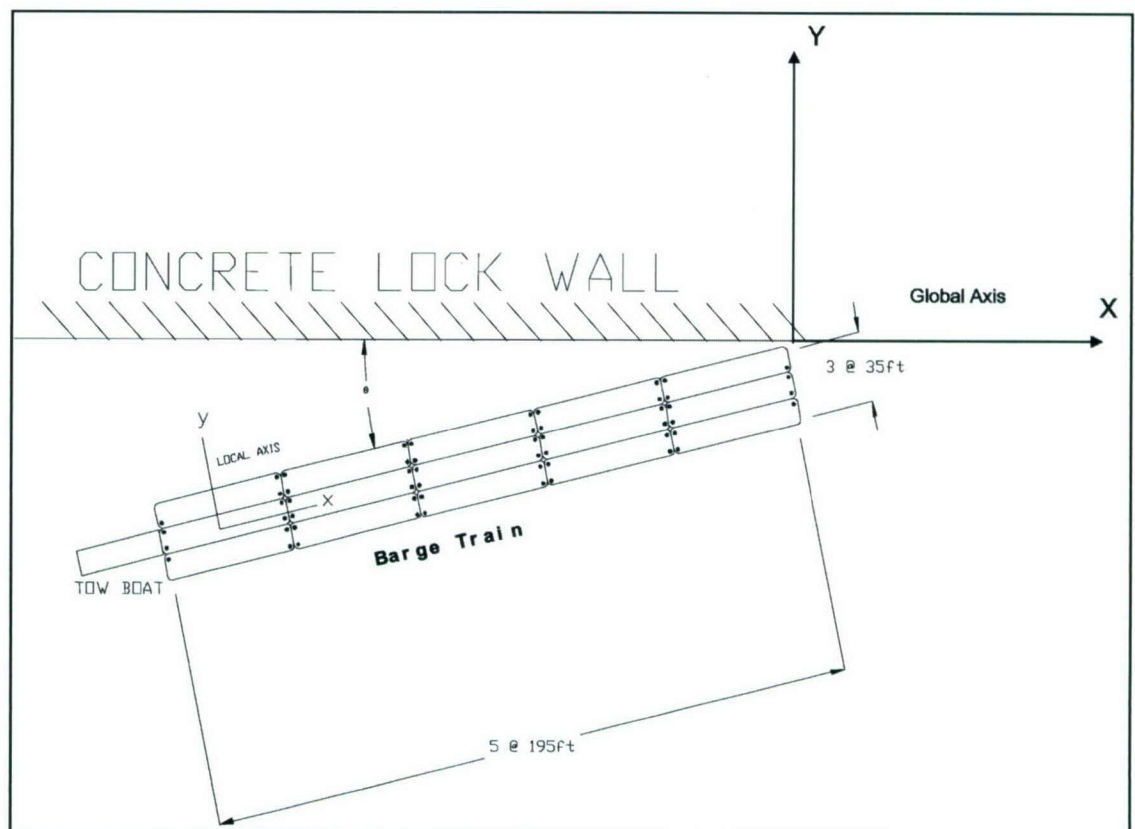
**US Army Corps  
of Engineers®**  
Engineer Research and  
Development Center

*Navigation Systems Research Program*

## **Barge Train Maximum Impact Forces Using Limit States for the Lashings between Barges**

José Ramón Arroyo and Robert M. Ebeling

March 2005



# **Barge Train Maximum Impact Forces Using Limit States for the Lashings between Barges**

José Ramón Arroyo

*General Engineering Department  
University of Puerto Rico  
PO Box 9044  
Mayagüez, PR 00681*

Robert M. Ebeling

*U.S. Army Engineer Research and Development Center  
Information Technology Laboratory  
3909 Halls Ferry Road  
Vicksburg, MS 39180-6199*

Final Report

Approved for public release; distribution is unlimited.

Prepared for      U.S. Army Corps of Engineers  
Washington, DC 20314-1000

Under              INP Work Unit 33143



## ABSTRACT:

In 1993, Headquarters, U.S. Army Corps of Engineers issued the first formal Corps-wide analysis procedure providing guidance for analyzing the effects of barge impact loading on navigation structures. According to the ETL 1110-2-338 engineering procedure, the magnitude of the impact forces generated by a particular collision event is dependent on: the mass including hydrodynamic added mass of the barge train, the approach velocity, the approach angle, the barge train moment of inertia, damage sustained by the barge structure, and friction between the barge and the wall. There have been two significant concerns raised since the ETL 1110-2-338 procedure had been released. Mainly, several engineers who have used the ETL 1110-2-338 engineering procedure have questioned the accuracy of the computed results.

In 2003, the U.S. Army Corps of Engineers issued a Technical Report that addresses the interpretation of eight of the 44 December 1998 full-scale, low-velocity controlled impact, barge train impact experiments conducted at the decommissioned Gallipolis Lock at Robert C. Byrd Lock and Dam. According to the ERDC/ITL TR-03-3, an easy to use empirical correlation is derived that reports the maximum impact force (normal to the wall) as a function of the linear momentum normal to the wall (immediately prior to impact), using the results from the impact forces measured during these full-scale impact experiments. This new empirical correlation will be used for impacts that do not involve damage during impact to either the corner barge of a barge train or to the wall. An alternate empirical correlation is given for the maximum impact force (normal to the wall) as a function of the kinetic energy normal to the wall (immediately prior to impact).

In 2004, the U.S. Army Corps of Engineers issued a Technical Report that considers the limit value of the force normal to the wall based on the empirical correlations and the limit states of the lashings that join the barges. According to the ERDC/ITL TR-04-2, the limit value of the force normal to the wall is based on the yield of the lashing. That is, predefined failure planes are analyzed and based on the yield of the lashing, and a maximum force normal to the wall is calculated. The three failure mechanisms studied were (1) Longitudinal, (2) Transverse, and (3) Corner. Finally, the maximum force normal to the struck wall is calculated from the equations of motion, the yielding of the lashings, and the empirical correlation.

However, previous research did not perform a parametric study to identify the tendencies of the maximum force normal to the wall with a variation of the principal variables that affect the models. This work presents the parametric analysis of the limit states of the lashing and an analysis of the tendencies. The models used to perform the parametric analysis are the corner (glancing blow) and longitudinal (head-on) failure mechanisms and the empirical correlation. The analyses are done with the help of Limit\_LASHING computer program, developed in the ERDC/ITL TR-04-2. This report also demonstrate the efficiency of Limit\_LASHING to estimate the maximum force normal to the wall based on the limit states of the lashing between barges.

**DISCLAIMER:** The contents of this report are not to be used for advertising, publication, or promotional purposes. Citation of trade names does not constitute an official endorsement or approval of the use of such commercial products. All product names and trademarks cited are the property of their respective owners. The findings of this report are not to be construed as an official Department of the Army position unless so designated by other authorized documents.

**DESTROY THIS REPORT WHEN IT IS NO LONGER NEEDED. DO NOT RETURN IT TO THE ORIGINATOR.**

# Contents

---

Conversion Factors .....	x
Preface.....	xi
1 Introduction.....	1
1.1 Background – Barge Train Maximum Impact Forces.....	1
1.1.1 Background – Full-Scale, Low-Velocity Controlled Barge Impact Experiments.....	3
1.1.2 Background – Empirical Correlations.....	5
1.1.3 Background – Three Idealized Failure Mechanisms.....	7
1.1.4 Background – Limit_Lashing .....	13
1.1.5 Limit_LASHING Results for the Eight Barge Impact Experiments.....	18
1.2 Engineering Properties of New and Used Lashings.....	22
1.2.1 Wire Rope Information .....	22
1.2.2 Mechanical Properties of New and Used Lashings.....	26
1.3 Report Contents .....	26
2 Glancing Blow Impact Forces.....	28
2.1 Introduction.....	28
2.2 Standard Lashing Layout .....	34
2.3 Parametric Study .....	37
2.3.1 Limiting Impact Forces Computed for 7/8-in. Diameter New Wire Rope.....	38
2.3.2 Limiting Impact Forces Computed for 7/8-in. Diameter Used Wire Rope.....	38
2.3.3 Limiting Impact Forces Computed for 1-in. Diameter New Wire Rope.....	39
2.3.4 Limiting Impact Forces Computed for 1-in. Diameter Used Wire Rope .....	46
2.4 Standard Lashing Layout With an Additional Wrap .....	52
2.4.1 Limiting Impact Forces Computed for 7/8-in. Diameter New Wire Rope.....	52
2.4.2 Limiting Impact Forces Computed for 7/8-in. Diameter Used Wire Rope.....	52
2.4.3 Limiting Impact Forces Computed for 1-in. Diameter New Wire Rope.....	53
2.4.4 Limiting Impact Forces Computed for 1-in. Diameter Used Wire Rope .....	62
2.5 Standard Lashing Layout Less One Wrap.....	62
2.5.1 Limiting Impact Forces Computed for 7/8-in. Diameter New Wire Rope.....	62
2.5.2 Limiting Impact Forces Computed for 7/8-in. Diameter Used Wire Rope.....	63
2.5.3 Limiting Impact Forces Computed for 1-in. Diameter New Wire Rope.....	72
2.5.4 Limiting Impact Forces Computed for 1-in. Diameter Used Wire Rope .....	72
2.6 “Glancing Blow” Results Summary .....	78
3 Head-On Impact Forces.....	80
3.1 Longitudinal Failure Mechanism .....	80



3.2 Longitudinal Failure Mechanism – Impact at 90 Degrees Without Eccentricity .....	83
3.3 Process of Lashing Failure for the Longitudinal Failure Mechanism.....	84
3.4 Additional Information of the Longitudinal Failure Mechanism.....	86
3.5 Parametric Study .....	87
3.5.1 Limiting Impact Forces Computed for 7/8-in. Diameter New Wire Rope.....	91
3.5.2 Limiting Impact Forces Computed for 7/8-in. Diameter Used Wire Rope.....	91
3.5.3 Limiting Impact Forces Computed for 1-in. Diameter New Wire Rope.....	92
3.5.4 Limiting Impact Forces Computed for 1-in. Diameter Used Wire Rope .....	94
3.6 Standard Lashing Layout With an Additional Wrap .....	94
3.6.1 Limiting Impact Forces Computed for 7/8-in. Diameter New Wire Rope.....	95
3.6.2 Limiting Impact Forces Computed for 7/8-in. Diameter Used Wire Rope.....	96
3.6.3 Limiting Impact Forces Computed for 1-in. Diameter New Wire Rope.....	97
3.6.4 Limiting Impact Forces Computed for 1-in. Diameter Used Wire Rope .....	98
3.7 Standard Lashing Layout Less One Wrap.....	99
3.7.1 Limiting Impact Forces Computed for 7/8-in. Diameter New Wire Rope.....	99
3.7.2 Limiting Impact Forces Computed for 7/8-in. Diameter Used Wire Rope.....	100
3.7.3 Limiting Impact Forces Computed for 1-in. Diameter New Wire Rope.....	101
3.7.4 Limiting Impact Forces Computed for 1-in. Diameter Used Wire Rope .....	102
3.8 Head-On Impact Results Summary.....	103
4 Conclusions and Recommendations .....	104
4.1 “Glancing Blow” Impact Event .....	104
4.2 “Head-On” Impact Event .....	106
References.....	107
Appendix A: Lashing Configurations .....	A1

SF 298

## List of Figures

---

Figure 1-1. Barge Train-Wall Systems.....	2
Figure 1-2. Asymptote of the Empirical Formulation.....	2
Figure 1-3. Velocity Vector Transformation—from Local to Global Axis .....	7
Figure 1-4. Empirical Correlation Using the Linear Momentum Normal to the Wall Concept (Figure 6.3 in Arroyo, Ebeling, and Barker, 2003) .....	7
Figure 1-5. Transverse Failure Mechanism .....	9
Figure 1-6. Pivot Point at the Starboard Side of the Barge Train.....	10
Figure 1-7. Pivot Point at the Port Side of the Barge Train .....	10
Figure 1-8. Scheme of Corner Failure Mechanism.....	11
Figure 1-9. Longitudinal Failure Mechanism for a Head-On Impact ( $\theta = 90$ deg).....	12
Figure 1-10. Example of a Progressive Barge Train Failure for the Transverse Failure Mechanism .....	14
Figure 1-11. Limit_LASHING Individual Barge Input Data.....	14

Figure 1-12. Limit_LASHING Barge Train Layout Screen .....	16
Figure 1-13. Limit_LASHING Approach Angle Input Data .....	16
Figure 1-14. Limit_LASHING Failure Mechanism Screen (Longitudinal failure mechanism shown on screen).....	17
Figure 1-15. Limit_LASHING Lashing Configuration Screen .....	18
Figure 1-16. Limit_LASHING Lashing Mechanical Properties Screen.....	19
Figure 1-17. Range of Applicability of the Failure Mechanisms.....	23
Figure 1-18. Wire Rope Scheme.....	24
Figure 1-19. Common Variations of Lay in Wires.....	24
Figure 1-20. 6X19 Wire Rope.....	25
Figure 1-21. How To Measure Ropes. ....	25
Figure 2-1. Glancing Blow Barge Train Impact .....	29
Figure 2-2. Transverse Failure Mechanism .....	30
Figure 2-3. No Relative Displacement Allowed in the Local “x” Axis in the Three Barge System .....	30
Figure 2-4. Scheme of Corner Failure Mechanism.....	31
Figure 2-5. No Local Rotation of Corner Barge is Allowed in the Transverse Failure Mechanism .....	31
Figure 2-6. Local Rotation of Corner Barge is Allow, Two Pivot Points Development – Corner Failure Mechanism .....	31
Figure 2-7. Effective Lashing Configurations in the Corner Failure Mechanism .....	33
Figure 2-8. Barge Train Configuration Used in the Parametric Study.....	35
Figure 2-9. Configuration 1 Located at Bow, Port, Aft, and Starboard Sides: Generic Sequence – 7,6,8,5.....	36
Figure 2-10. Configuration 2 Located at the Bottom Layer in the Inside Connection: Generic Sequence – 7, 6, 8, 5 and 3, 2, 4, 1 .....	36
Figure 2-11. Configuration 3 Located at the Middle Layer in the Inside Connection: Generic Sequence – 6, 3, 5, 6, 4 and 7, 1, 2, 7, 1 .....	36
Figure 2-12. Configuration 4 Located at the Top Layer in the Inside Connection: Generic Sequence – 5, 2, 5 and 8, 3, 8 .....	37
Figure 2-13. Maximum FW for a 2x2 Barge Train System – Case A.....	39
Figure 2-14. Maximum FW for a 2x3 Barge Train System – Case A.....	40
Figure 2-15. Maximum FW for a 3x2 Barge Train System – Case A.....	40
Figure 2-16. Maximum FW for a 3x3 Barge Train System – Case A.....	41
Figure 2-17. Maximum FW for a 3x4 Barge Train System – Case A.....	41
Figure 2-18. Maximum FW for a 3x5 Barge Train System – Case A.....	42
Figure 2-19. Maximum FW for a 2x2 Barge Train System – Case B.....	43



Figure 2-20. Maximum FW for a 2x3 Barge Train System – Case B.....	43
Figure 2-21. Maximum FW for a 3x2 Barge Train System – Case B.....	44
Figure 2-22. Maximum FW for a 3x3 Barge Train System – Case B.....	44
Figure 2-23. Maximum FW for a 3x4 Barge Train System – Case B.....	45
Figure 2-24. Maximum FW for a 3x5 Barge Train System – Case B.....	45
Figure 2-25. Maximum FW for a 2x2 Barge Train System – Case C.....	46
Figure 2-26. Maximum FW for a 2x3 Barge Train System – Case C.....	47
Figure 2-27. Maximum FW for a 3x2 Barge Train System – Case C.....	47
Figure 2-28. Maximum FW for a 3x3 Barge Train System – Case C.....	48
Figure 2-29. Maximum FW for a 3x4 Barge Train System – Case C.....	48
Figure 2-30. Maximum FW for a 3x5 Barge Train System – Case C.....	49
Figure 2-31. Maximum FW for a 2x2 Barge Train System – Case D.....	49
Figure 2-32. Maximum FW for a 2x3 Barge Train System – Case D.....	50
Figure 2-33. Maximum FW for a 3x2 Barge Train System – Case D.....	50
Figure 2-34. Maximum FW for a 3x3 Barge Train System – Case D.....	51
Figure 2-35. Maximum FW for a 3x4 Barge Train System – Case D.....	51
Figure 2-36. Maximum FW for a 3x5 Barge Train System – Case D.....	52
Figure 2-37. Maximum FW for a 2x2 Barge Train System – Case AWA.....	53
Figure 2-38. Maximum FW for a 2x3 Barge Train System – Case AWA.....	54
Figure 2-39. Maximum FW for a 3x2 Barge Train System – Case AWA.....	54
Figure 2-40. Maximum FW for a 3x3 Barge Train System – Case AWA.....	55
Figure 2-41. Maximum FW for a 3x4 Barge Train System – Case AWA.....	55
Figure 2-42. Maximum FW for a 3x5 Barge Train System – Case AWA.....	56
Figure 2-43. Maximum FW for a 2x2 Barge Train System – Case AWB.....	56
Figure 2-44. Maximum FW for a 2x3 Barge Train System – Case AWB.....	57
Figure 2-45. Maximum FW for a 3x2 Barge Train System – Case AWB.....	57
Figure 2-46. Maximum FW for a 3x3 Barge Train System – Case AWB.....	58
Figure 2-47. Maximum FW for a 3x4 Barge Train System – Case AWB.....	58
Figure 2-48. Maximum FW for a 3x5 Barge Train System – Case AWB.....	59
Figure 2-49. Maximum FW for a 2x2 Barge Train System – Case AWC.....	59
Figure 2-50. Maximum FW for a 2x3 Barge Train System – Case AWC.....	60
Figure 2-51. Maximum FW for a 3x2 Barge Train System – Case AWC.....	60
Figure 2-52. Maximum FW for a 3x3 Barge Train System – Case AWC.....	61
Figure 2-53. Maximum FW for a 3x4 Barge Train System – Case AWC.....	61



Figure 2-54. Maximum FW for a 3x5 Barge Train System – Case AWC.....	62
Figure 2-55. Maximum FW for a 2x2 Barge Train System – Case AWD .....	63
Figure 2-56. Maximum FW for a 2x3 Barge Train System – Case AWD .....	64
Figure 2-57. Maximum FW for a 3x2 Barge Train System – Case AWD .....	64
Figure 2-58. Maximum FW for a 3x3 Barge Train System – Case AWD .....	65
Figure 2-59. Maximum FW for a 3x4 Barge Train System – Case AWD .....	65
Figure 2-60. Maximum FW for a 3x5 Barge Train System – Case AWD .....	66
Figure 2-61. Maximum FW for a 2x2 Barge Train System – Case LWA .....	66
Figure 2-62. Maximum FW for a 2x3 Barge Train System – Case LWA .....	67
Figure 2-63. Maximum FW for a 3x2 Barge Train System – Case LWA .....	67
Figure 2-64. Maximum FW for a 3x3 Barge Train System – Case LWA .....	68
Figure 2-65. Maximum FW for a 3x4 Barge Train System – Case LWA .....	68
Figure 2-66. Maximum FW for a 3x5 Barge Train System – Case LWA .....	69
Figure 2-67. Maximum FW for a 2x2 Barge Train System – Case LWB.....	69
Figure 2-68. Maximum FW for a 2x3 Barge Train System – Case LWB.....	70
Figure 2-69. Maximum FW for a 3x2 Barge Train System – Case LWB.....	70
Figure 2-70. Maximum FW for a 3x3 Barge Train System – Case LWB.....	71
Figure 2-71. Maximum FW for a 3x4 Barge Train System – Case LWB.....	71
Figure 2-72. Maximum FW for a 3x5 Barge Train System – Case LWB.....	72
Figure 2-73. Maximum FW for a 2x2 Barge Train System – Case LWC.....	73
Figure 2-74. Maximum FW for a 2x3 Barge Train System – Case LWC.....	73
Figure 2-75. Maximum FW for a 3x2 Barge Train System – Case LWC.....	74
Figure 2-76. Maximum FW for a 3x3 Barge Train System – Case LWC.....	74
Figure 2-77. Maximum FW for a 3x4 Barge Train System – Case LWC.....	75
Figure 2-78. Maximum FW for a 3x5 Barge Train System – Case LWC.....	75
Figure 2-79. Maximum FW for a 2x2 Barge Train System – Case LWD.....	76
Figure 2-80. Maximum FW for a 2x3 Barge Train System – Case LWD.....	76
Figure 2-81. Maximum FW for a 3x2 Barge Train System – Case LWD.....	77
Figure 2-82. Maximum FW for a 3x3 Barge Train System – Case LWD.....	77
Figure 2-83. Maximum FW for a 3x4 Barge Train System – Case LWD.....	78
Figure 2-84. Maximum FW for a 3x5 Barge Train System – Case LWD.....	78
Figure 3-1. Longitudinal Failure Mechanism for a Head-On Impact ( $\square = 90$ deg) .....	80
Figure 3-2. Nominal and Finite Tensile Strength of Lashing.....	82
Figure 3-3. Scheme of Barge Train with a Direct Impact without Eccentricity.....	83

Figure 3-4. Progressive Longitudinal Failure of Lashings Across a Longitudinal Failure Plane Within the Barge Train.....	85
Figure 3-5. Barge Train Configuration Used in the Parametric Study.....	88
Figure 3-6. Configuration 1 Located at Bow, Port, Aft, and Starboard Sides: Generic Sequence – 7,6,8,5.....	90
Figure 3-7. Configuration 2 Located at the Bottom Layer in the Inside Connection: Generic Sequence – 7, 6, 8, 5 and 3, 2, 4, 1.....	90
Figure 3-8. Configuration 3 Located at the Middle Layer in the Inside Connection: Generic Sequence – 6, 3, 5, 6, 4 and 7, 1, 2, 7, 1.....	91
Figure 3-9. Configuration 4 Located at the Top Layer in the Inside Connection: Generic Sequence – 5, 2, 5 and 8, 3, 8.....	91
Figure 3-10. Maximum Head-On Impact FW – Case A.....	92
Figure 3-11. Maximum Head-On Impact FW – Case B.....	93
Figure 3-12. Maximum Head-On Impact FW – Case C.....	94
Figure 3-13. Maximum Head-On Impact FW – Case D.....	95
Figure 3-14. Maximum Head-On Impact FW – Case AWA.....	96
Figure 3-15. Maximum Head-On Impact FW – Case AWB.....	97
Figure 3-16. Maximum Head-On Impact FW – Case AWC.....	98
Figure 3-17. Maximum Head-On Impact FW – Case AWD.....	99
Figure 3-18. Maximum Head-On Impact FW – Case LWA.....	100
Figure 3-19. Maximum Head-On Impact FW – Case LWB.....	101
Figure 3-20. Maximum Head-On Impact FW – Case LWC.....	102
Figure 3-21. Maximum Head-On Impact FW – Case LWD.....	103
Figure 4-1. Range of Applicability of the Failure Mechanisms.....	105
Figure A1. Configuration 1 located at bow, port, aft, and starboard sides: generic sequence – 7,6,8,5.....	A2
Figure A2. Configuration 2 located at the bottom layer in the inside connection: generic sequence – 7, 6, 8, 5 and 3, 2, 4, 1.....	A2
Figure A3. Configuration 3 located at the middle layer in the inside connection: generic sequence – 6, 3, 5, 6, 4 and 7, 1, 2, 7, 1.....	A3
Figure A4. Configuration 4 located at the top layer in the inside connection: generic sequence – 5, 2, 5 and 8, 3, 8.....	A3
Figure A5. Constitutive relationship of the lashings.....	A4



## List of Tables

---

Table 1-1. Impact Velocity/Angle Data for Bumper Experiment.....	4
Table 1-2. Comparison of Results.....	21
Table 1-3. Comparison of Results.....	23
Table 1-4. Dimensions and Mechanical Properties of Lashing used in the Parametric Analysis.....	26
Table 2-1. Results of Example of Corner and Transverse Failure Mechanisms .....	35
Table 2-2. Mechanical Properties of Wire Rope Used in the Parametric Study.....	38
Table 2-3. Mechanical Properties of Lashing – Case A .....	39
Table 2-4. Mechanical Properties of Lashing – Case B. ....	42
Table 2-5. Mechanical Properties of Lashing – Case C .....	45
Table 2-6. Mechanical Properties of Lashing – Case D.....	49
Table 2-7. Mechanical Properties of Lashing – Case AWA .....	53
Table 2-8. Mechanical Properties of Lashing – Case AWB.....	56
Table 2-9. Mechanical Properties of Lashing – Case AWC.....	59
Table 2-10. Mechanical Properties of Lashing – Case AWD.....	63
Table 2-11. Mechanical Properties of Lashing – Case LWA.....	66
Table 2-12. Mechanical Properties of Lashing – Case LWB.....	69
Table 2-13. Mechanical Properties of Lashing – Case LWC.....	72
Table 2-14. Mechanical Properties of Lashing – Case LWD .....	75
Table 3-1. Mechanical Properties of Wire Rope Used in the Parametric Study.....	88
Table 3-2. Mechanical Properties of Lashing – Case A.....	91
Table 3-3. Mechanical Properties of Lashing – Case B.....	93
Table 3-4. Mechanical Properties of Lashing – Case C.....	93
Table 3-5. Mechanical Properties of Lashing – Case D.....	94
Table 3-6. Mechanical Properties of Lashing – Case AWA .....	95
Table 3-7. Mechanical Properties of Lashing – Case AWB.....	96
Table 3-8. Mechanical Properties of Lashing – Case AWC.....	97
Table 3-9. Mechanical Properties of Lashing – Case AWD.....	98
Table 3-10. Mechanical Properties of Lashing – Case LWA.....	100
Table 3-11. Mechanical Properties of Lashing – Case LWB.....	101
Table 3-12. Mechanical Properties of Lashing – Case LWC .....	101
Table 3-13. Mechanical Properties of Lashing – Case LWD .....	102
Table A1. Typical Lashing Properties (Full Scale Experiments) .....	A4

# Conversion Factors

---

Non-SI\* units of measurement in this report can be converted to SI units as follows:

Multiply	By	To Obtain
acres	4,046.873	square meters
cubic feet	0.02831685	cubic meters
cubic inches	0.00001638706	cubic meters
degrees (angle)	0.01745329	radians
degrees Fahrenheit	$(5/9) \times (^\circ\text{F} - 32)$	degrees Celsius
degrees Fahrenheit	$(5/9) \times (^\circ\text{F} - 32) + 273.15$	kelvins
feet	0.3048	meters
gallons (U.S. liquid)	0.003785412	cubic meters
horsepower (550 ft-lb force per second)	745.6999	watts
inches	0.0254	meters
kips per square foot	47.88026	kilopascals
kips per square inch	6.894757	megapascals
miles (U.S. statute)	1.609347	kilometers
pounds (force)	4.448222	newtons
pounds (force) per square inch	0.006894757	megapascals
pounds (mass)	0.4535924	kilograms
square feet	0.09290304	square meters
square miles	2,589,998	square meters
tons (force)	8,896.443	newtons
tons (2,000 pounds, mass)	907.1847	kilograms
yards	0.9144	meters

---

\* *Système International d'Unités* ("International System of Measurement"), commonly known as the "metric system."

# Preface

---

The research described in this report was authorized by Headquarters, U.S. Army Corps of Engineers (HQUSACE), as part of the Navigations Systems Research Program. This study was conducted under Work Unit (WU) 33143, "Design of Innovative Lock Walls for Barge Impact." Focus Area Leader was Ms. Yazmin Seda-Sanabria, Geotechnical and Structures Laboratory, U.S. Army Engineer Research and Development Center (ERDC). Dr. Robert M. Ebeling of the ERDC Information Technology Laboratory (ITL), Vicksburg, MS, is the Principal Investigator of this work unit.

Dr. Sandra Knight, Coastal and Hydraulics Laboratory (CHL), Vicksburg, MS, ERDC, was the Technical Director for Navigation. The Navigation Business Line Leader was Mr. Barry Holliday, HQUSACE. Mr. James E. Clausner, Technical Programs Office, CHL, was Navigation Systems Program Manager.

This research was jointly conducted and the report prepared by Dr. José Ramón Arroyo, General Engineering Department, University of Puerto Rico at Mayagüez; and Dr. Robert M. Ebeling, Computer-Aided Engineering Division (CAED), ITL. Dr. Ebeling authored the scope of work for the research effort discussed in this report. The research was monitored by Dr. Ebeling, under the supervision of Dr. Charles R. Welch, Chief of Engineering and Informatics Systems Division, ITL; Mr. David R. Richards, Technical Director, ITL; and Dr. Jeffery P. Holland, Director, ITL.

ITL is an element of the U.S. Army Engineer Research and Development Center (ERDC), U.S. Army Corps of Engineers. At the time of publication of this report, Dr. James R. Houston was Director of ERDC, and COL James R. Rowan, EN, was Commander and Executive Director.



# 1 Introduction

---

## 1.1 Background – Barge Train Maximum Impact Forces

Locks are a necessary structural feature found at every dam within the U.S. inland waterways navigation system. This network of rivers is an essential component of the nation's transportation infrastructure system, a system key to national commerce. Locks allow for groups of barges, lashed together to form barge trains, to negotiate the changes in river elevation at the dams. One of the most frequent loads applied to the locks of the U.S. inland waterway system is the impact made by a barge train on the approach walls as the barge train aligns itself to transit the lock. Consequently, this load case represents one of the primary design loads considered for lock approach walls.

Lock approach walls are designed for usual, unusual, and extreme loads. In the past, the primary focus of engineers performing impact computations has been on the lock approaches where the worst-case events and damage to the barge train and/or wall are likely to occur (e.g., extreme loads where vessel control is lost). The Corps' original guidance for computing glancing-blow maximum impact forces for barge trains impacting approach walls, Engineer Technical Letter (ETL) 1110-2-338, was rescinded in 2001. ETL 1110-2-338 impact force computations were based on crushing of the impact corner of the barge, a response that is usually associated with an extreme load case. In April 2004, ETL 1110-2-563, *Barge Impact Analysis for Rigid Walls*, was issued by Headquarters, U.S. Army Corps of Engineers (HQUSACE). The impact force computations are based on the "Empirical Correlation" developed by and presented in Arroyo, Ebeling, and Barker (2003). Limiting impact forces contained in this second document were not available (April 2004) and were consequently based on engineering judgment.

Recent advances in the computations of usual and some unusual impact design loads during which no damage occurs to the wall and the barges, and no failure occurs in the lashings that bind the barges together were presented in Arroyo, Ebeling, and Barker (2003). This report discusses the reduction of load data measured during full-scale, low-velocity, controlled barge impact experiments of a 15-barge train impacting a wall (Figure 1.1) at a decommissioned U.S. Army Corps of Engineers lock, and the resulting empirical correlation.

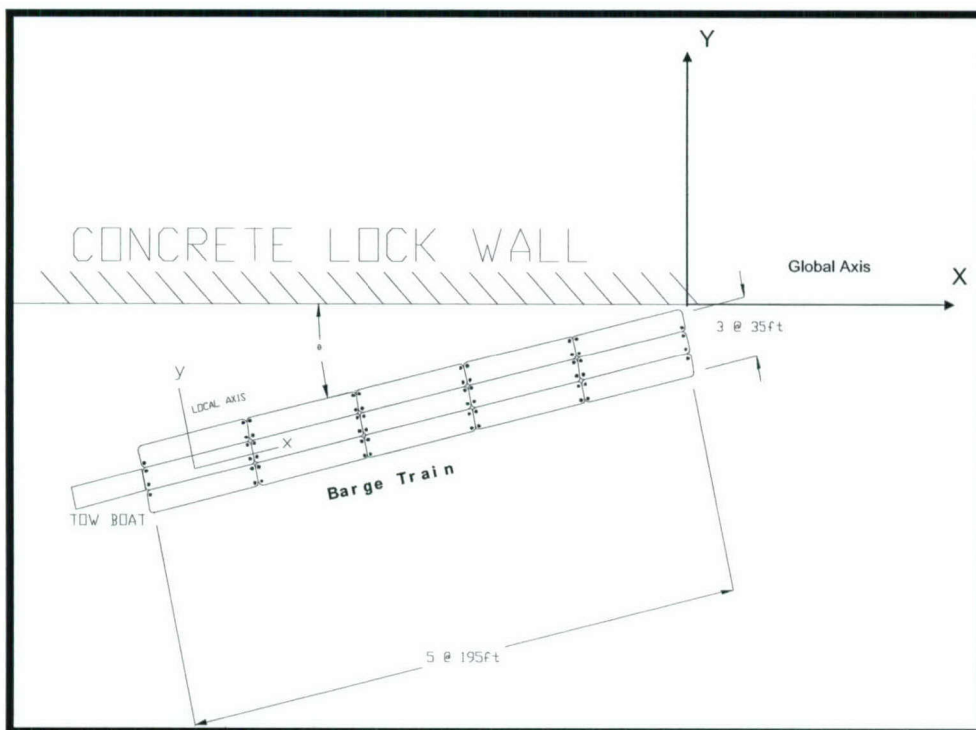


Figure 1-1. Barge Train-Wall Systems

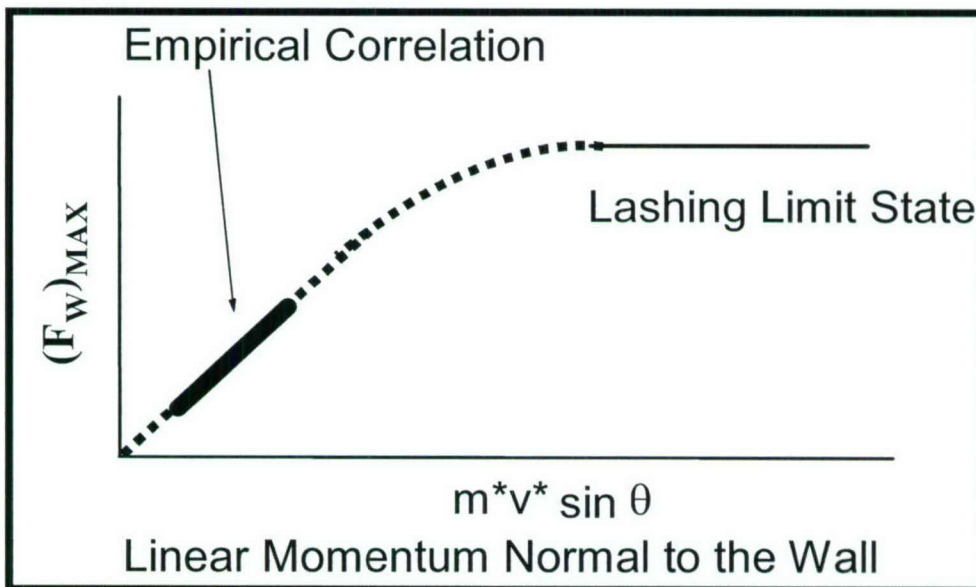


Figure 1-2. Asymptote of the Empirical Formulation

Figure 1.2 shows an idealized image of the interrelationship between maximum impact force imparted to the wall and the linear momentum (just prior to impact) of the barge train normal to the wall. Linear momentum conveniently represents two key demand variables: the mass of the barge train and its velocity normal to the wall.



There exists an upper bound for the force normal to the wall that is described by the weakest zone in the barge train; either the lashing connections or the nonlinear deformation of the corner of the barge in contact with the wall. The lashing limit state can be represented graphically (Figure 1.2). The limit state force shown in this figure results from either the failure of the lashings that bind the barges of the barge train together or to plastic yielding of the structural members (i.e., deck and skin plates and internal structural frame) within the corner of the barge that impacts the wall, whichever is less. Arroyo and Ebeling (2004) developed and fully described the theory for three probable idealized lashing failure mechanisms. These failure mechanisms are: the transverse, the corner, and the longitudinal failure mechanisms. This Technical Report presents a full assessment and a parametric study of these failure mechanisms. It is important to conduct a parametric study to quantify the magnitude of the maximum impact force as a function of a range of values of each of the primary variables within the barge train system.

### 1.1.1 Background – Full-Scale, Low-Velocity Controlled Barge Impact Experiments

In December 1998, full-scale, low-velocity, controlled barge impact experiments were conducted by Patev, Barker, and Koestler (2003) at the decommissioned Gallipolis Lock at Robert C. Byrd Lock and Dam, Gallipolis Ferry, WV. One of the many goals of these experiments was to measure the actual impact forces normal to the wall using a load-measuring device. The focus of these experiments was to obtain and measure the baseline response of an inland waterway barge, quantify a multiple-degree-of-freedom system during the impact, and investigate the use of energy-absorbing fenders. The full-scale experiment used a 297-m- (975-ft-) long, 15-barge, commercial barge train in a 3-wide by 5-long configuration (Figure 1.1). Each barge was a jumbo open-hopper design 10.67 by 59.45 m (35 by 195 ft) with rake barges at the front of the tow. The barges were ballasted with anthracite coal to a draft of 2.74 m (9 ft). The total weight of the flotilla was 267,000 kN (30,012 short tons) with a total mass of 27,228,228 kg (1,865.59 kip-sec<sup>2</sup>/ft), which is equal to the total weight divided by the gravitational constant,  $g$ . A total of 44 impact experiments were successfully conducted against the unaltered guide wall and a prototype fendering system that was attached to the wall. Approach velocity for the 12 bumper experiments conducted at the lock, ranged from 268 mm/sec to 875 mm/sec (0.88 to 2.87 fps), with approach angles ( $\theta$ ) ranging from 8.8 to 21.1 degrees. These shallow approach angles are typical of the approach angles with lock approach walls during glancing-blow impacts. For each of these tests, the barge train was brought in at a constant approach angle  $\theta$  and at a constant velocity. The target area was the stiff-to-rigid concrete upper guide wall, *lacking* the friction-reducing steel armor found on modern lock walls. The data in Table 1.1 summarize the approach angle and velocity for the 12 most credible bumper experiments.

The load bumper (or more specifically, the arc load beam) used to record the impact force time histories during the experiments was constructed of mild-steel with an outer radius of 72.6 in., outer arc-length of 43.6 in., cross section measuring 9 in. in width by 5 in. in height, and separation between the 6-in.-diam load pins of 35.5 in. The interpretation of the instrumentation data recorded by Patev, Barker and Koestler (2003)



is discussed in Arroyo, Ebeling, and Barker (2003). The following summarizes key aspects of the Arroyo/Ebeling/Barker interpretation. Once the time of impact was identified, the impact angle (the angle formed by the port side of the corner barge with the lock wall) was determined from the corrected GPS data. This angle is critical to the bumper geometry and resulting force system.

Table 1-1. Impact Velocity/Angle Data for Bumper Experiment

Experiment Number	Impact Angle, deg	Velocity		Velocity Normal to the Wall	
		fps	mph	fps	mph
28	9.7	2.41	1.64	0.41	0.28
29	12.7	2.21	1.50	0.48	0.33
30	12.2	2.35	1.60	0.50	0.34
31	10.6	1.62	1.10	0.30	0.20
37	10.3	1.96	1.33	0.35	0.24
38	11.9	1.84	1.25	0.38	0.26
39	14.1	1.62	1.10	0.39	0.27
40	17.5	1.91	1.30	0.57	0.39
41	8.8	2.87	1.95	0.44	0.30
42	17.5	1.84	1.25	0.55	0.38
43	21.1	0.88	0.60	0.32	0.22
44	20.9	1.22	0.83	0.44	0.30

Velocity (actually speed) is simply calculated from the displacement of the front corner GPS unit per unit time (1 sec). The initial orientation of the bumper relative to the longitudinal axis of the barges was adopted to be 54 degrees from the longitudinal axis (local axis of the model) of the barges. Initially, the recorded forces at the pins were assumed to be in the radial direction. The precise orientation of the bumper on the barge is critical to this effort. The as-built orientation of the bumper was then determined from a combination of design drawings and documentary photos. The survey data were intended for this purpose; however, the uncertainty caused by the barges shifting and the tow drifting against its moorings between sightings compromised the accuracy of these measurements sufficiently to make them unusable for this purpose.

Subsequently, it was established from the design drawings and documentary photos that the recorded forces orientation were not aligned in the radial direction of the arc load beam. A new-recorded forces orientation that took this observed discrepancy into account was established. This second configuration was analyzed considering the magnitude of the angles associated with the support reactions orientation. The results of this analysis indicated that an impossible geometrical arrangement was produced by this second set of assumptions. A final geometrical configuration was then established based on: (1) the range of probable angles for the force orientations relative to the radial direction, (2) the location of the bumper related to the longitudinal axis of the barges, and (3) the appropriate coefficient of friction between concrete (for the unarmored wall face) and (barge corner) steel. It was demonstrated in Arroyo, Ebeling, and Barker (2003) that this final configuration produces reasonable results based on the values of the coefficient of friction between the wall and the steel bumper found in technical literature, and using



the fact that the bumper must be in compression during the impact process. Based on a careful assessment of the results from this bumper study, only eight of the initial 12 bumper impact experiments were used in the empirical correlation developed by Arroyo, Ebeling, and Barker (2003) to estimate the maximum impact force normal to the wall.

### 1.1.2 Background – Empirical Correlations

Using values for the maximum normal force  $F_w$  and the Linear Momentum normal to the wall, a best fit straight line was calculated for the eight good experiments of 1998. This approach relates the maximum  $F_w$  obtained from the experiments directly to the linear momentum. The least squares regression procedure was used to develop the best fit straight line through the eight data points for the empirical correlation. The line was assumed to start at the origin (i.e., no intercept term was used for the linear equation). The resulting best-fit equation for this set of eight data values was

$(F_w)_{\max} = 0.435mv \sin \theta$ . That is, a coefficient times the linear momentum normal to the wall determines the maximum force normal to the wall. We can observe that the greater the magnitude for the linear momentum, the larger will be the maximum value for the impact force normal to the wall. This relationship was based on low velocity, shallow impact (up to 21.1 degrees) experiments that, by definition, do not account for factors that manifest themselves at higher velocities. Additionally, no damage occurred to the barge train and no lashings broke during these eight impact experiments.

The empirical correlation between the maximum force normal to the wall and the linear momentum normal to the wall immediately prior to impact developed using the field data from Patev, Barker, and Koestler (2003) (development of empirical correlation described in Arroyo and Ebeling [2004], and Arroyo, Ebeling, and Barker [2003]) was based on statistical procedures and the values of force obtained from the acceptable bumper configuration.

The mathematical form of Newton's second law states that a resultant external force applied to a body is equal to the mass of the body multiplied by the absolute acceleration the body experiences. Also, it can be expressed in terms of the absolute velocity of the body by introducing the first derivative with respect to time of the velocity, which is the acceleration. One useful tool that can be derived from Newton's second law,  $F = ma$ , is obtained by integrating both sides of the equation with respect to time. This integration can be done only if the forces acting on the particle are known functions of time. The external forces acting on the particle change the linear momentum. The mathematical form of the resulting expression after the process of integration states that the impulse during a period of time due to the applied impulsive force is equal to the difference in linear momentum during the same interval of time. This relationship establishes the *Principle of Impulse and Linear Momentum*. The units of both impulse and momentum are force and time; therefore, impulse and momentum are expressed in Newton-second, or kip-second. The impulsive force is a function of time and generally varies during its period of application. A large force that acts over a short period of time is called an *impulsive force*.



The linear momentum is defined as the mass of the particle multiplied by the velocity of the particle. It is a vector quantity oriented in the same direction as the velocity of the particle (tangent to the trajectory). The velocity of a barge train is usually specified in the local barge axis; longitudinal - local "x" axis and transverse - local "y" axis. In this case two velocities are specified, that is  $V_x$  and  $V_y$ . To obtain the velocity normal to the wall, an axis transformation equation is needed. This expression is:

$$\begin{Bmatrix} V_{par} \\ V_{norm} \end{Bmatrix} = [C]^{-1} \begin{Bmatrix} V_x \\ V_y \end{Bmatrix} \quad (1.1)$$

Where:

$$[C]^{-1} = \begin{bmatrix} \cos \theta & -\sin \theta \\ \sin \theta & \cos \theta \end{bmatrix}$$

and  $V_{par}$  and  $V_{norm}$  are the velocity parallel (global "X" axis) and normal (global "Y" axis) to the wall, respectively.

Equation (1.1) can be easily obtained from Figure 1.3.

The empirical correlation between the maximum force normal to the wall and the linear momentum normal to the wall immediately prior to impact, developed by Arroyo, Ebeling, and Barker (2003) was based on statistical procedures and the values of maximum impact force obtained from the acceptable bumper configuration. Using values for the maximum normal force  $F_W$  and the Linear Momentum normal to the wall, a best fit straight line was calculated using data from eight of the full-scale impact experiments. This approach relates the maximum  $F_W$  directly to the linear momentum.

It is important to note that only one data point of the entire  $F_W$  time history for each of the eight experiments were used to develop this empirical correlation. The least squares regression procedure was used to develop the best fit straight line through the eight data points (for the eight impact experiments) for the empirical correlation. The line was assumed to start at the origin (i.e., no intercept term was used for the linear equation). The resulting best fit straight line, average minus one standard error, and average plus one standard error lines were developed and shown in Figure 1.4.

The resulting best-fit equation for this set of eight data values is  $(F_W)_{max} = 0.435mV_{norm}$ , with units of the resulting force in kip, mass (including the mass of the loaded barges and tow boat, but excluding hydrodynamic added mass) in kip-sec<sup>2</sup>/ft and approach angle in degrees. That is, a coefficient times the linear momentum normal to the wall determines the maximum force normal to the wall.

As noted earlier, it can be observed that the greater the magnitude for the linear momentum, the larger will be the maximum value for the impact force normal to the wall. This relationship was based on low velocity, shallow impact (up to 21.1 degrees) experiments that, by definition, do not account for factors that manifest themselves at higher velocities. Additionally, no damage occurred to the flotilla of barges and no lashings broke during these eight impact experiments. This empirical correlation was derived using data obtained from a (3 by 5) barge train that had a velocity normal to the wall up to and not exceeding 173.74 mm/s (0.57 fps) with no damage occurring during

impact events, for impact angles up to 21.1 deg, and for a barge train with a linear momentum normal to the wall between 2885.29 kN-sec (649.84 and 1,025.48 kip-sec).

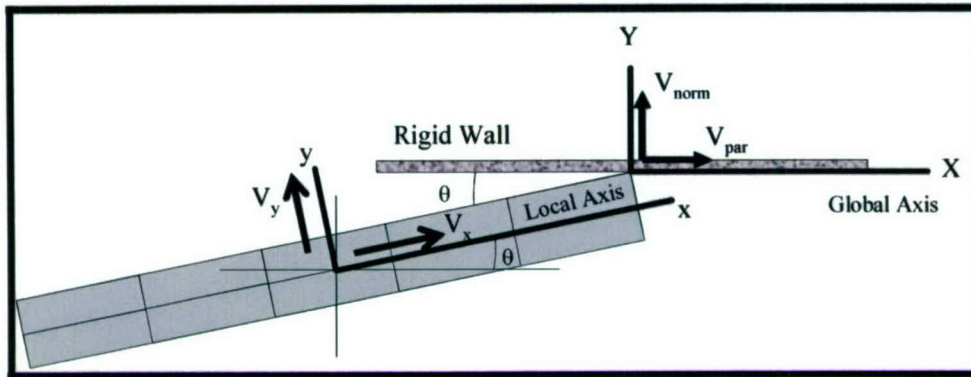


Figure 1-3. Velocity Vector Transformation—from Local to Global Axis

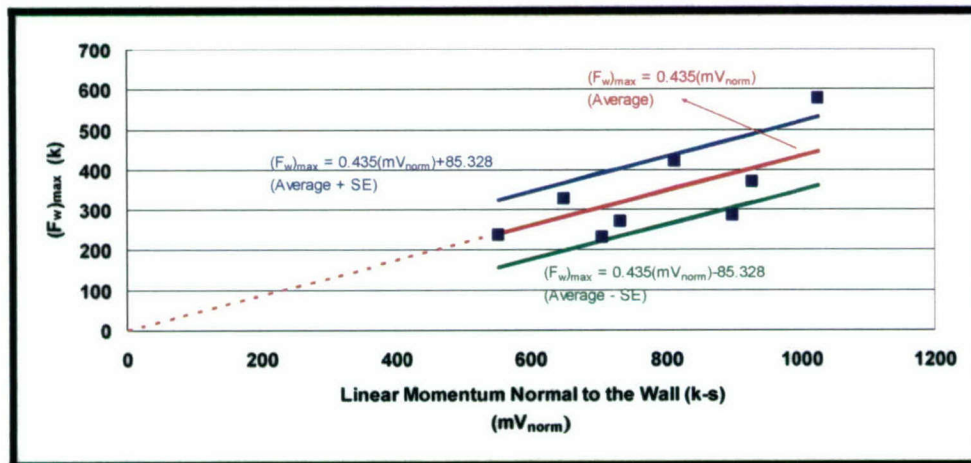


Figure 1-4. Empirical Correlation Using the Linear Momentum Normal to the Wall Concept (Figure 6.3 in Arroyo, Ebeling, and Barker, 2003)

The maximum normal force  $(F_w)_{max}$  by the empirical correlation is equal to the reaction force provided by the lock wall on the barge train during the impact. Note that the masses used to develop the correlation of linear momentum normal to the wall with values of  $(F_w)_{max}$  uses the mass of the barge train and does *not* include the computation of any hydrodynamic added masses. (However, hydrodynamic effects on the barge train are accounted for in the measured impact forces.) A single lumped mass was used to characterize the barge train in this simplified correlation.

### 1.1.3 Background – Three Idealized Failure Mechanisms

The empirical correlation given in Figure 1.4 is based on data from eight low-velocity, controlled barge impact experiments in which there was *no damage* to the barge and *no failure* of the lashing(s). Thus these two linear empirical correlations are only valid below a limit state in which either crushing of the corner of the impacted barge occurs or ultimate strength of the lashing(s) occurs. Either limit state would introduce an asymptote to the empirical correlation shown in Figure 1.4. The Figure 1.2 idealization



demonstrates the point that the Empirical Correlations must have a limiting force value that occurs, for example, when the lashings yield and the barge train breaks apart into individual barges.

A barge train system consists of a group of nearly rigid barges joined together with steel cables, referred to as lashings. These lashings define a barge train system where the weak zones are assumed to occur at each barge connection. The motion of each barge relative to the other is how the system distributes the impact forces among the barges during the impact process.

During the impact of a barge train against the wall, forces are transferred from the point of contact to the barges that form the barge train. These forces are transferred by means of the contact between the barges and the lashing that join the barges. The lashings are pre-stressed in an attempt to prevent any initial angular motion between the barges before the internal stress begins to increase within the lashings. At the instant of impact, a failure plane can be defined such that all lashings break along this plane. Three principal lashing failure mechanisms were identified. These failure planes were designated as the (1) Longitudinal, (2) Transverse, and (3) Corner failure mechanisms and are fully described in Arroyo and Ebeling (2004). In each case, a single type of failure plane was required to occur in such a way that the force normal to the wall was computed. Each of these idealized failure planes defines two systems of barges. That is, two systems of barges are obtained by analyzing each of the barge systems created; one on each side of the potential failure plane. The limit state can be reached as soon as the lashing achieves its ultimate (tensile) stress and possibly even breaks across a predefined plane that is designated as a potential failure plane.

#### *1.1.3.1 Glancing Blow – Transverse Failure Mechanism*

As has been observed during barge train impact events at shallow approach angles (i.e., “glancing” blows, cf. Figure 1.5), the impact event can produce a failure of the lashings in an “opening wedge” fashion along a transverse plane between barges. The lashings develop tensile strains across the wedge-opening transverse plane as this opening develops. The barges rotate a small amount in such a way that the force normal to the wall is transferred to the connections between the barges. This transverse failure mechanism occurs in the local barge “y” axis along the first transverse line of lashing connections behind the row of barges that form the bow to the barge train. This type of failure has a significant contribution from the rotation of the first column of three barges that form the bow.

Figure 1.5 depicts the barge train impacting a rigid wall and the development of a failure plane along the transverse axis of the barge train system. Two systems of barges are identified in this figure. The system in a direct contact to the wall is referred to as “System one” and the remaining barges form “System two.” System one rotates with a pivot assumed at the first connection from the bow on the starboard side. All the lashings across this potential failure plane will elongate, resulting in an increase in the internal lashing forces. The lashings on the port side of this transverse plane will be the most stressed and will be the first to fail.



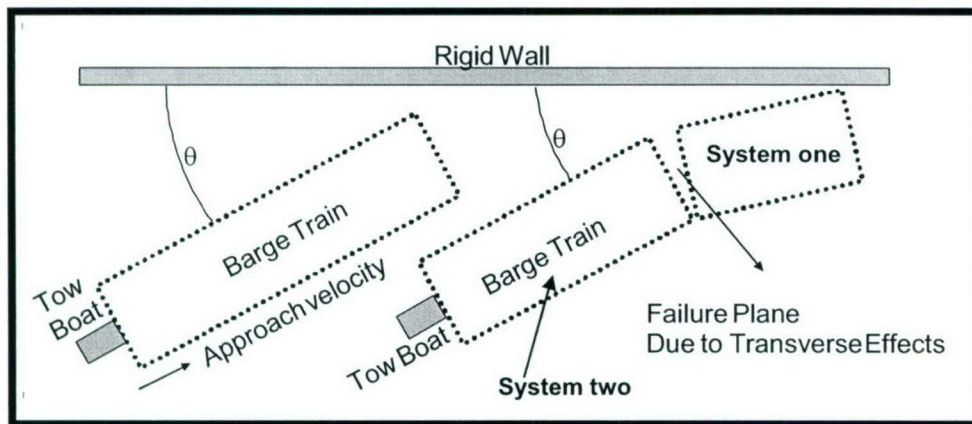


Figure 1-5. Transverse Failure Mechanism

The idealized failure mechanism assumes the internal connections will rupture in sequence towards the pivot point as System one continues the rotation. In this failure mechanism, both systems of barges are assumed to be rigid and no longitudinal relative motion is assumed. It is recognized that this is an idealization; however this simple model attempts to capture a failure mechanism whereby most of the energy comes from the rotational degree(s) of freedom.

This transverse failure mechanism makes the following general assumptions:

- The barges of System one have zero acceleration normal to the wall immediately after impact occurs with the “rigid” wall.
- System two continues the forward motion, and System one continues the rotation, increasing the internal force of the lashing(s) across the failure plane.
- Each of the two barge systems is assumed to be a rigid body.
- The lashings are modeled as having elasto-plastic behavior that break when an ultimate (tensile) strain value is achieved within the lashing.

There are two possible tendencies of rotation in the transverse failure mechanism. If the line of action of the resultant force at the point of contact lies to the front of the center of mass of System one, then the pivot point will be at the starboard side of the barge train as shown in Figure 1.6. On the other hand, if the line of action of the resultant force at the point of contact of the barge train and the rigid wall lie behind the center of mass, then the pivot point will be at the port side of the barge train (Figure 1.7). Arroyo and Ebeling (2004) describe these two failure possibilities and the parameters for their occurrence.

#### 1.1.3.2 Glancing Blow – Corner Failure Mechanism

As has been observed during barge train impacts events at shallow approach angles (i.e., “glancing” blows), the impact event can produce a failure of the lashings in an “opening wedge” fashion along a transverse plane between barges. (The lashings develop tensile strains across the wedge-opening transverse plane as this opening develops.)

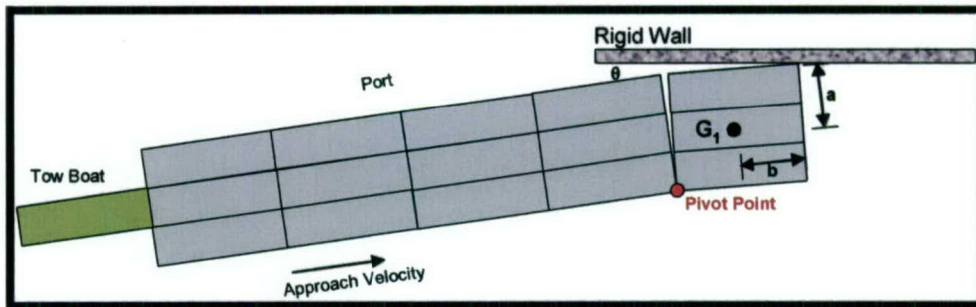


Figure 1-6. Pivot Point at the Starboard Side of the Barge Train

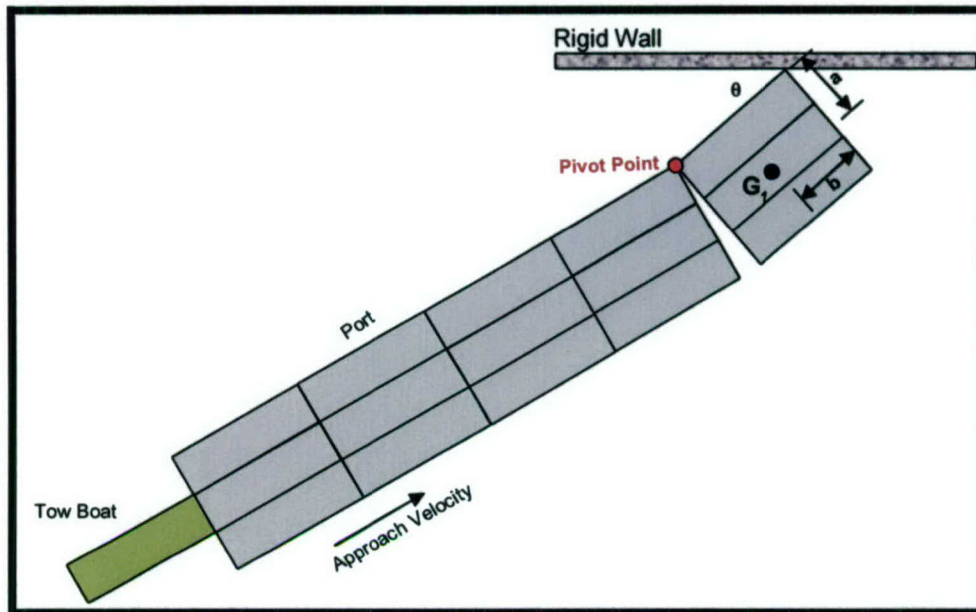


Figure 1-7. Pivot Point at the Port Side of the Barge Train

The barges move and rotate a small amount in such a way that the force normal to the wall is transferred to the connections between the barges. However, the actual failure process may not be as simple as the simple transverse "wedge opening" fashion. A local rotation of the corner barge (barge one) is likely to occur, as depicted in Figure 1.8. A second pivot point is generated after the first pivot point is developed in the starboard side of the barge train. This second pivot point is located at the corner barge at the bow opposite to the impact point.

This failure mechanism is believed to be a more realistic model than the Transverse failure mechanism alone. In the Transverse failure mechanism, the three-barge system in contact with the wall was considered as a (single) rigid body; no local rotation was allowed to occur. In this potential failure mechanism, designated the Corner failure mechanism, local rotation of the corner barge is allowed.



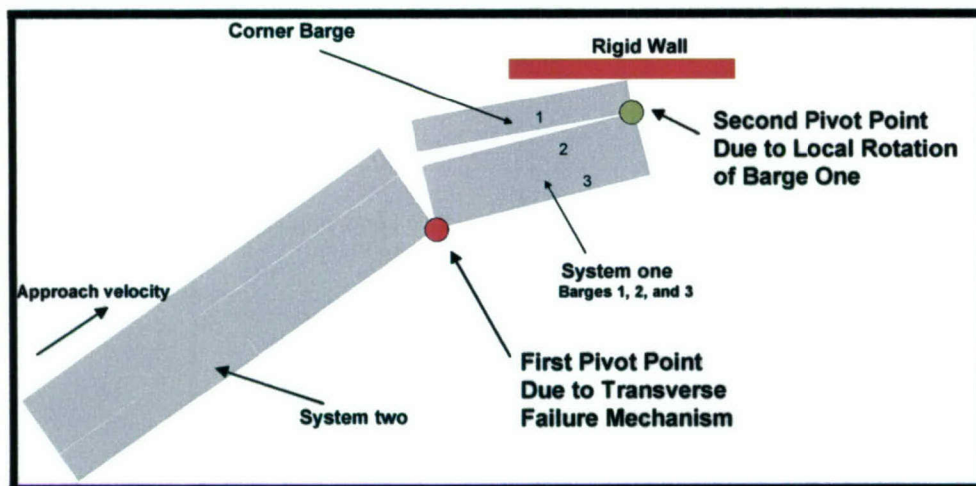


Figure 1-8. Scheme of Corner Failure Mechanism

This Corner failure mechanism makes the following general assumptions:

- The barges of System one have zero acceleration normal to the wall immediately after impact occurs.
- System two continues its forward motion, and System one continues the rotation, increasing the internal force within the lashings across the failure plane.
- The connections of barges in System one are flexible, allowing the relative rotation shown in Figure 1.8.
- The lashings are modeled as having elasto-plastic behavior that break when an ultimate (tensile) strain value is achieved within the lashings.

#### 1.1.3.3 Head-on Impact – Longitudinal Failure Mechanism

As has been observed during barge train impact events, an almost direct impact of a barge train system on a nose pier or a cell can produce a failure of lashings in the longitudinal axis of the barge system. This failure extends from the bow to the aft of the barge train system. This is comparable to a shear failure mechanism in which the barge train separates into two columns of barges with one system of barges moving relative to the other system of barges. Figure 1.9 shows an example of this idealized failure mechanism for a barge train of 15 barges that impacts a concrete lock wall at an approach angle  $\theta = 90$  degrees. This potential failure mechanism is designated as the Longitudinal Failure Mechanism. This failure mechanism is based on the relative motion of a two system barge train with each system of barges developing on each side of a longitudinal failure plane.

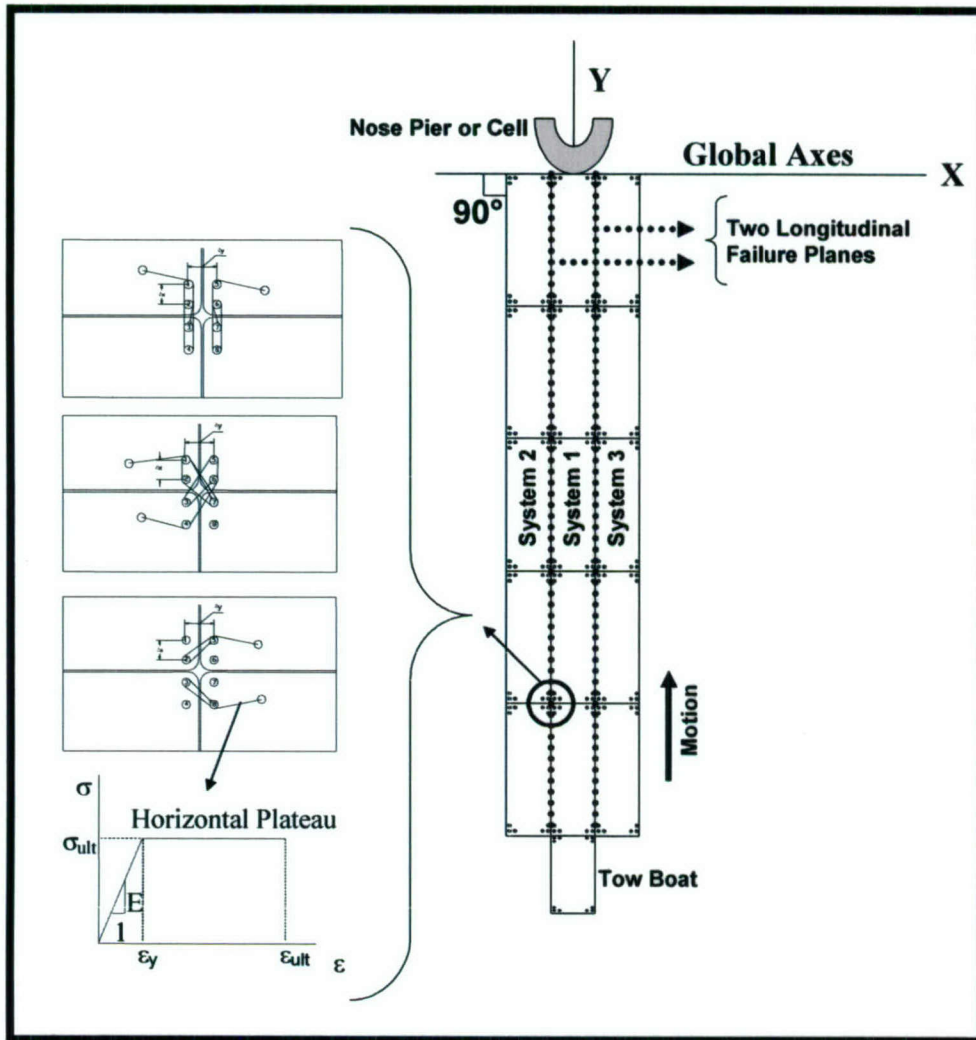


Figure 1-9. Longitudinal Failure Mechanism for a Head-On Impact ( $\theta = 90$  deg)

Figure 1.9 shows an idealized collision in which a barge train impacts a nose pier or cell and develops failure planes along the longitudinal axis of the system. Based on this figure, two systems of barges can be identified. The system that is in a direct contact with the wall is called System one and the remaining row of barges form System two and three. If the impact occurs at the corner barge of the barge train, then the row of lashings between the first and second row of barges along the longitudinal axis will deform more than the other lashings in the barge train. In this idealized failure mechanism both systems of barges are assumed to be rigid and no transverse relative motion is allowed. Also, Figure 1.9 shows a typical lashing configuration used during the 1998 experiments and the assumed elasto-plastic mechanical behavior of the lashings.

#### *Progressive Yielding of Lashings*

Lastly, the limit state, which is defined as an event that occurs when lashings yield, can be used to define a value of  $(FW)_{\max}$  due to the impact process. This maximum force normal to the wall can be calculated assuming the lashings provide the maximum strength to the connections between barges. The idealized image in Figure 1.10 shows the



progressive process that defines the failure of the system for the Transverse failure mechanism. This figure presents the state of the lashings as the process of impact develops. As impact begins, the internal stress within the lashing increases, but this increase occurs within the elastic zone (Figure 1.10.a). Later, as the rotation of the front barges (i.e., System one) increase, the lashing at the port side of the transverse failure plane is in a state of ultimate stress, but the internal lashings are in an elastic state (Figure 1.10.b). Finally, the rotation continues increasing until all lashings across the failure plane achieves ultimate stress and their ultimate (tensile) strain value, producing a transverse failure of the lashings across the transverse failure plane of the barge system. This sketch idealizes the progressive development of the Transverse failure mechanism process assuming an elasto-plastic behavior of the lashings and ultimate rupture of the lashings. A similar process will apply to the Longitudinal and Corner failure mechanisms. In the Longitudinal failure mechanism process, the ultimate strength is reached as the relative motion between System one and System two increase. The Corner failure mechanism exhibits the same general behavior as depicted in Figure 1.10 but includes a relative rotation between the corner barge and the remaining barges of System one, resulting in a failure of the lashing that joins the corner barge to the rest of the barge train.

#### **1.1.4 Background – Limit\_Lashing**

Limit\_LASHING is a user-friendly, PC-based computer program developed to analyze the barge train impact on the lock walls, approach walls, guide walls, and guard walls. This program uses the methodology developed in Arroyo and Ebeling (2004) and other theories such as impulse and linear momentum and coefficient of friction, as discussed in Arroyo, Ebeling, and Barker (2003). The program was written using FORTRAN code and uses a preprocessor and postprocessor written in Visual Basic, which provides a user-friendly Windows® interface. The program can analyze the combination of the effects of mass of the barges and the effect of lashings at the moment the barge train reaches the ultimate deformation for three different failure mechanisms: the transverse failure mechanism, longitudinal failure mechanism, and the corner failure mechanism. The program conducts the analysis with user-provided data for the approach angle, number of barges, lashing configuration, etc. It presents all the results of the analysis for the possible failure mechanism in graphical form and reports the maximum normal force in the wall. The following sub-sections present the Limit\_Lashing input variables.

##### *1.1.4.1 Individual Barge Data*

This option of Limit\_LASHING is used to define the geometric properties of the individual barge as width, length, edge distance of the bits, and separation of the bits; the coefficient of friction between the barges; and the coefficient of friction between barge and impacted wall. The program assumes that all the barges are the same. Figure 1.11 shows the screen used to enter the input data mentioned above.

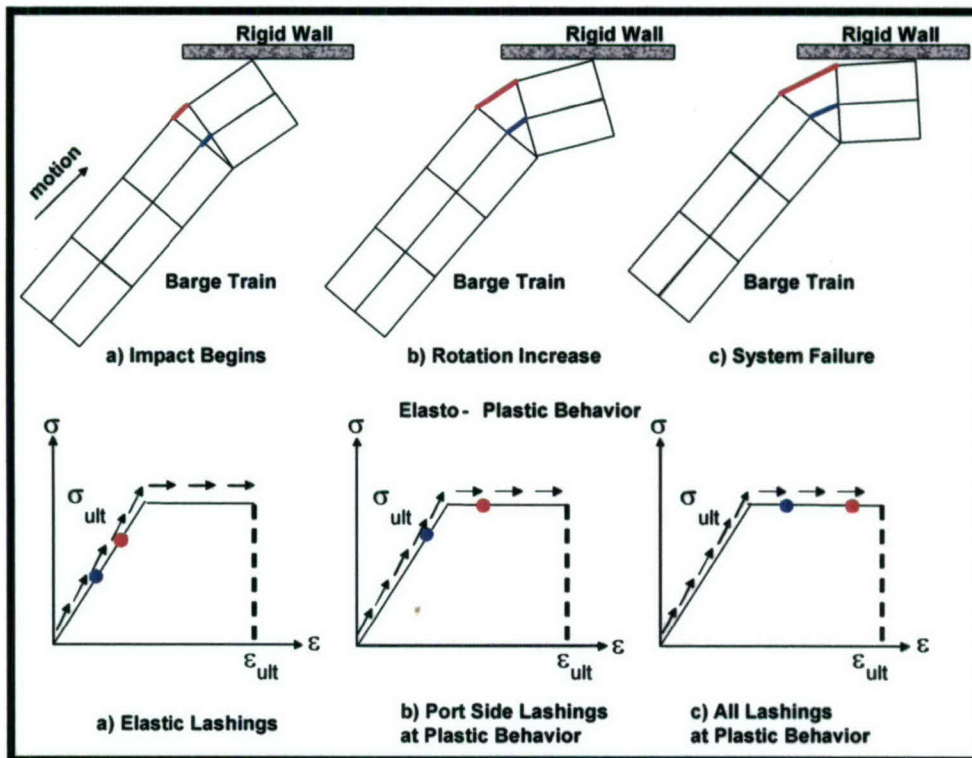


Figure 1-10. Example of a Progressive Barge Train Failure for the Transverse Failure Mechanism

**Individual Barge Data**

**Barge Dimension**

Width (W): 35 ft

Length (L): 195 ft

Mass: 124.37 Kips<sup>2</sup>

**Bit Spacing**

Edge Distance (c): 1.25 ft

Separation (s): 3 ft

**Friction Coefficients**

Between Barges: 0.2

Barge & Wall: 0.2

OK

Cancel

Figure 1-11. Limit\_LASHING Individual Barge Input Data




The width of the barge is measured as the shortest side of the barge. The length of the barge is the longest side of the barge. The mass of the barge can be calculated as the total weight of the barge train plus the tow boat divided by the gravitational constant,  $g$ , and divided by the number of barges in the barge train. The edge distance is the distance between the edges of the barge to the center of the corner bit. The separation is the distance between the center of adjacent bits. The coefficient of friction between barges and between barge to wall is in the range between 0.2 and 0.5, as discussed in Arroyo, Ebeling, and Barker (2003), and Arroyo and Ebeling (2004).

#### *1.1.4.2 Barge Train Layout*

This screen requests the number of barges in the local x- and y-axes coordinate system (LCS). By using the Display Barge button, the program will display the layout in the local coordinate system. Also the Hydrodynamics Added Mass Coefficients must be provided in this screen. The default values of these coefficients are 0.05, 0.4, and 0.4 in the x, y, and rotational component, respectively. Finally, Figure 1.12 shows that, if the user wants to define a different mass for each barge, the lower list of masses values can be modified for a particular case in which a barge train has a different mass.

#### *1.1.4.3 Approach Angle*

The approach angle of the barge train system can be defined by using the  icon located on the toolbar. The angle will be between 0 and 90 degrees (head-on impacts are 90 degrees). Then, a new screen is presented where the user can define the approach velocity in the local x- and y-direction. This screen also presents the orientation of the global coordinate system (Figure 1.13).

#### *1.1.4.4 Failure Mechanism*

The failure mechanism to be analyzed can be selected from the Failure Mechanism screen (Figure 1.14). That screen presents the failure planes of the system. The failure plane is produced between the barges in green (barge System 1) and the barges in red (barge System 2) defined by the joints (J1, J2, J3, ...). This screen shows the local (blue) and global (GCS) coordinate systems. After the failure mechanism is selected, it is necessary to establish the configuration of lashing using the Lashing Configuration button.

After the failure mechanism is selected and the Lashing Configuration button is pressed, two screens will appear. In the left screen appears the barge train system indicating the failure plane and the joints defining this plane. The right screen presents bits associated with each joint and the table of connectivity based on the lashing configuration desired. The three idealized failure mechanisms that the program can analyze are explained in Arroyo and Ebeling (2004).

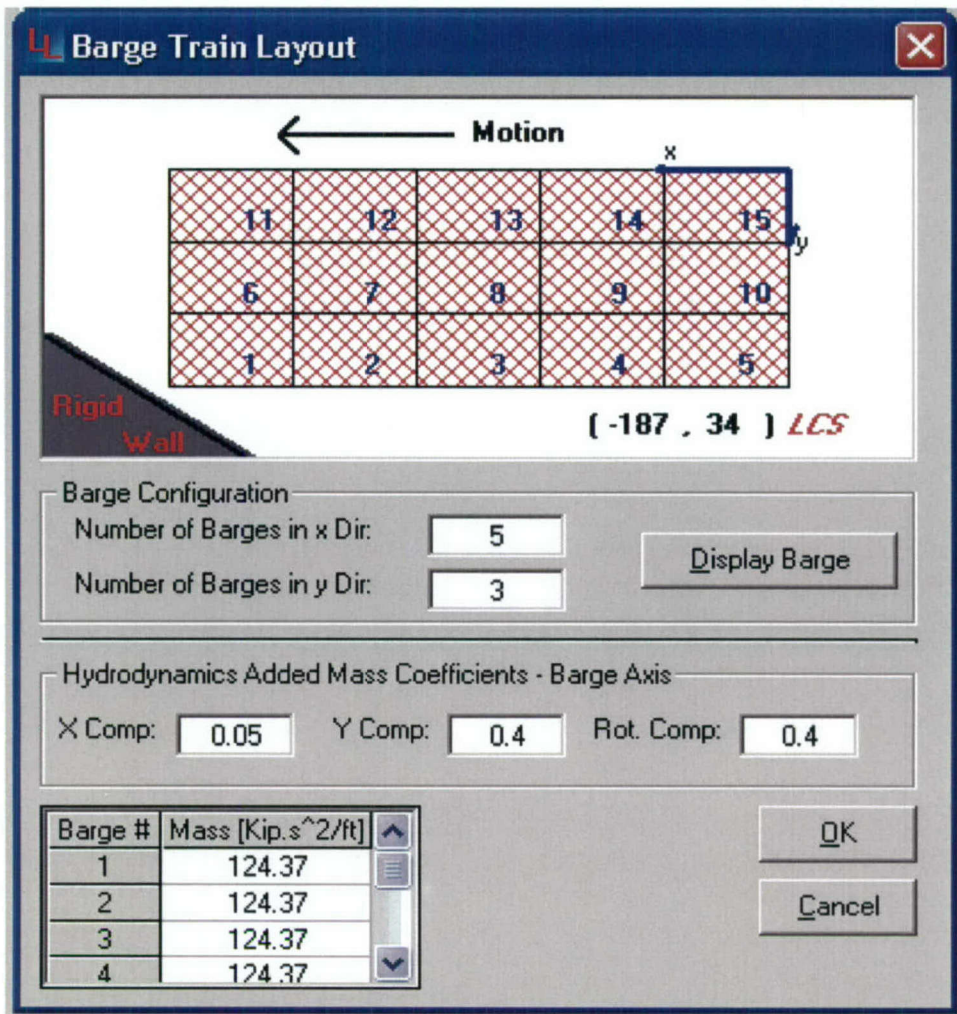


Figure 1-12. Limit\_LASHING Barge Train Layout Screen

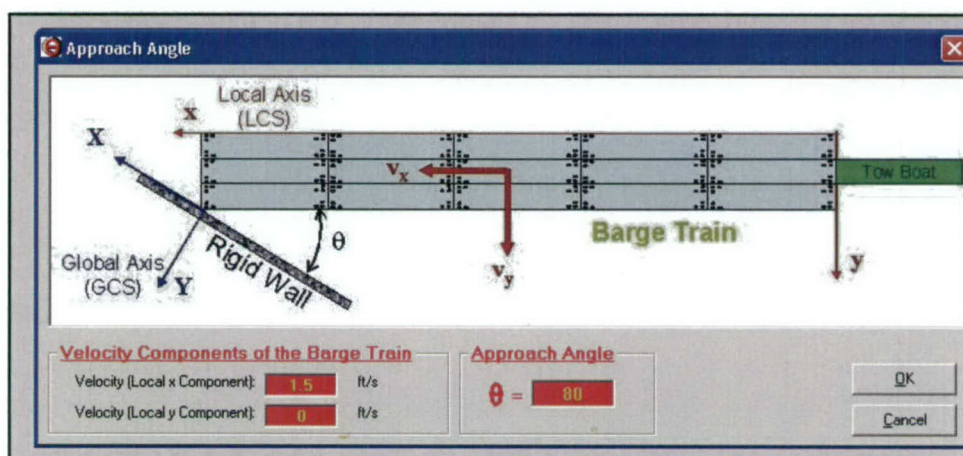


Figure 1-13. Limit\_LASHING Approach Angle Input Data



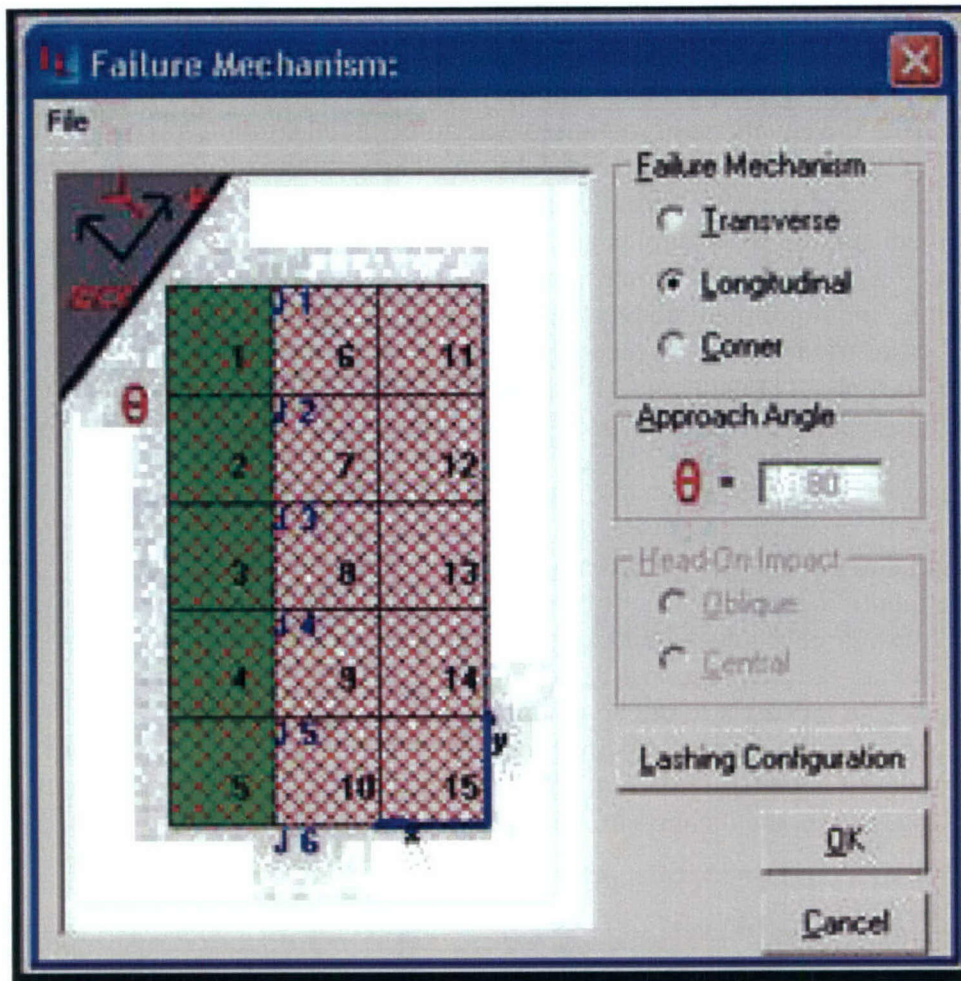


Figure 1-14. Limit\_LASHING Failure Mechanism Screen (Longitudinal failure mechanism shown on screen)

To define the lashing configuration, it is necessary to use the right screen of Figure 1.15. After the Lashing Configuration button is selected, it is necessary to define the number of lashings that act across the failure plane. Then, the user can zoom in on the bits arrangement of every joint along the failure plane by using the pull-down menu Display Bit Layout at Current Joint. The bits are presented in two colors, green and red. The green color bits are associated with barge System 1, and the red color bits are associated with barge System 2. At the bottom of the screen appears a table with the number of rows equal to the number of lashings. It is necessary to enter the number of wraps of each lashing in this table. One lashing can have  $n$  wraps. The wraps are defined in the columns that indicate From and To. Always define the wraps from barge System 1 (green) to barge System 2 (red).

Clicking on the lashing number (first column) causes a new screen to appear to define the mechanical properties of this lashing. Next, it is necessary to define the diameter of the lashing, modulus of elasticity, the initial tension (i.e., lashing pre-stress), ultimate load capacity, and the ultimate rupture strain of the lashing. Also, Figure 1.16 shows a diagram of the elasto-plastic stress-strain behavior of lashing. Section 1.2 gives more information about typical lashing configurations.



### 1.1.5 Limit\_LASHING Results for the Eight Barge Impact Experiments

Arroyo and Ebeling (2004), discuss the complex dynamic problem of a barge train-rigid wall system using the equations of motion to determine the maximum force applied to the rigid wall by a barge train during an impact event. Three failure mechanisms were studied. As this study concludes, the longitudinal failure mechanism is a failure that can occur at high approach angles, for example, greater than 70 degrees. This failure mechanism is based on the relative motion of one set of barges to another set of barges. All the lashings along the first line of connection and parallel to the port side will fail first. Two special cases of this failure mechanism were also studied, that is, a direct impact to a cell or nose pier, (1) with, and (2) without eccentricity. In the case of no eccentricity, two failure planes were identified.

The second failure mechanism presented was the transverse failure mechanism, which consisted of a flexure fashion failure. In this case, the first line of lashings parallel to the bow breaks due to the rotation of the barges at the bow of the system. In this model, no relative motion between the front barges was allowed. This failure mechanism can occur for shallow approach angles, for example less than 30 degrees. For higher approach angles, another failure plane will be adopted by the system. In this failure mechanism, two possible locations of the pivot point exist. An expression was determined to determine where the pivot point occurs, on the port side or on the starboard side. This location depends both on the coefficient of friction between the barge system and the armored wall, and on the location of the center of mass of System 1.

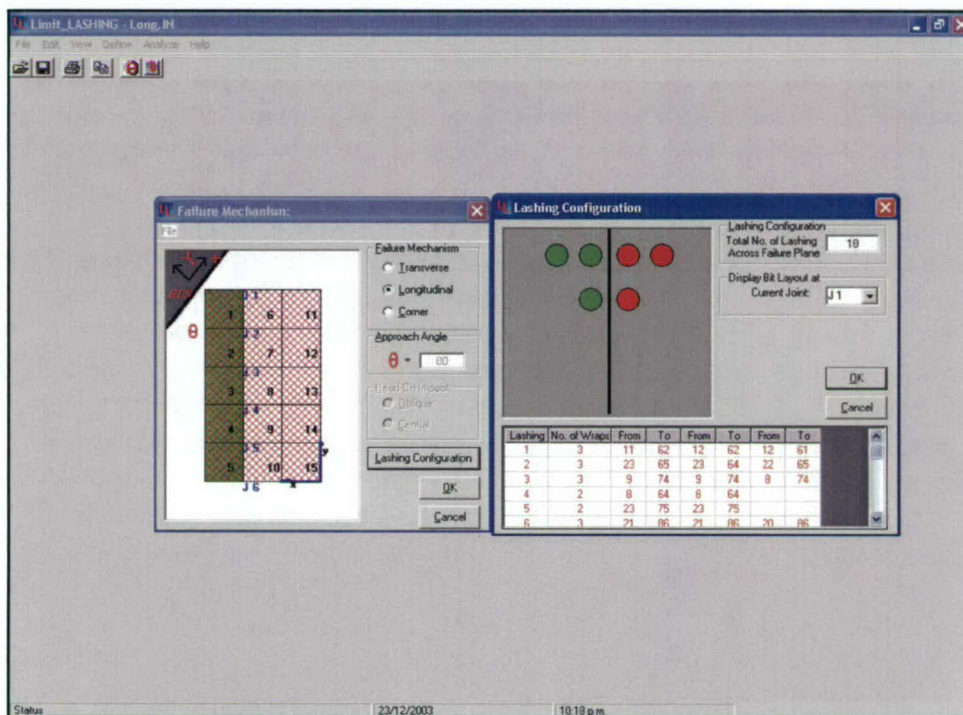


Figure 1-15. Limit\_LASHING Lashing Configuration Screen



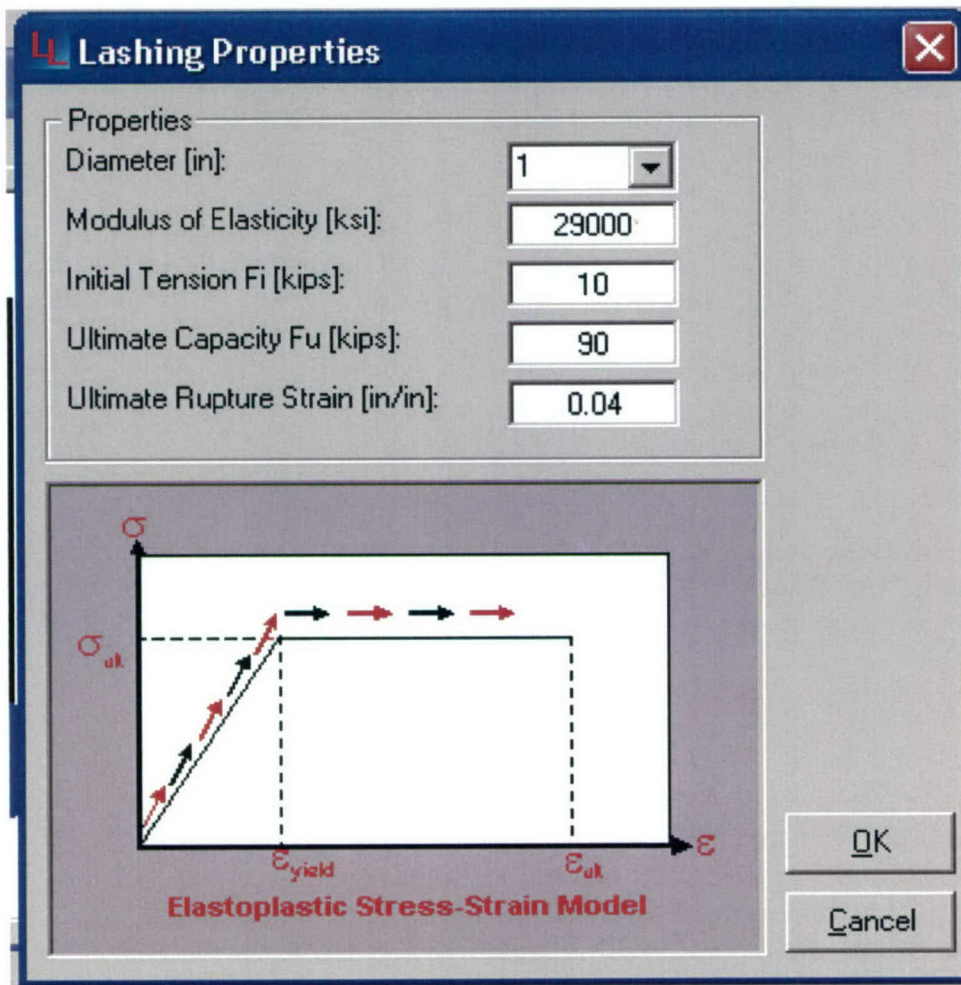


Figure 1-16. Limit\_LASHING Lashing Mechanical Properties Screen

A third failure mechanism was the corner failure mechanism. This model is similar to the transverse failure mechanism. The difference is that the rotation toward the wall of the corner barge is allowed. This effect can be introduced into the formulation of the transverse failure mechanism by including the lashing forces that join the corner barge to the rest of the barge train. In other words, the transverse failure mechanism assumes the front barges as a single rigid body, and the corner failure mechanism assumes that the corner barge is joined by the lashings to the other barges in System 1.

Arroyo and Ebeling (2004) present a comparison of the maximum force normal to the wall obtained by several methods:

- Full-Scale Experiment 1998 data
- ETL 1110-2-338 (rescinded)
- Lashing Limit State plus Empirical Correlation (Transverse and Corner Failure Mechanism).

The ETL 1110-2-338 engineering procedure had been used to compute values of maximum impact force normal to the wall,  $(F_w)_{max}$ . A key aspect of this engineering formulation is computation of collision energy dissipated in non-recoverable, plastic hull

deformation of (i.e., damage to) the corner of the barge where impact with the wall occurs. However, as no damage was observed to the barge corner during any of these low velocity, controlled impact experiments at Robert C. Byrd Lock. The failure due to lashing yielding could dominate over the crushing of the corner barge corner.

Based on the formulation described in Arroyo and Ebeling (2004), for shallow approach angles, the Limit\_LASHING corner failure mechanism predicts lower forces normal to the wall than the other two lashing failure mechanisms. This condition could be explained if one notices that the corner failure mechanism has more degrees of freedom. That is, this failure mechanism provides a primary degree of freedom, "rotation of System one," and a secondary degree of freedom, "rotation of the corner barge." For that reason, for a shallow approach angle ( $< 30$  degrees), the corner failure mechanism is recommended.

Several examples based on the data from the Full-Scale Experiment 1998 are presented. Table 1.2 lists the relevant information of the eight most credible experiments, the computed normal force at the wall based on the ETL 1110-2-338 computation, the field test results, and the force normal to the wall computed based on the Transverse and Corner failure mechanism as presented in Arroyo and Ebeling (2004).

The results listed in Table 1.2 show that, in all experiments, the results provided by the Corner failure mechanism are lower than the Transverse failure mechanism indicating that the Corner mechanism is more probable to occur than the Transverse failure mechanism. In most of the experiments, the value of the force normal to the wall obtained using the Corner failure mechanism (System 2) plus the Empirical Correlation (System 1) was above the value obtained from the field test. Only experiment 42 produced a field value greater than the Limit\_LASHING numerical model. The reason for obtaining a lower force normal to the wall is due to the very low value for the kinetic coefficient of friction between steel-steel (0.09). As found in the technical literature, this value is typically between 0.2 and 0.5.

Results of column (7) reflect the impact force from the eight full-scale, low velocity, controlled impact, barge experiments in which no lashing failure occurred. Results of columns (9) and (11) must be larger than column (7) because they were calculated assuming failure of the lashing. Results from column (11) are lower than the results from column (9) indicating that the corner failure mechanism will dominate if the lashings break.



Table 1-2. Comparison of Results

(1)	(2)	(3)	(4)	(5)	(6)	(7)	(8)	(9)	(10)	(11)	(12)
Experiment Number	Approach Velocity fps	Approach Angle deg	Velocity Normal to the Wall fps	Coefficient of Friction(1) (1)	Linear Momentum kip * sec	Computed (Fw)Max by ETL 1110-2-338 (2) (2)	Field Test (Fw) Max (1) (1)	(Fw)Max Transverse Failure Mechanism kip	(Fw) Max Transverse Failure Mechanism + Emp. Correlation kip	(Fw) Max Corner Failure Mechanism kip	(Fw) Max Corner Mechanism + Emp. Correlation kip
29	2.21	12.63	0.48	0.60	895.48	410	287	838	916	438	516
30	2.35	12.19	0.50	0.48	932.80	421	370	789	870	413	494
31	1.62	10.60	0.30	0.43	559.68	264	236	754	803	394	443
37	1.96	10.29	0.35	0.52	652.96	317	327	776	833	406	463
38	1.84	11.94	0.38	0.57	708.92	328	230	816	878	427	489
39	1.62	14.12	0.39	0.51	727.58	317	272	828	891	433	496
41	2.87	8.76	0.44	0.51	820.86	424	419	754	825	394	465
42	1.84	17.48	0.55	0.09	1,026.07	387	577	716	805	374	463

(1) Table 5.3 in Arroyo, Ebeling, and Barker (2003)

(2) Table 5.4 in Arroyo, Ebeling, and Barker (2003)

Mass without hydrodynamic added mass = 1,865.59 kip\*s<sup>2</sup>/ft

The results from column (11) provide greater (FW)max values than column (7) (as expected) because no breaking of the lashing occurred during the full-scale, low-velocity, controlled impact, barge experiments.

The calculations were repeated, but using a kinetic coefficient of friction between the armored wall and the barge train equal to 0.5 and a kinetic coefficient of friction between barge system one and barge system two equal to 0.25. Table 1.3 lists the results for this case. In all cases, the computed force normal to the wall was greater than the field test results. In these cases, the field test values must be lower than the computed values because no lashing failure occurred during the experiments.

In summary; Figure 1.17 presents the range of applicability of the Limit\_LASHING computer program. For example, the Corner failure mechanism will dominate over the other two Limit\_LASHING limit state mechanisms if the approach angle is below 30 degrees. The green line in Figure 1.17 (below the purple and blue lines) shows this condition. These results were obtained using a kinetic coefficient of friction between steel-steel of 0.5. The lashings properties and configurations were the ones presented in Section 1.2. The Longitudinal failure mechanism is appropriate when the approach angle is greater than 70 degrees because produce non-negative values of FW. The other mechanism predicts negative values of FW, which is impossible because the barge train pushes the wall, and does not pull on the wall.

## **1.2 Engineering Properties of New and Used Lashings**

### **1.2.1 Wire Rope Information**

Wire rope is a length of flexible, multi-wired, stranded machinery made of many precision parts. Generally there exists a core, with several multi-wired strands laid helically around the core. There are two types of cores: fiber and wire cores. The towing industry generally uses wire cores. Figure 1.18 illustrates the basics of wire rope. The direction in which the wires and strands are twisted around the rope gives the wire rope important material characteristics. This is called "lay." Figure 1.19 shows the different types of lay.

Wire rope is generally classified by two groups of numbers. For the first numerical classification, the first integer will define how many strands are laid around the core; the second number defines how many wires are used per strand. For example, 6x19 signifies a type of wire rope with 6 helical strands each consisting of 19 wires. Figure 1.20 shows an example of 6x19 wire rope.

The second important number refers to the diameter. Obviously, the thicker the diameter, the greater load the rope can hold. In general, the more wires per strand, the more flexible the rope, and the lower its resistance to abrasion. Figure 1.21 shows the correct way to measure the diameter of ropes.



Table 1-3. Comparison of Results.

Experiment Number	Assumed Coefficient of Friction	Field Test (FW) Max (1) (kip)	(FW)Max Corner Mechanism + Emp. Correlation (kip)
29	0.50	287	647
30	0.50	370	644
31	0.50	236	596
37	0.50	327	601
38	0.50	230	623
39	0.50	272	650
41	0.50	419	601
42	0.50	577	721

(1) Table 5.3 in Arroyo, Ebeling, and Barker (2003)  
 Mass without hydrodynamic added mass = 1,865.59 kip\*s<sup>2</sup>/ft

Depending on the particular application, two common classifications of wire rope used in the waterways towing industry are 6x25 and 6x37. The 6x25 is more flexible, however has a lower nominal breaking force. Standard practice is that maximum tensions allowed in the lines should not exceed 1/3 of the breaking strength of the rope. While allowing for this safety factor is recommended, one must also take into account wear on the rope over time. Fatigue failure is a failure due to repeated stresses that may be below yield strength. For example, due to repeated friction, a rope going around a sheave will break eventually due to wear. Occasional visual inspection of wire rope is highly recommended to avoid this.

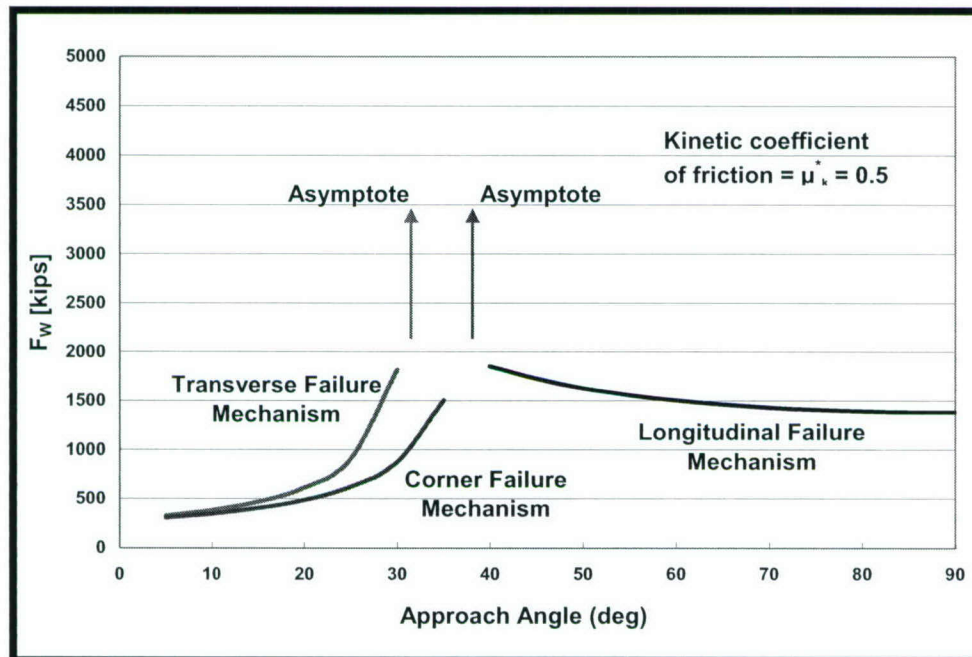


Figure 1-17. Range of Applicability of the Failure Mechanisms

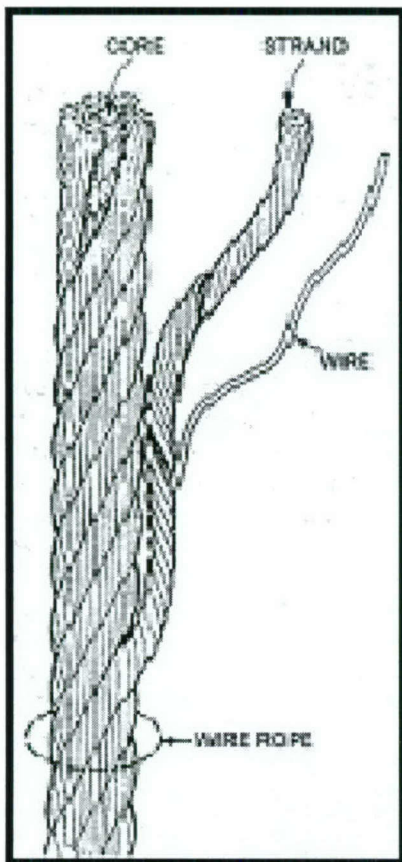


Figure 1-18. Wire Rope Scheme

Lay	Definition	Characteristics
<b>Regular Lay</b> 	Most common lay in which the wires wind in one direction and the strands the opposite direction. (right lay shown)	Less likely to kink and untwist; easier to handle; more crush resistant than lang lay.
<b>Lang Lay</b> 	Wires in strand and strands of rope wind the same direction. (right lay shown)	Increased resistance to abrasion; greater flexibility and fatigue resistance than regular lay; will kink and untwist.
<b>Right Lay</b> 	Strands wound to the right around the core. (regular lay shown)	The most common construction
<b>Left Lay</b> 	Strands wound to the left around the core. (regular lay shown)	Used in a few special situations - cable tool drilling line, for example.
<b>Alternate Lay</b> 	Alternate strands of right regular lay and right lang lay.	Combines the best features of regular and lang lay for boom hoist or winch lines.

Figure 1-19. Common Variations of Lay in Wires



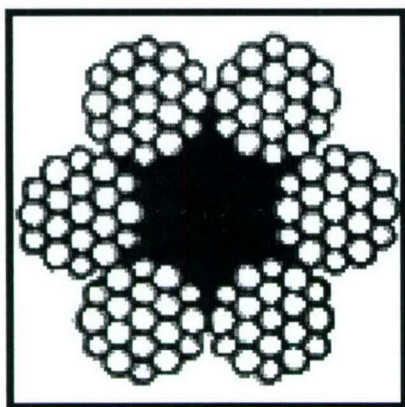


Figure 1-20. 6X19 Wire Rope

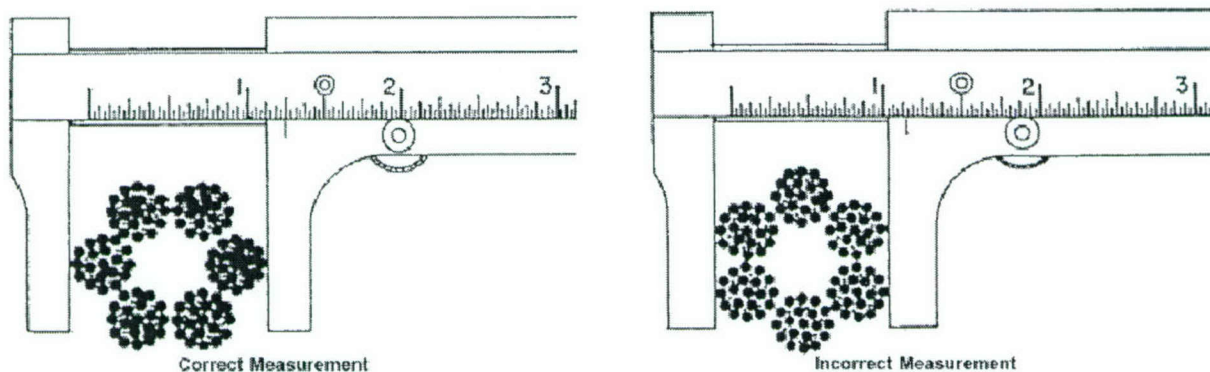


Figure 1-21. How To Measure Ropes.

As required by the ASTM A 1023, the levels of acceptance of wire are:

*Wire before Fabrication*—Wire samples tested before fabrication shall meet the requirements for the size and grade (level) specified by the supplier and as found in the appropriate wire specification.

*Wire after Fabrication*—For each requirement, a maximum of 5 percent of wires tested is permitted to lie outside the values specified, rounded to the nearest whole number of wires. Failure of the same wire to satisfy more than one requirement shall be considered as a single failure.

*Diameter*—The diameter of 5 percent of the wires may exceed, by up to 50 percent, the specified tolerance for the nominal diameter.

*Tensile Strength*—When tested in accordance with the requirements of Specification A 1007, the measured values shall be within the tolerance specified with an additional tolerance of 7000 psi (50 N/mm<sup>2</sup>) below the minimum value. The measured value of wire diameters less than 0.5 mm (0.020 in.) shall be greater than the minimum values specified in the appropriate wire specification.

*Torsion*—When tested in accordance with the requirements of Specification A 1007, the measured values of wires of 0.5 mm (0.020 in.) diameter and greater shall be at least 85 percent of the values specified, rounded down to the next whole number. The measured value of wire diameters less than 0.5 mm (0.020 in.) shall be greater than the minimum values specified.

### 1.2.2 Mechanical Properties of New and Used Lashings

To perform the parametric analyses, one kind of lashing was selected. The one used was the Independent Wire Rope Core (IWRC) 6x19. Two diameters of this wire rope classification were used, that is with a diameter of 22.225 mm (7/8 in.) and 25.40 mm (1 in.). For all cases, the modulus of elasticity was the same and equal to 96519.44 MPa (14,000 ksi). If the case analyzed considers the new wire rope then the breaking strength is 69.2 kip and the rupture strain is 6 percent for a lashing with a diameter of 7/8 in. (cf. Table 1-4).

Table 1-4. Dimensions and Mechanical Properties of Lashing used in the Parametric Analysis.

Wire Rope	Diameter (in.)	New Wire Rope Nominal Breaking Strength, $P_{ult}$ (kip)	E (ksi)	Nominal Area (in. <sup>2</sup> )	New Wire Rope Rupture Strain, Rupture (%)	Used Wire Rope Nominal Breaking Strength, $P_{ult}$ (kip)	Used Wire Rope Rupture Strain, Rupture (%)
6 x 19 With IWRC	7/8	69.2	14 x 10 <sup>3</sup>	0.37	6	55.4	5
	1	89.8		0.48		71.8	

In the case where the new wire rope is considered, the breaking strength is 89.8 kip and the rupture strain is 6 percent for a lashing with a diameter of 1 in. If the case analyzed considers the used wire rope then the breaking strength is 55.4 kip and the rupture strain is 5 percent for a lashing with a diameter of 7/8 in. Finally, when a used wire rope is considered, a breaking strength of 71.8 kip and the rupture strain of 5 percent is adopted for a lashing with a diameter of 1 in.

## 1.3 Report Contents

Chapter one presents an introduction to the parametric analysis performed in this research project. Previous works developed in recent research are also described. A description of the basic input data required by the computer program Limit\_LASHING is also presented. One of the most important aspects in the parametric analysis is the mechanical properties of the lashing. These properties are described in this chapter. The results produced by Limit\_LASHING were compared and discussed against the results obtained from other technical approaches.

Chapter two presents the discussion of what failure mechanism controls the results of the glancing blow impact. A numerical example is presented to show and support the selection of the Limit\_LASHING failure mechanism that controls the glancing blow



impact process. This Chapter presents the results of 4,320 analyses of glancing blow impact forces. The variables used in the parametric study of this Chapter are:

1. Approach angle: Glancing Blows – 2, 5, 8, 10, 12, 15, 18, 20, 25, 30 degrees
2. Size of barge train system: (rows x columns) 3x5, 3x3, 2x2, 3x2, 3x4, and 2x3
3. Approach velocity: 1 – 6 fps
4. Mass per barge = 1,865.59 kip-sec<sup>2</sup>/ft and mass of towboat = 34.20 kip-sec<sup>2</sup>/ft
5. Lashing Layout:
  - a. Lashing layout used during the experiments 1998 (base line)
  - b. Increase number of wraps of the base line by one
  - c. Decrease number of wraps of the base line by one
6. Size of lashing: (values specified as in Section 1.2)
  - a. Lashing diameter (i.e., 7/8 in. and 1 in.)
  - b. Rupture strain (new wire, used wire)
  - c. Ultimate load (new wire, used wire).

Chapter three presents the discussion of what failure mechanism controls the results of the head-on impact. A numerical example is presented to show and support the selection of the Limit\_LASHING failure mechanism that controls the head-on impact event. This Chapter presents the results of 288 analyses of head-on impact events. The variables used in the parametric study of this Chapter are the following:

1. Approach angle: Head-on – 90 degrees
2. Size of barge train system: (rows x columns) 3x5, 3x3, 3x2, and 3x4
3. Approach velocity: 1 – 6 fps
4. Mass per barge = 1,865.59 kip-sec<sup>2</sup>/ft and mass of towboat = 34.20 kip- sec<sup>2</sup>/ft
5. Lashing Layout:
  - a. Lashing layout used during the experiments 1998 (base line)
  - b. Increase number of wraps of the base line by one
  - c. Decrease number of wraps of the base line by one
6. Size of lashing: (values specified as in Section 1.2)
  - a. Lashing diameter (i.e., 7/8 in. and 1 in.)
  - b. Rupture strain (New wire, used wire)
  - c. Ultimate load (New wire, used wire)

Chapter four presents the conclusions regarding these parametric analyses. Appendix A shows the standard lashing layout configuration used during the 1998 Experiment.

## 2 Glancing Blow Impact Forces

---

### 2.1 Introduction

A barge train system consists of a group of nearly rigid barges joined together with steel cables, referred to as lashings. These lashings define a barge train system where the weak zones are assumed to occur at each barge connection. The motion of each barge relative to the other is how the system distributes the impact forces among the barges during the impact process. As has been observed during barge train impact events at shallow approach angles (i.e., “glancing” blows, cf. Figure 2.1), the impact event can produce a failure of the lashings in an “opening wedge” fashion along a transverse plane between barges. The lashings develop tensile strains across the wedge-opening transverse plane as this opening develops. The barges rotate a small amount in such a way that the force normal to the wall is transferred to the connections between the barges. This transverse failure mechanism occurs in the local barge “y” axis along the first transverse line of lashing connections behind the row of barges that form the bow to the barge train. This type of failure has a significant contribution from the rotation of the first column of three barges that form the bow.

Figure 2.2 depicts the barge train impacting a rigid wall and the development of a failure plane along the transverse axis of the barge train system. Two systems of barges are identified in this figure. The system that is in a direct contact to the wall is referred to as System one and the remaining barges form System two. System one rotates with a pivot assumed at the first connection from the bow on the starboard side. All the lashings across this potential failure plane will elongate, resulting in an increase in the internal lashing forces. The lashings on the port side of this transverse plane will be the most stressed and will be the first to fail. The idealized failure mechanism assumes the internal connections will rupture in sequence towards the pivot point as System one continues the rotation. In this failure mechanism both systems of barges are assumed to be rigid and no longitudinal relative motion is assumed. As mention in Arroyo and Ebeling (2004), this is an idealization; however this simple model attempts to capture a failure mechanism whereby most of the energy comes from the rotational degree(s) of freedom.

This Transverse failure mechanism model allows for the rotation of the first column of barges (Figure 2.2). In this way, all the lashings along the transverse failure plane will break by means of the rotation between barges of System one and System two. In this



model, different linear accelerations (in actuality, decelerations) in the global “Y” direction for System one and System two were assumed. It is reasoned that, when System one stops its forward global “Y” motion with its impact with a rigid wall, barge System one will decelerate at a more rapid rate than System two. Consequently, it is envisioned for this simplified model that the deceleration of System two will be far different and at a lower deceleration rate than occurs for System one. A zero linear global acceleration in the “Y” direction of System one is assumed in this simplified model because the impact with a *rigid* wall occurs with this system in the global “Y” direction. System two motions continue and the lashings that connect System one to System two will try to rotate System two toward the wall. Thus, the deceleration of System two in the global “Y” direction is nonzero. The Transverse failure mechanism does not allow for the relative displacement between barges that form System one nor in System two in the local “x” direction. In this manner, all lashings located in the Figure 2.3 shaded zone break by means of the transverse mechanism with no contribution made by the longitudinal relative displacement between barges.

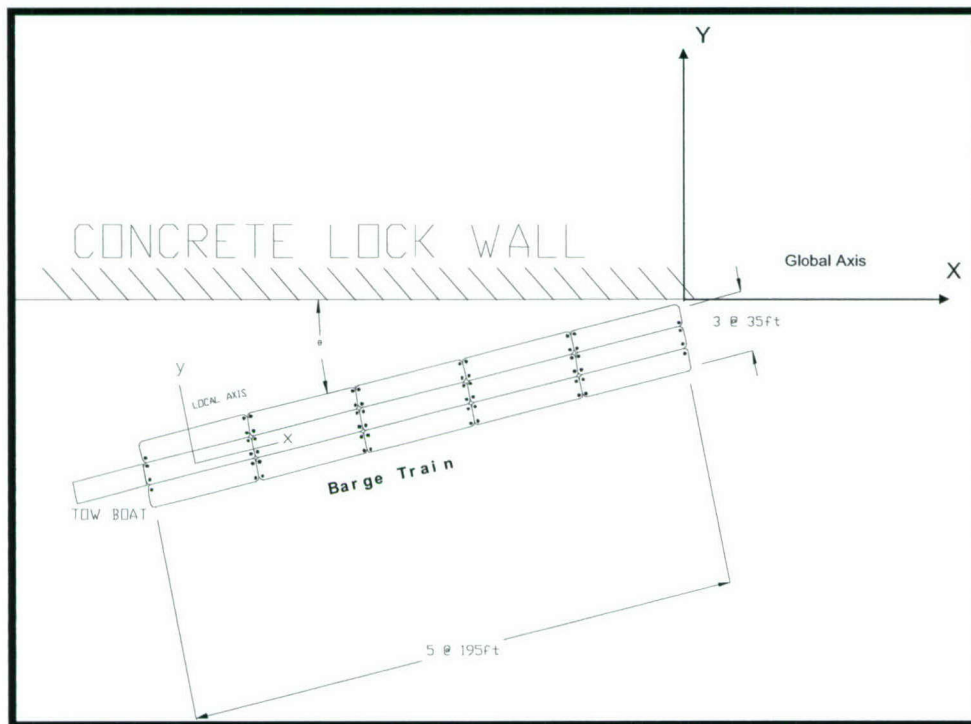


Figure 2-1. Glancing Blow Barge Train Impact

As mentioned above, a barge train system consists of a group of nearly rigid barges joined together with steel cables, referred to as lashings. These lashings define a barge train system where the weak zones are assumed to occur at each barge connection. The motion, including rotation, of each barge relative to the other is how the system distributes the impact forces among the barges during the impact process. As has been observed during barge train impacts events at shallow approach angles (i.e., “glancing” blows), the impact event can produce a failure of the lashings in an “opening wedge” fashion along a transverse plane between barges. (The lashings develop tensile strains across the

wedge-opening transverse plane as this opening develops.) The barges move and rotate a small amount in such a way that the force normal to the wall is transferred to the connections between the barges. In Arroyo and Ebeling (2004), this potential failure mechanism was designated as the Transverse Failure Mechanism. However, the actual failure process may not be as simple as the simple transverse “wedge opening” fashion. A local rotation of the corner barge (barge one) is likely to occur (Figure 2.4).

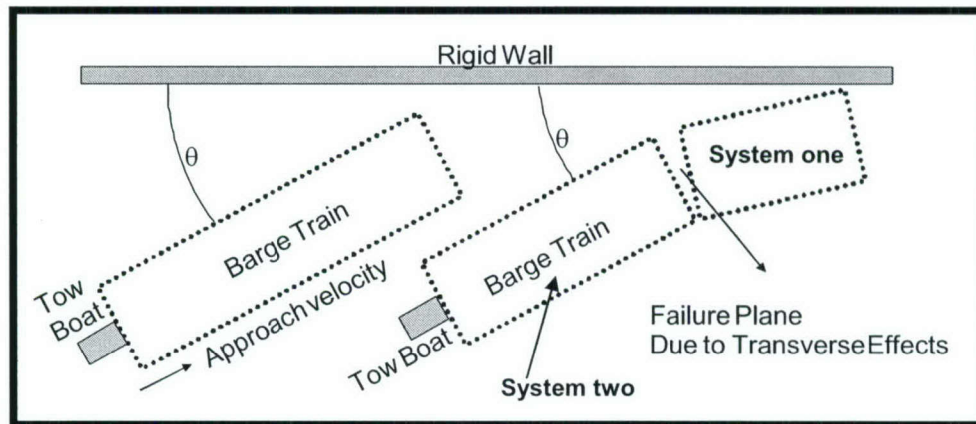


Figure 2-2. Transverse Failure Mechanism

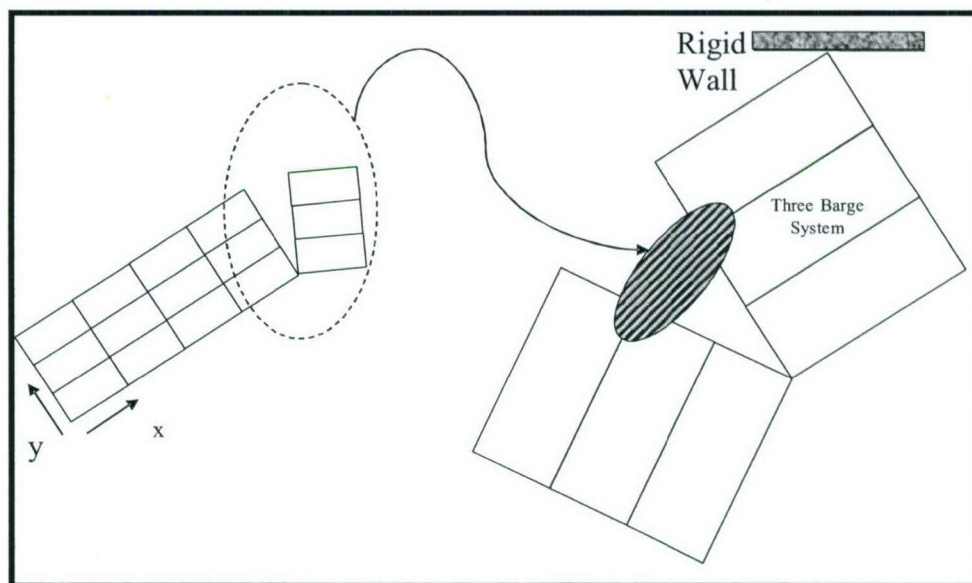


Figure 2-3. No Relative Displacement Allowed in the Local “x” Axis in the Three Barge System

A second pivot point is generated after the first pivot point is developed in the star-board side of the barge train. This second pivot point is located at the corner barge at the bow opposite to the impact point.

This “corner barge” failure mechanism is believed to be a more realistic model than the Transverse failure mechanism alone. In the Transverse failure mechanism, the three barge system in contact with the wall was considered as a (single) rigid body; no local rotation was allowed to occur, as shown in Figure 2.5. In the Corner failure mechanism,



local rotation of the corner barge is allowed. Thus, the lashings in the shaded zone will break by means of the transverse shearing mechanisms and the local rotation of barge one as depicted in Figure 2.6.

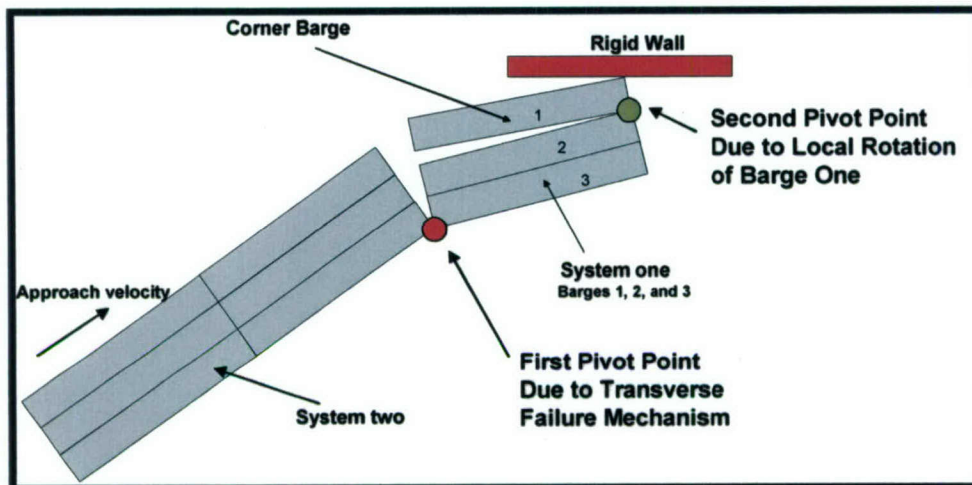


Figure 2-4. Scheme of Corner Failure Mechanism

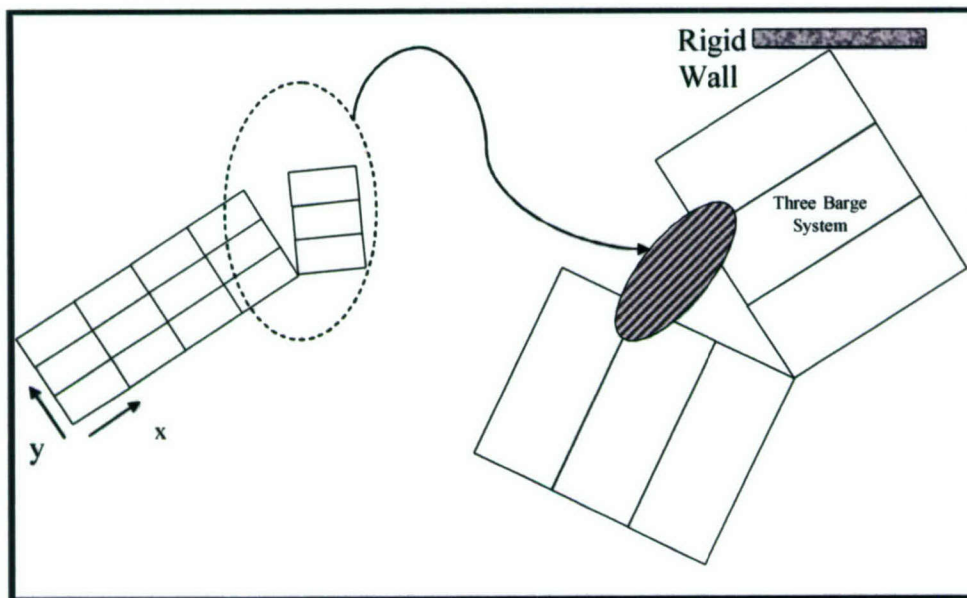


Figure 2-5. No Local Rotation of Corner Barge is Allowed in the Transverse Failure Mechanism

In the Corner failure mechanism, one additional typical lashing configuration must be included when compared against the lashing configurations used in the Transverse failure mechanism. The following section provides typical lashing layouts used during the 1998 full-scale experiments (see Patev, Barker, and Koestler [2003], or Arroyo, Ebeling, and Barker [2003]). From these typical lashing configurations, three layouts (Figure 2.7) must exist at ultimate load condition for the Corner failure mechanism to occur. The lashings that go across the “L” failure plane are the lashings that have to fail to produce the rotation toward the wall of the corner barge alone. The corner barge, defined as the one that is in contact with the wall during the impact (upper right barge in Figure 2.4), has to lose contact with the rest of the system for the Corner failure mechanism to occur.

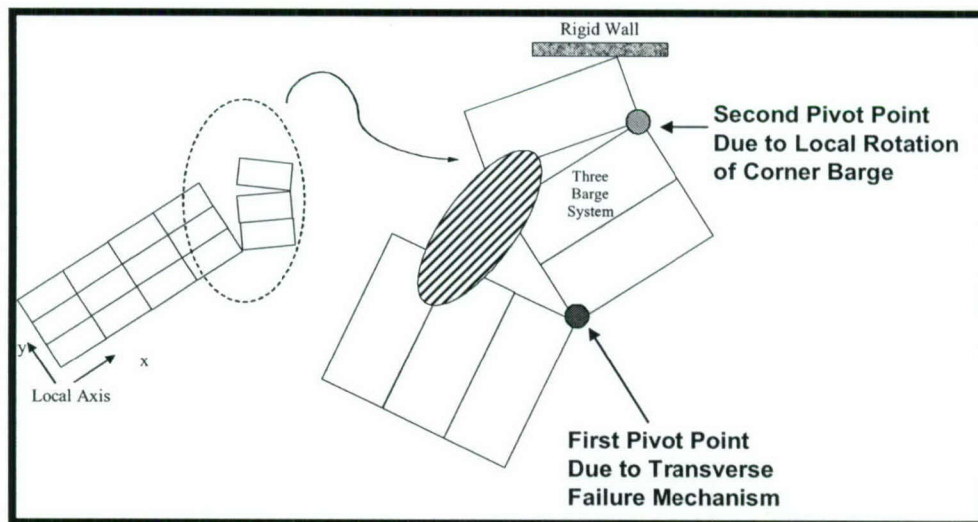


Figure 2-6. Local Rotation of Corner Barge is Allow, Two Pivot Points Development – Corner Failure Mechanism

If the lashings presented in Figure 2.7 break, then the contact between the corner barge and the rest of the barge train system will be lost. This simplified failure mechanism produces a rotation of the corner barge alone towards the wall because the lashings fails and the connection with all other barges are lost. *Note that the only difference between this failure mechanism and the Transverse failure mechanism is that the lashing layout presented in Figure 2.7.d must be included in this analysis.* The Transverse failure mechanism must break the lashing configurations shown in Figure 2.7.a, 2.7.b, and 2.7.c.

The lashings involved with the Corner failure mechanism must also include the lashings along the Transverse planes between the three front barges (i.e., a local, Transverse failure mechanism, plus the lashings that restrain the relative rotation of System one relative to System two). The incremental analysis stop after the lashing configurations presented in Figure 2.7 reaches ultimate strain.

For the Corner failure mechanism, the lashings in System one (see Figure 2.4) located at the bow (i.e., the lashings at the bow that joins the corners of barge 1 to barge 2) are not included in the calculation of the lashing forces because, if barge 1 tries to rotate, then the rotation will be around the connection at the bow. If the Corner failure mechanism occurs, the corner barge (barge 1) is assumed to rotate with a “pivot” point at the bow at the connection of barge one and two. In this manner, the corner barge rotates towards the wall as soon as all lashings joining it to the rest of the barge train fails. This process does not include the lashings that join barges of System one at the bow.

To numerically demonstrate that the corner failure mechanism controls over the transverse failure mechanism, an example is presented. Consider a three by five barge train joined using the lashing configuration used in Experiments 1998, as shown in Appendix A. This example assumes a 6x19 wire rope with independent wire rope core (IWRC) with a diameter of 7/8 in., and a modulus of elasticity for the lashings of 14,000 ksi. If the lashing is assumed to be new, then it has a nominal breaking strength of 69.2 kip and a rupture strain of 6 percent. The approach angle is assumed to be 10 degrees and an approach velocity in the local “x” axis is assumed equal to 1.5 fps. The total mass of the



barge train system is  $1899.75 \text{ kip} \cdot \text{s}^2/\text{ft}$  and the kinetic coefficient of friction between the barges and between the barge train and the rigid armored wall equal to 0.2, respectively. Using these values as the input data, Limit\_LASHING gives the following results.

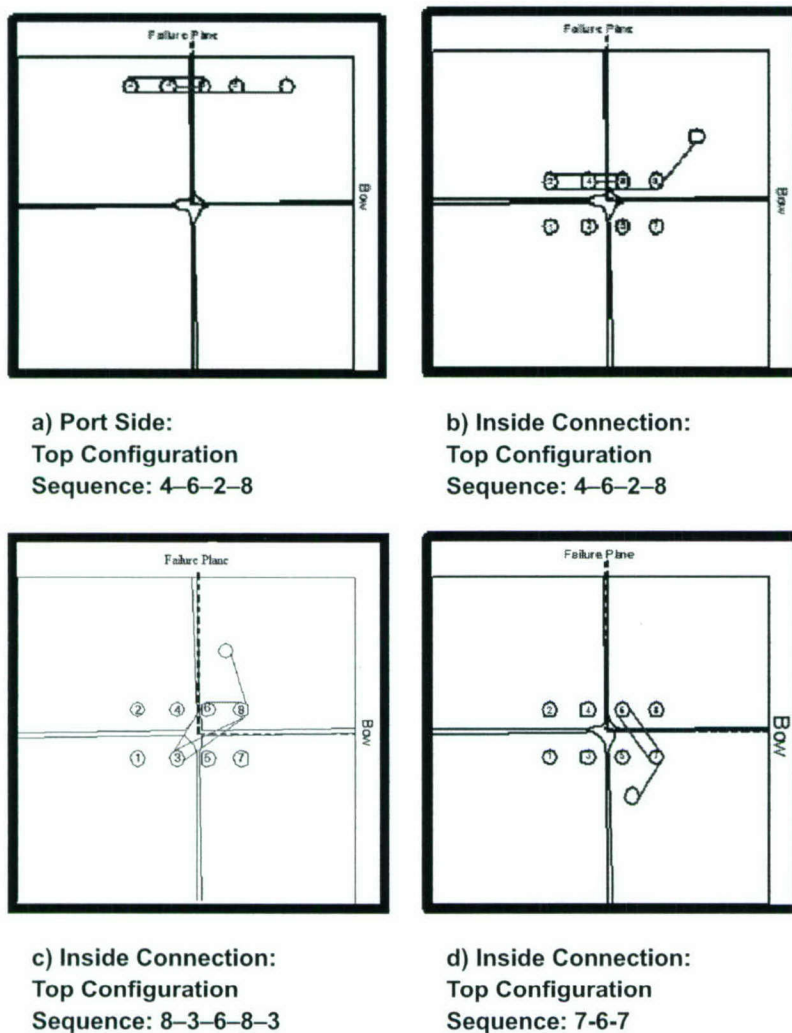


Figure 2-7. Effective Lashing Configurations in the Corner Failure Mechanism

The data listed in Table 2.1 show that the total force computed normal to the wall is greater for the Transverse failure mechanism than for the Corner failure mechanism. This is a general trend that depends on the number of lashings used in the configuration (as shown in Figure 2.7.d), and on the mechanical properties of these lashings. As fewer, more flexible lashings are used, the possibility of the Corner failure mechanism increases, and vice versa. For example, suppose that no lashing is used for the configuration of Figure 2.7.d, and then the Corner failure mechanism will dominate as soon as the other three configurations shown in Figure 2.7 break. Note that, to complete the Transverse failure mechanism, several additional lashings have to fail after the configurations presented in Figure 2.7 fails. For this reason, in general, the Corner failure mechanism is more likely to occur than the Transverse failure mechanism.

Finally, subsequent sections present the results of the parametric study performed to a series of typical barge train configurations. Among the configurations used are the 2x2, 2x3, 3x2, 3x3, 3x4, and 3x5 barge train. The first number means the number of barges in the local “y” axis and the second number identifies the amount of barges in the local “x” axis. That is, a 3x5 barge train consists of three rows of barges and five columns of barges. Figure 2.8 shows the barge train configuration used in the parametric analysis.

## 2.2 Standard Lashing Layout

In the parametric study, three lashing layouts were used. The principal layout was the one used in the full-scale experiments performed in 1998 and reported in Patev, Barker and Koestler (2003), and Arroyo and Ebeling (2004). Figures 2.9 through 2.12 show these lashing configurations. These configurations were taken as the baseline for the parametric study.

Configuration one (Figure 2.9) was the arrangement used in the 1998 full-scale experiments to join a pair of barges along the outside edge of the barge train. It is also the configuration used on the bow, port, aft, and starboard sides. It consists of three turns of the bits along the edge of the two joined barges. The generic sequence of the bits connected is also shown in Figure 2.9. The name “generic sequence” means that the assigned numbers can change in each model configuration. However, the lashing configuration must follow the sequence shown in Figure 2.9.

At the center joints where four barges come together, three configuration levels were available. In the 1998 experiments there were eight of these connections because 15 barges were joined together. Figures 2.9 through 2.12 show the top, middle, and bottom configurations. The bottom layer, designated configuration two, is similar to configuration one. We consider this configuration as a separate configuration because it is associated to the center connections between barges. The middle configuration at the inner connections, designated configuration three, is like a “scissor” passing each lashing over the edge of the joined barges three times. Finally, configuration four, or the top layer in the inner connection, has two turns for each lashing over the edge of the joined barges. Note that the configurations shown in these figures are not the only configurations available for use in Limit\_LASHING computer program.

To determine the angle that each force (within the lashing) makes with the local axis of the system, the coordinates of each bit on the barges are specified by the user. Using these coordinates, Limit\_LASHING calculates the necessary angles to determine the components of the internal force for the lashings in the local axis. It is important to note that these arrangements are prepared for both a forward and backward motion of the lashings.

Two additional lashing configurations were used to describe the barge train impact process. The lashing properties and configurations are the most important parameter in the limit states based on the lashing ultimate strength. One additional wrap and one less wrap for each lashing of the baseline layout used for the 1998 experiments are the two additional layouts used on the parametric study. These two conditions cover the cases



where the barge train is well connected and weakly connected. In the next subsections, the data used for the parametric study and the results obtained are described.

Table 2-1. Results of Example of Corner and Transverse Failure Mechanisms

Failure Mechanism	F <sub>w</sub> (kip)		
	Limit_Lashing	Empirical Correlation	Total
Corner	525.37	43.1	568.47
Transverse	579.04	43.1	622.14

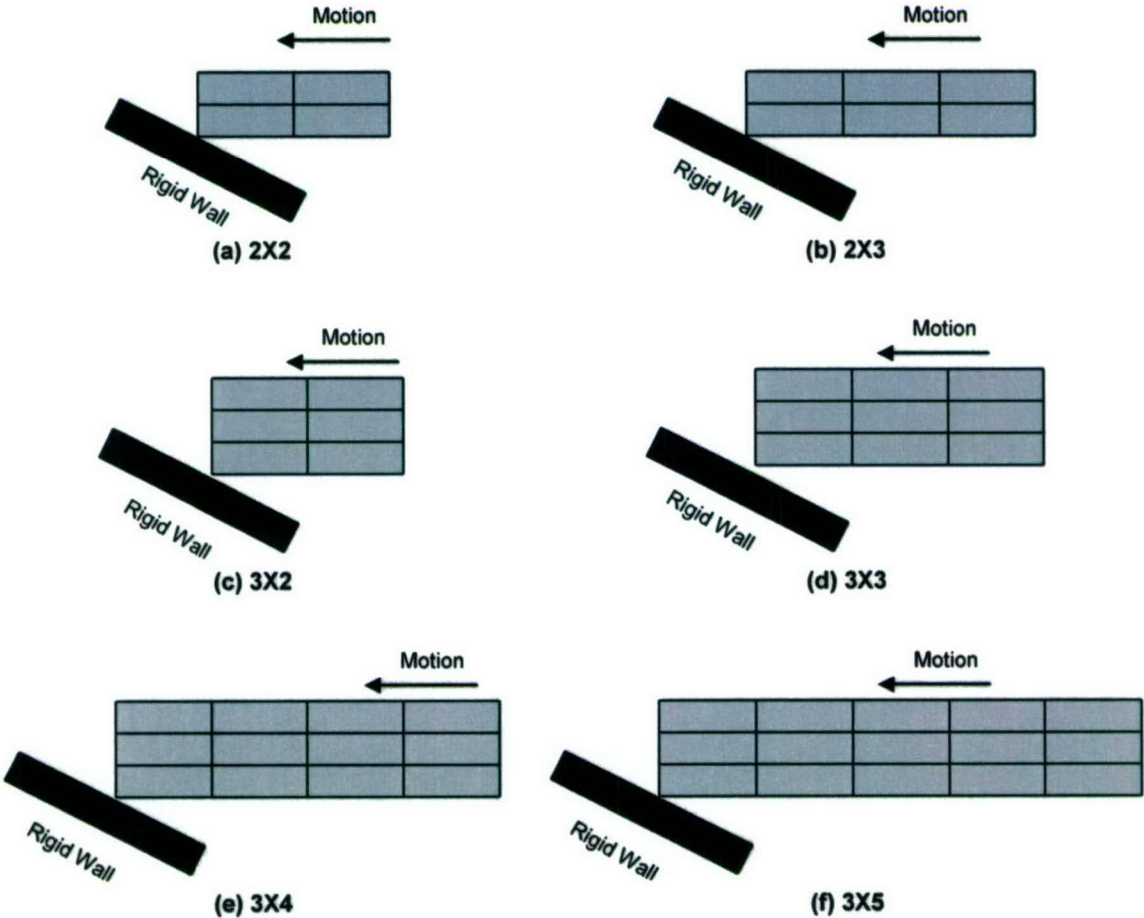


Figure 2-8. Barge Train Configuration Used in the Parametric Study

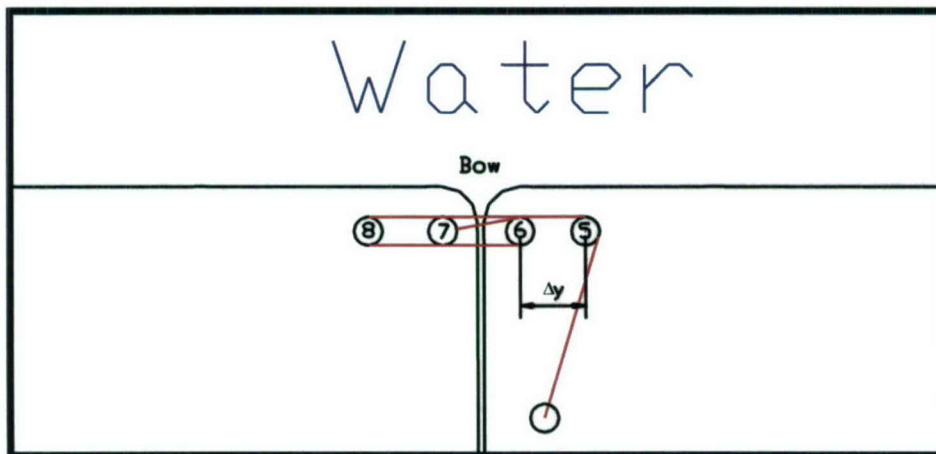


Figure 2-9. Configuration 1 Located at Bow, Port, Aft, and Starboard Sides: Generic Sequence - 7,6,8,5

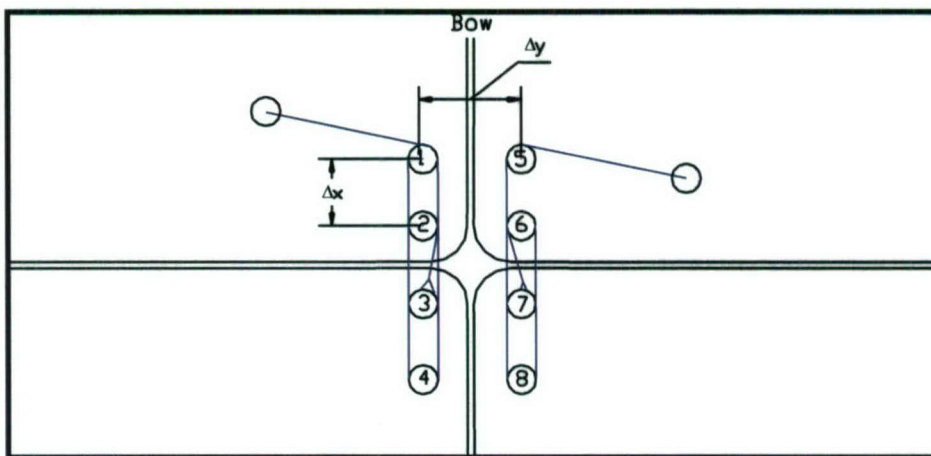


Figure 2-10. Configuration 2 Located at the Bottom Layer in the Inside Connection: Generic Sequence - 7, 6, 8, 5 and 3, 2, 4, 1

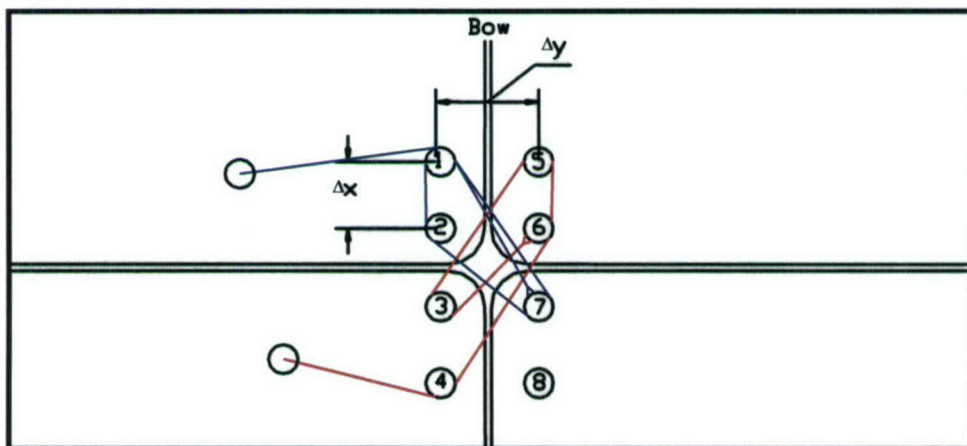


Figure 2-11. Configuration 3 Located at the Middle Layer in the Inside Connection: Generic Sequence - 6, 3, 5, 6, 4 and 7, 1, 2, 7, 1



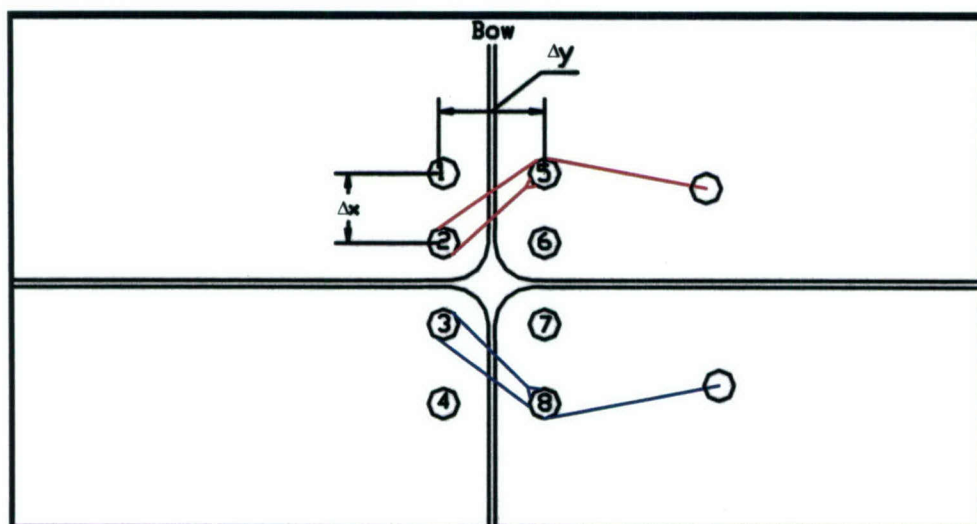


Figure 2-12. Configuration 4 Located at the Top Layer in the Inside Connection: Generic Sequence – 5, 2, 5 and 8, 3, 8

## 2.3 Parametric Study

This section presents the variation of the force normal to the wall during the impact event. The parametric study was done by modifying the following parameters: (1) approach angle, (2) approach velocity, (3) wire rope diameter, (4) wire rope nominal breaking strength, (5) wire rope rupture strain, (6) size of barge train, and (7) lashing layouts. Each one of these variables will be discussed next.

The approach angle is the angle that makes the longitudinal axis of the barge train with respect to the longitudinal axis of the rigid wall (Figure 2.1). During the impact process, the approach angle is assumed as a constant value. The values of the approach angle used for the parametric study for the “glancing blow” events are 2, 5, 8, 10, 12, 15, 18, 20, 25, and 30 degrees.

The approach velocity is the velocity of the barge train system measured in the (local barge) longitudinal axis of the barge train system. There are two kinds of approach velocity that can be given to Limit\_LASHING computer program. That is, the approach velocity of the barge train system in each local “x” and “y” axes. In the parametric study, the approach velocity refers to the velocity in the local “x” axis of the barge train. The velocity in the local “y” axis is assumed to be zero for all the cases in the parametric study. The approach velocity in the local “x” axis used for the parametric study for the “glancing blow events are 1, 2, 3, 4, 5, and 6 feet per second (fps).

One kind of wire rope (lashings) was used in the parametric study. This is the 6x19 Independent Wire Rope Cores (6x19 IWRC). The parametric study considers two diameters, 7/8 in. and 1 in. These are the two most used dimensions in the towing industry. It is important to mention that the nominal areas for each of these lashings are 0.37 sq in. and 0.48 sq in. for lashings with diameters of 7/8 in. and 1 in. respectively. The Young’s modulus of elasticity for this kind of wire rope is estimated to be 14,000 ksi.

The breaking strength of this lashing is another important parameter in the parametric analysis. The breaking strength is estimated based on the condition of the lashing. If the wire rope is new, the breaking strength is estimated to be 69.2 kip and 89.8 kip for the 7/8-in.- and 1-in.-diameter lashing, respectively. However, if the lashing is assumed to be used, the breaking strength is lower. In the parametric study, the breaking strength for the used wire rope was estimated as 55.4 kip and 71.8 kip for the lashings with diameters of 7/8 in. and 1 in., respectively.

The rupture strain is a property of the wire rope that is related to the nominal breaking strength. This is the maximum strain the lashing can reach before the lashing breaks. Also, the condition of the wire rope affects the value of this property. For a new wire rope and a used wire rope, the rupture strain is estimated to be 6 percent and 5 percent, respectively.

Figures 2.7 through 2.12 show the barge train and the lashing layout discussed in the previous section. Table 2.2 lists the mechanical properties of the wire rope used in the parametric study.

Table 2-2. Mechanical Properties of Wire Rope Used in the Parametric Study

Wire Rope	Diameter (in.)	New Wire Rope Nominal Breaking Strength, $P_{ult}$ (kip)	E (ksi)	Nominal Area (sq in.)	New Wire Rope Rupture Strain, $\epsilon_{Rupture}$ (%)	Used Wire Rope Nominal Breaking Strength, $P_{ult}$ (kip)	Used Wire Rope Rupture Strain, $\epsilon_{Rupture}$ (%)
6 x 19 with IWRC	7/8	69.2	14 x 10 <sup>3</sup>	0.37	6	55.4	5
	1	89.8		0.48		71.8	

### 2.3.1 Limiting Impact Forces Computed for 7/8-in. Diameter New Wire Rope

The results of the limiting impact forces computed for the 7/8-in. diameter new wire rope are presented next. Table 2.3 lists the parameters used in the analyses.

Figures 2.13 through 2.18 present the variation of the maximum force normal to the wall for barge train systems 2x2, 2x3, 3x2, 3x3, 3x4, and 3x5, respectively. Additional input data are the mass of the barge train, mass of the towboat, and the lashing initial load. Each figure shows the values used in this set of calculations.

### 2.3.2 Limiting Impact Forces Computed for 7/8-in. Diameter Used Wire Rope

The results of the limiting impact forces computed for the 7/8-in. diameter used wire rope are presented next. Table 2.4 lists the parameters used.

Figures 2.19 through 2.24 present the variation of the maximum force normal to the wall for barge train systems 2x2, 2x3, 3x2, 3x3, 3x4, and 3x5, respectively. Additional



input data are the mass of the barge train, mass of the towboat, and the lashing initial load. Each figure shows the values used in this set of calculations.

### 2.3.3 Limiting Impact Forces Computed for 1-in. Diameter New Wire Rope

The results of the limiting impact forces computed for the 1-in. diameter new wire rope are presented next. Table 2.5 lists the parameters used.

Table 2-3. Mechanical Properties of Lashing – Case A

Lashing Layouts	As in the Experiments	
Lashing Diameter	7/8	in.
Breaking Strength	69.2	kip
Nominal Area	0.37	sq in.
Rupture Strain	6	%

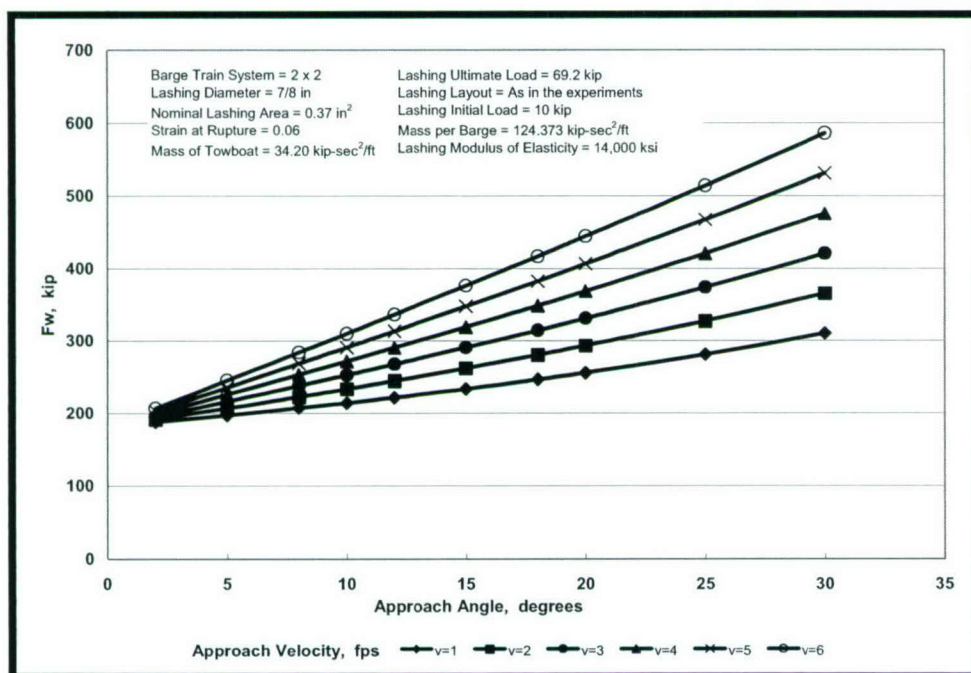


Figure 2-13. Maximum  $F_w$  for a 2x2 Barge Train System – Case A

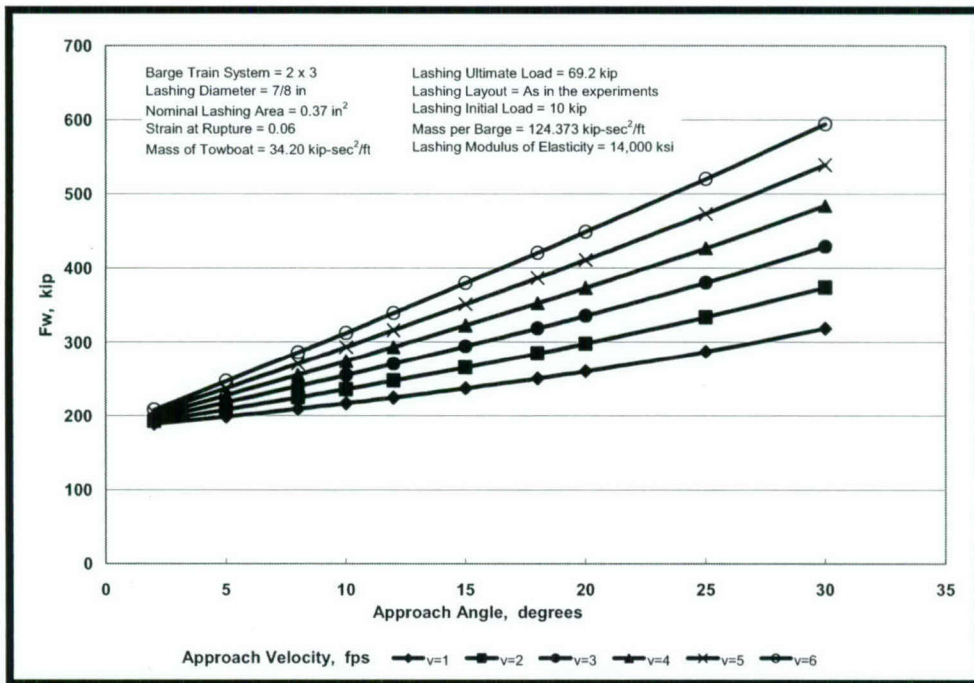


Figure 2-14. Maximum  $F_w$  for a 2x3 Barge Train System – Case A

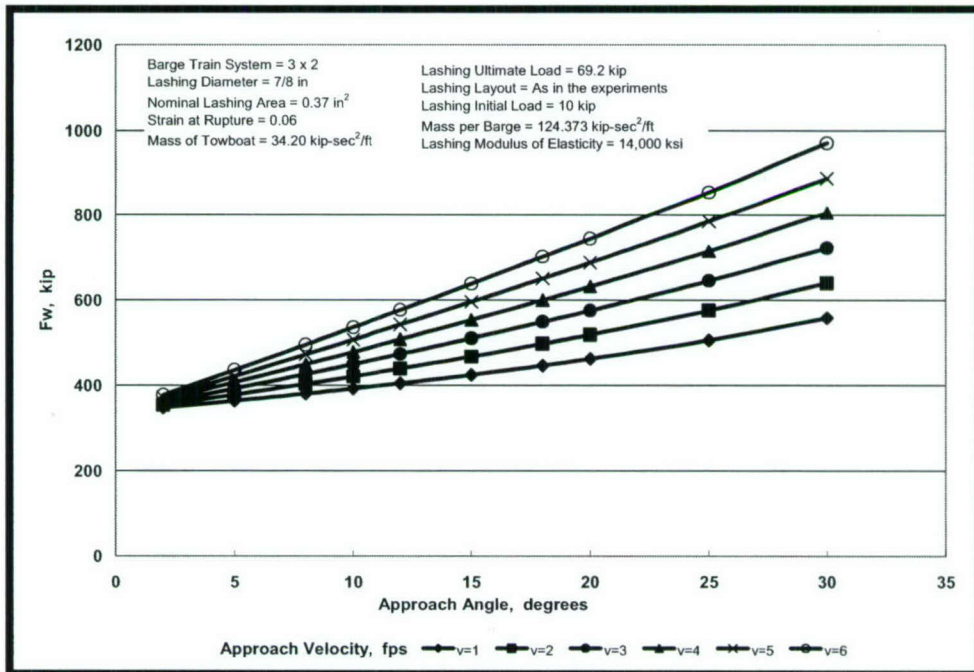


Figure 2-15. Maximum  $F_w$  for a 3x2 Barge Train System – Case A



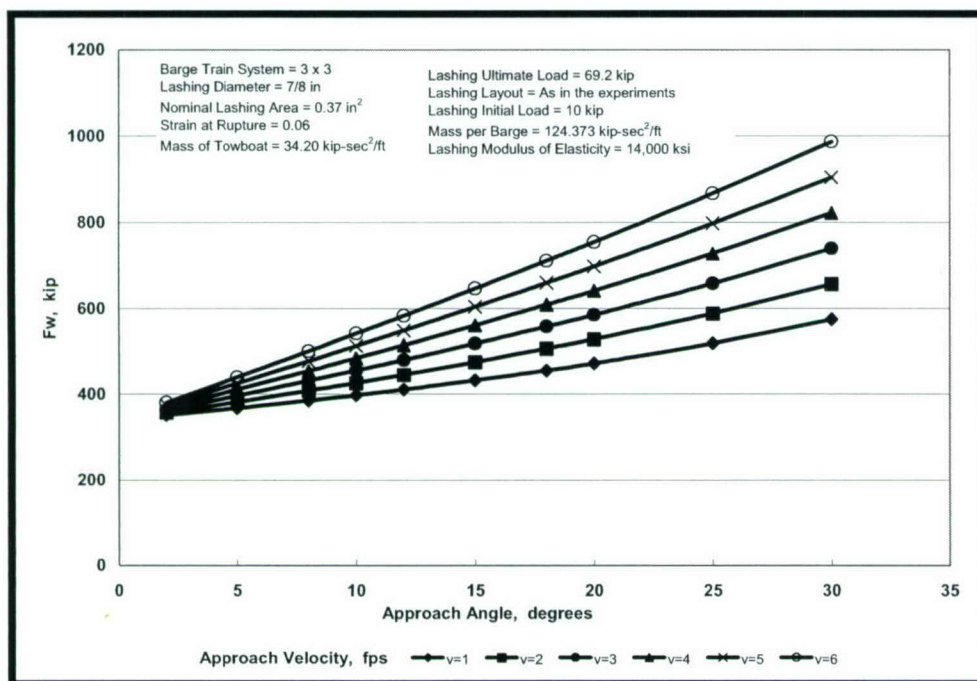


Figure 2-16. Maximum  $F_w$  for a 3x3 Barge Train System – Case A

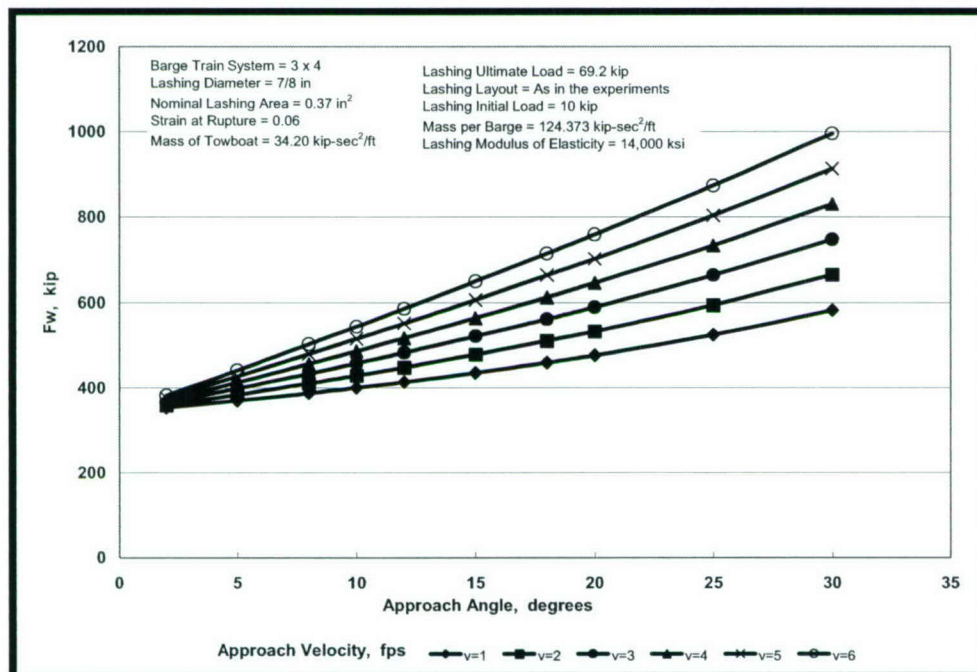


Figure 2-17. Maximum  $F_w$  for a 3x4 Barge Train System – Case A

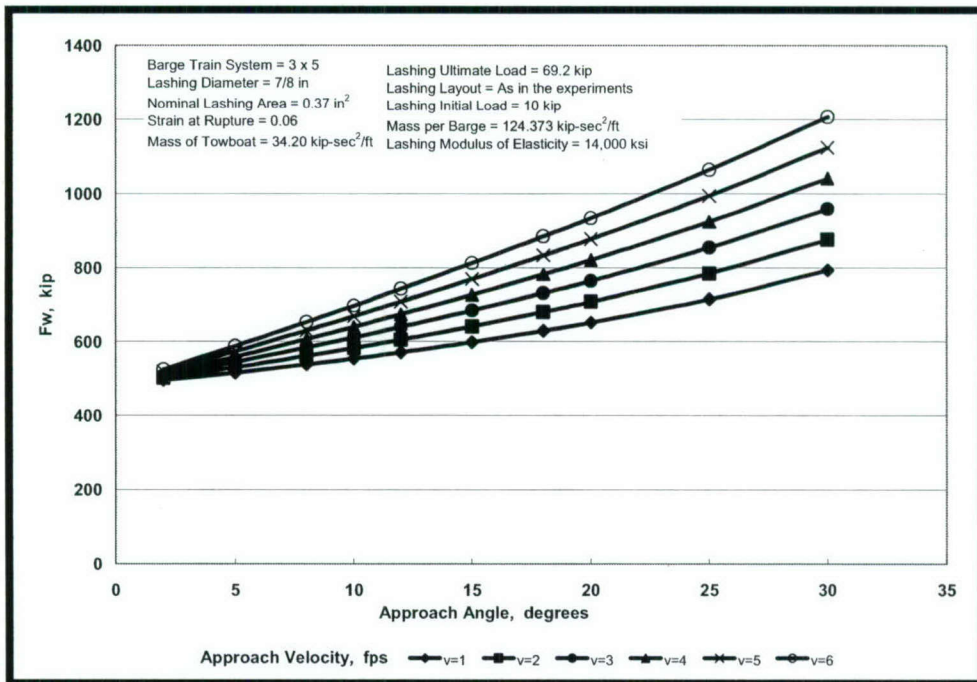


Figure 2-18. Maximum  $F_w$  for a 3x5 Barge Train System – Case A

Table 2-4. Mechanical Properties of Lashing – Case B.

Lashing Layouts	As in the Experiments	
Lashing Diameter	7/8	in.
Breaking Strength	55.4	kip
Nominal Area	0.37	sq in.
Rupture Strain	5	%



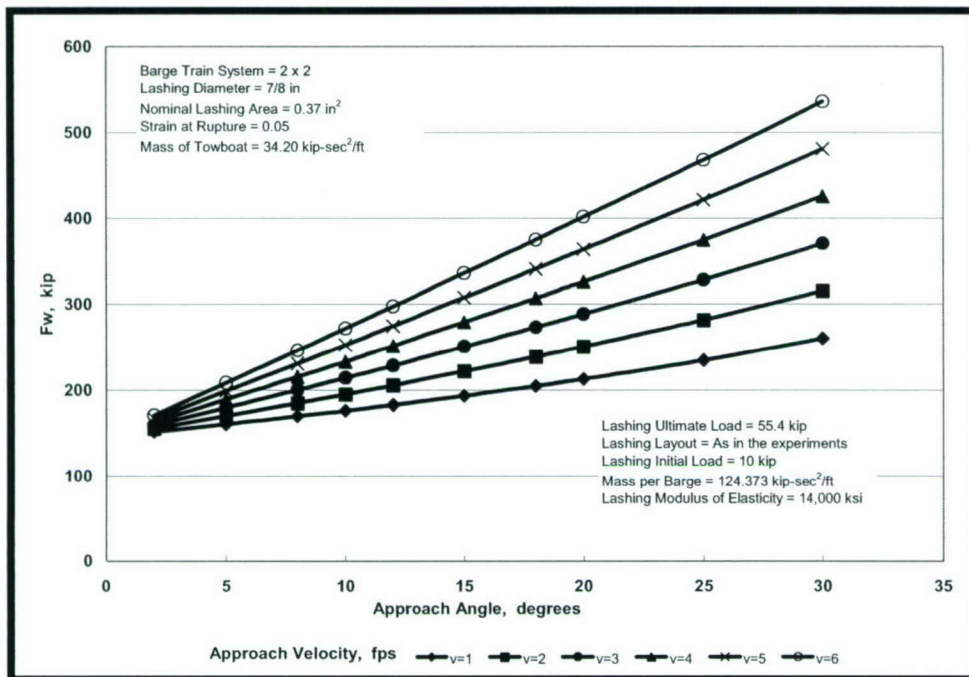


Figure 2-19. Maximum  $F_w$  for a 2x2 Barge Train System – Case B

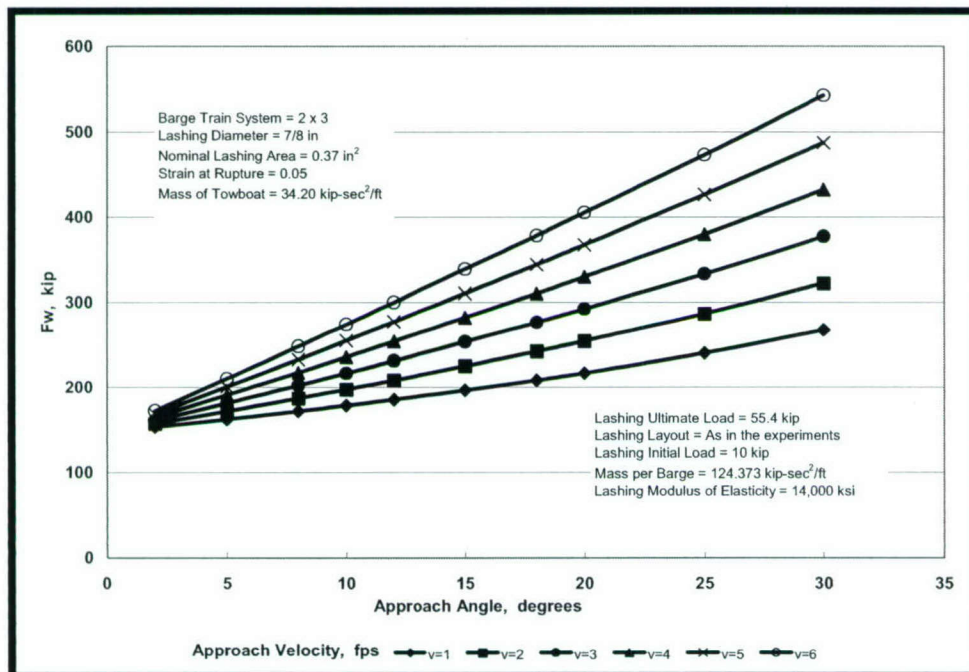


Figure 2-20. Maximum  $F_w$  for a 2x3 Barge Train System – Case B

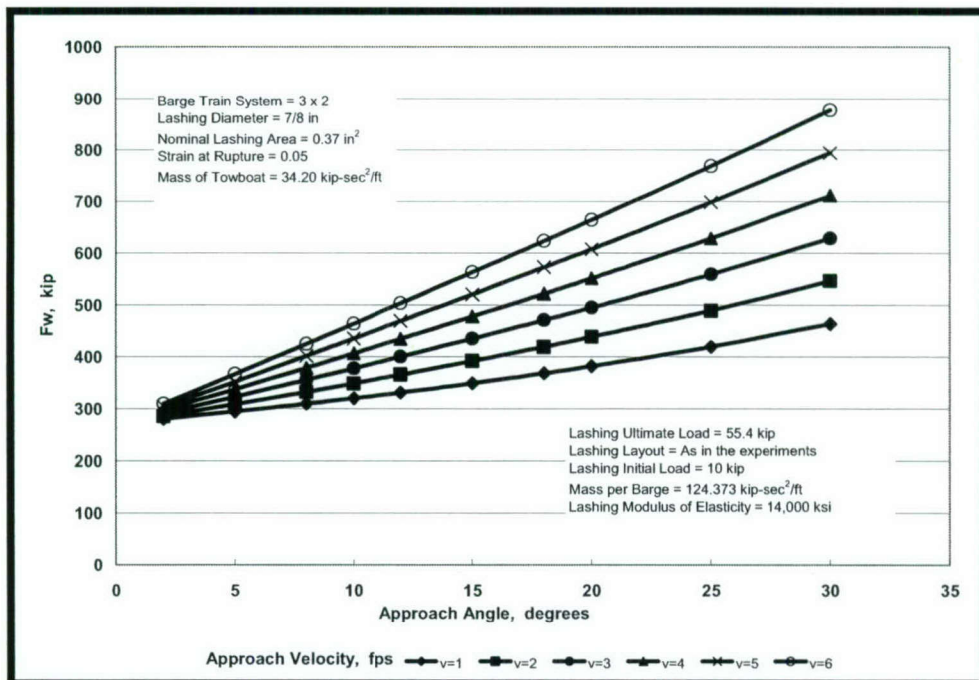


Figure 2-21. Maximum  $F_w$  for a 3x2 Barge Train System – Case B

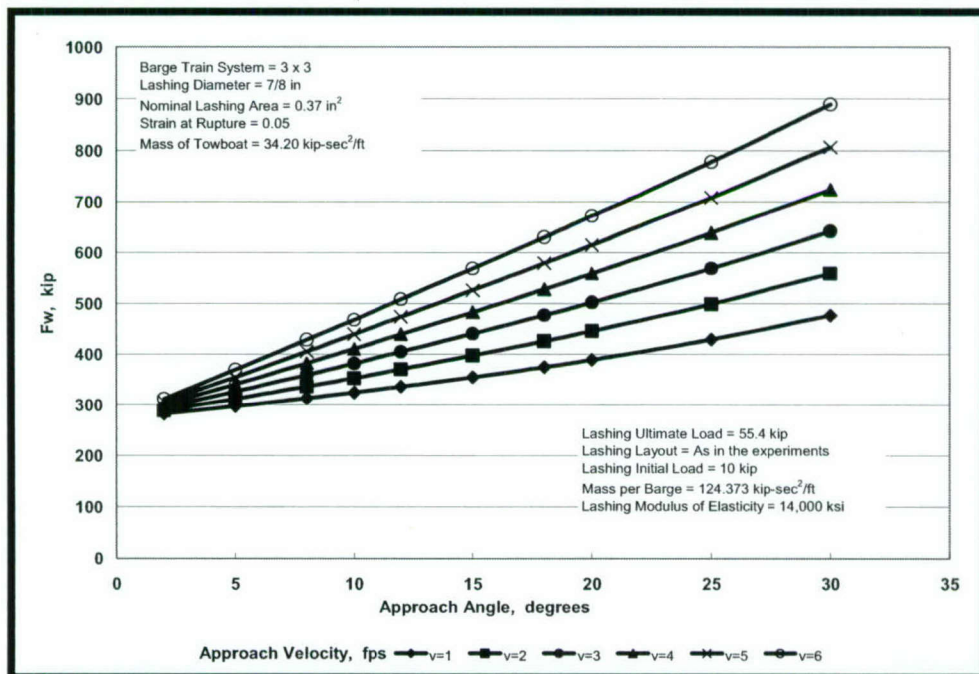


Figure 2-22. Maximum  $F_w$  for a 3x3 Barge Train System – Case B



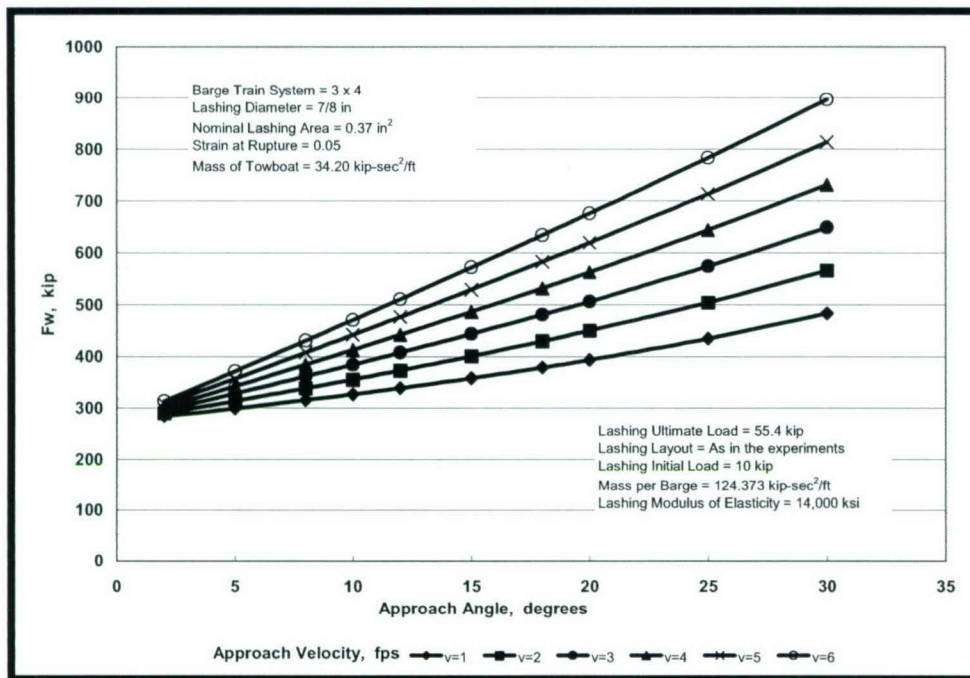


Figure 2-23. Maximum  $F_w$  for a 3x4 Barge Train System – Case B

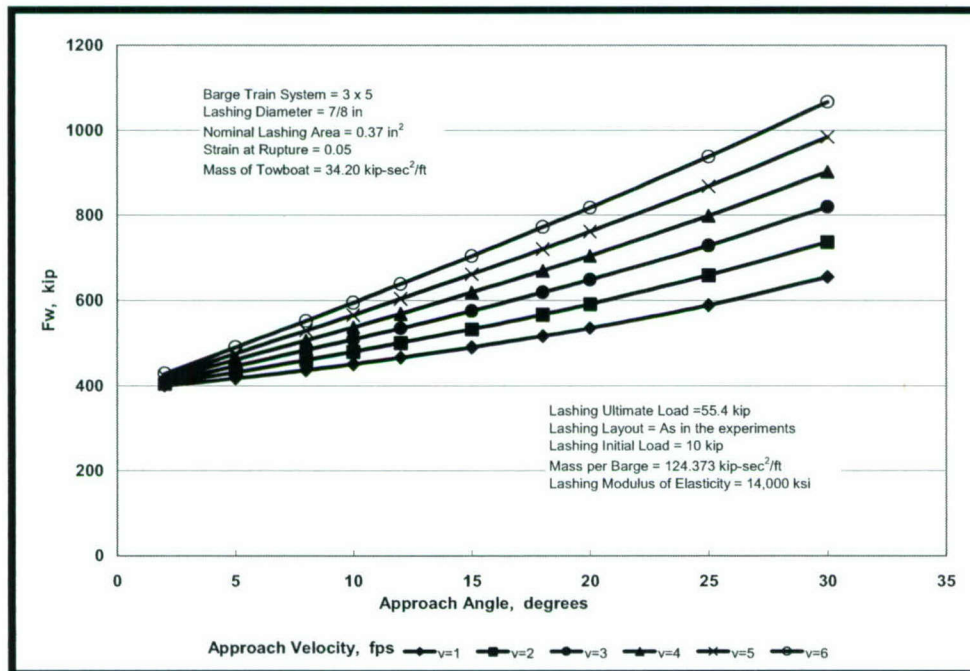


Figure 2-24. Maximum  $F_w$  for a 3x5 Barge Train System – Case B

Table 2-5. Mechanical Properties of Lashing – Case C

Lashing Layouts	As in the Experiments	
Lashing Diameter	1	in.
Breaking Strength	89.8	kip
Nominal Area	0.48	sq in.
Rupture Strain	6	%

Figures 2.25 through 2.30 present the variation of the maximum force normal to the wall for barge train systems 2x2, 2x3, 3x2, 3x3, 3x4, and 3x5, respectively. Additional input data are the mass of the barge train, mass of the towboat, and the lashing initial load. Each figure shows the values used in this set of calculations.

### 2.3.4 Limiting Impact Forces Computed for 1-in. Diameter Used Wire Rope

The results of the limiting impact forces computed for the 1-in. diameter used wire rope are presented next. Table 2.6 lists the parameters used.

Figures 2.31 through 2.36 present the variation of the maximum force normal to the wall for barge train systems 2x2, 2x3, 3x2, 3x3, 3x4, and 3x5, respectively. Additional input data are the mass of the barge train, mass of the towboat, and the lashing initial load. Each figure shows the values used in this set of calculations.

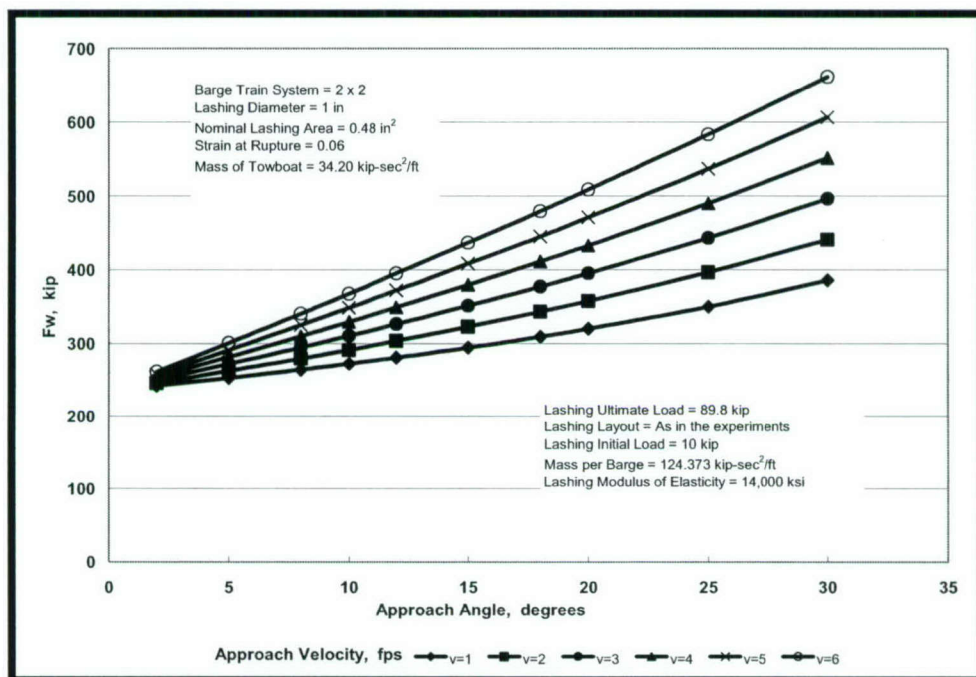


Figure 2-25. Maximum  $F_w$  for a 2x2 Barge Train System – Case C



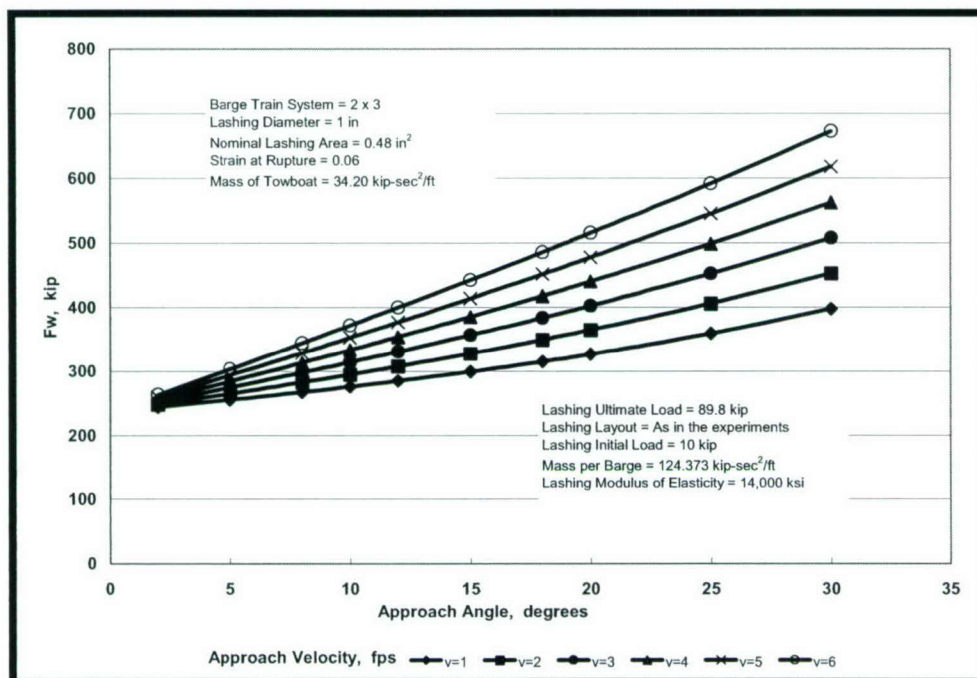


Figure 2-26. Maximum  $F_w$  for a 2x3 Barge Train System – Case C

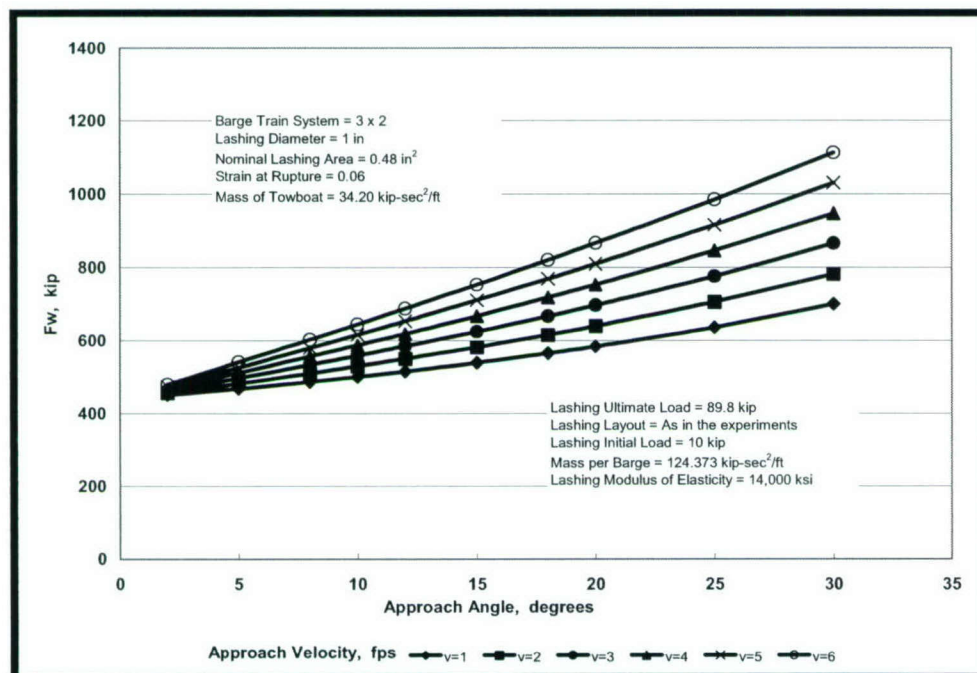


Figure 2-27. Maximum  $F_w$  for a 3x2 Barge Train System – Case C

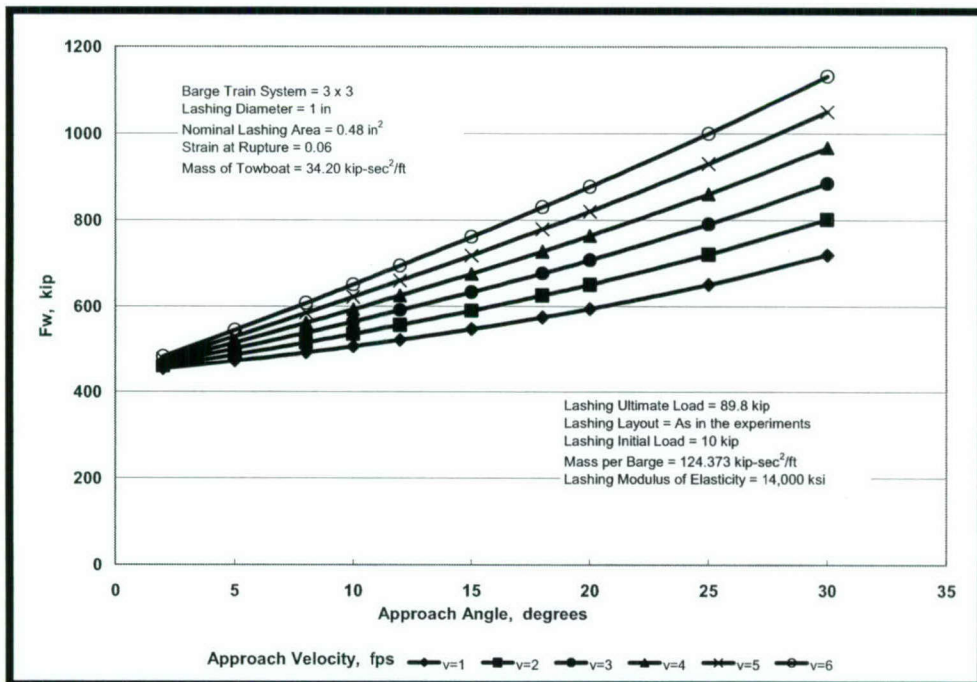


Figure 2-28. Maximum  $F_w$  for a 3x3 Barge Train System – Case C

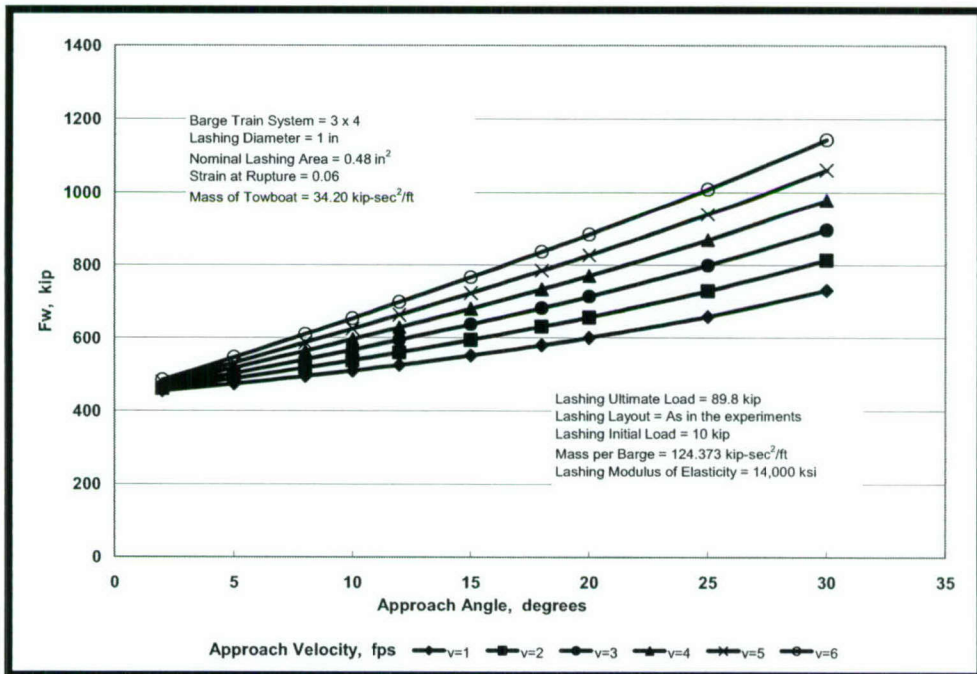


Figure 2-29. Maximum  $F_w$  for a 3x4 Barge Train System – Case C



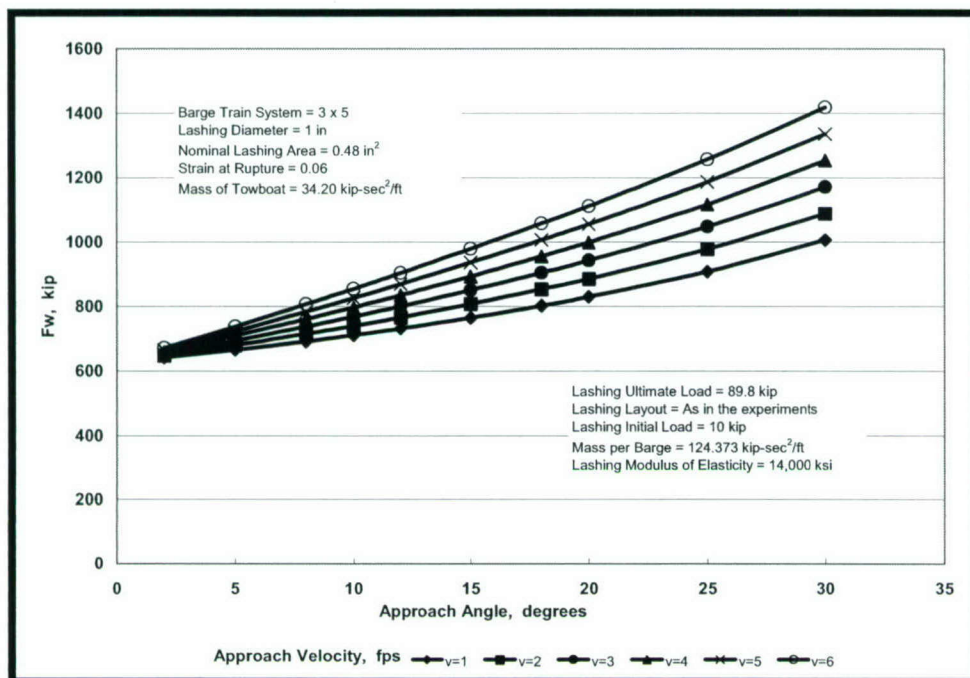


Figure 2-30. Maximum  $F_w$  for a 3x5 Barge Train System – Case C

Table 2-6. Mechanical Properties of Lashing – Case D

Lashing Layouts	As in the Experiments	
Lashing Diameter	1	in.
Breaking Strength	71.8	kip
Nominal Area	0.48	sq in.
Rupture Strain	5	%

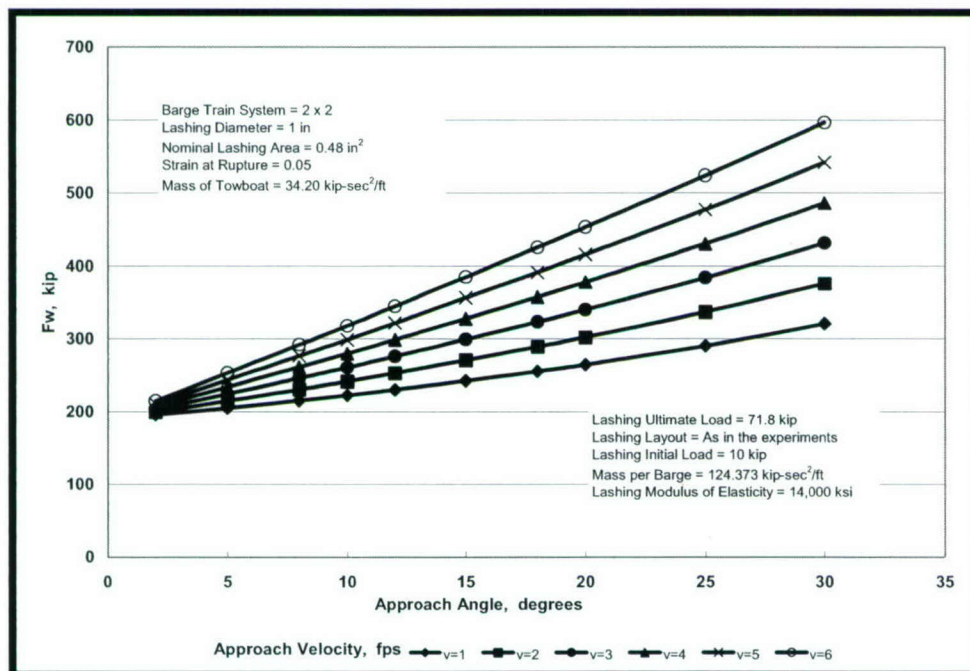


Figure 2-31. Maximum  $F_w$  for a 2x2 Barge Train System – Case D

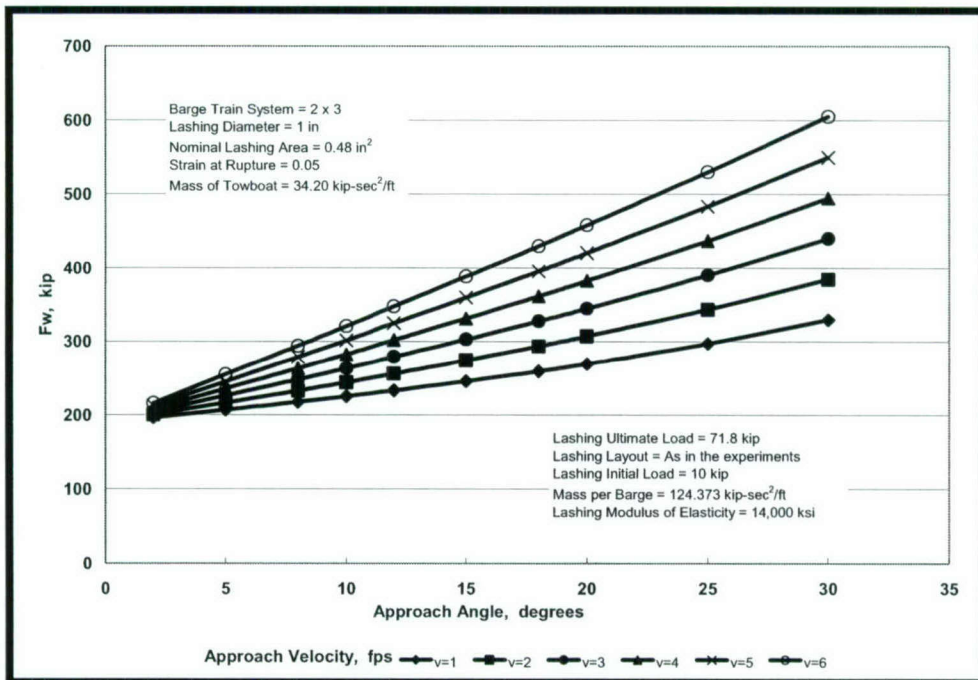


Figure 2-32. Maximum  $F_w$  for a 2x3 Barge Train System – Case D

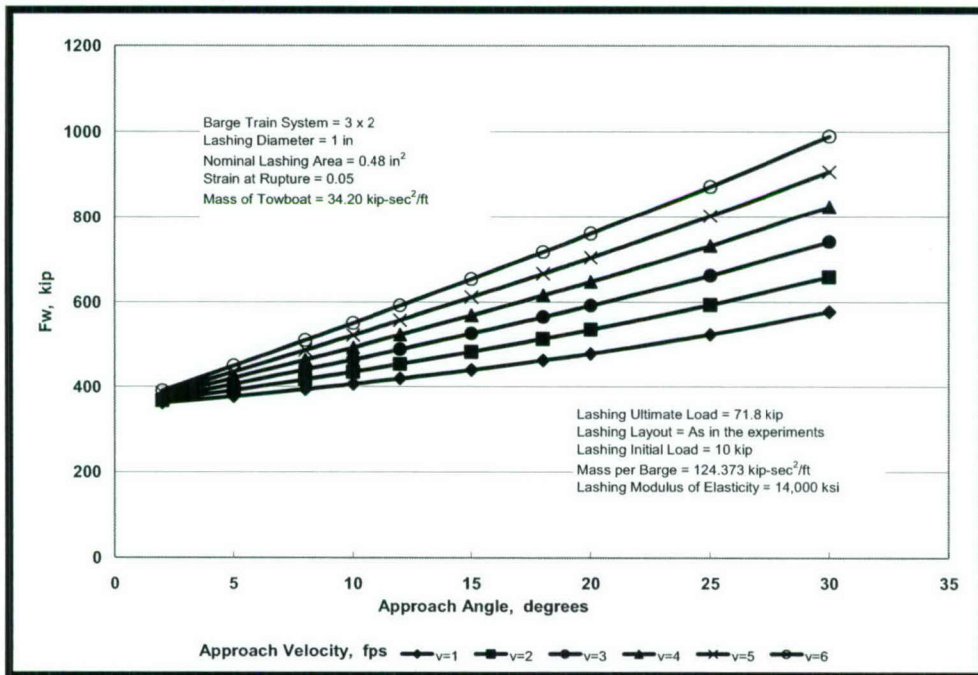


Figure 2-33. Maximum FW for a 3x2 Barge Train System – Case D



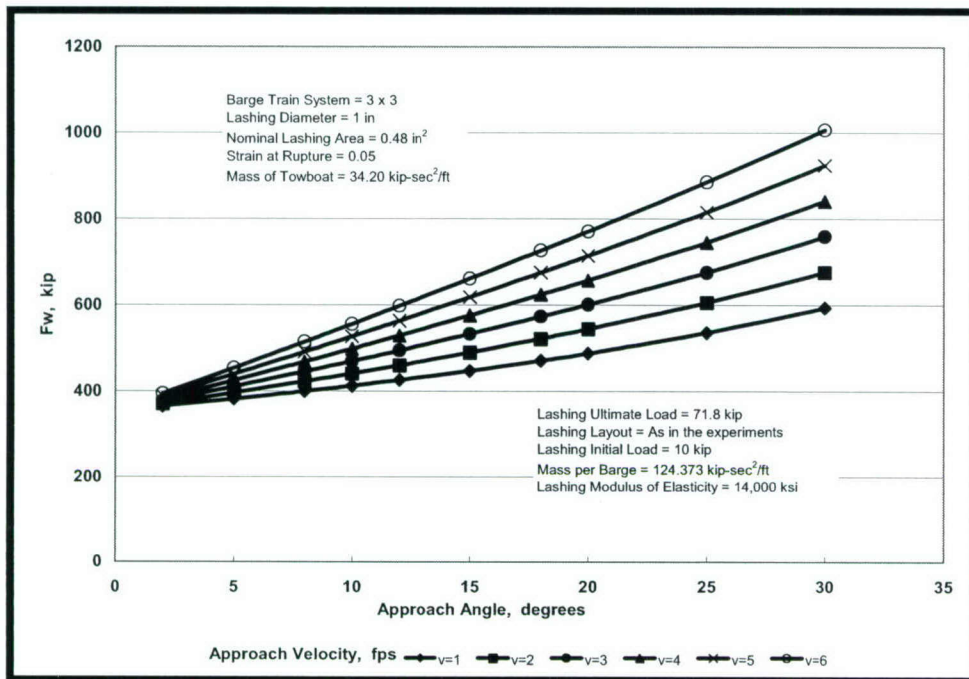


Figure 2-34. Maximum  $F_w$  for a 3x3 Barge Train System – Case D

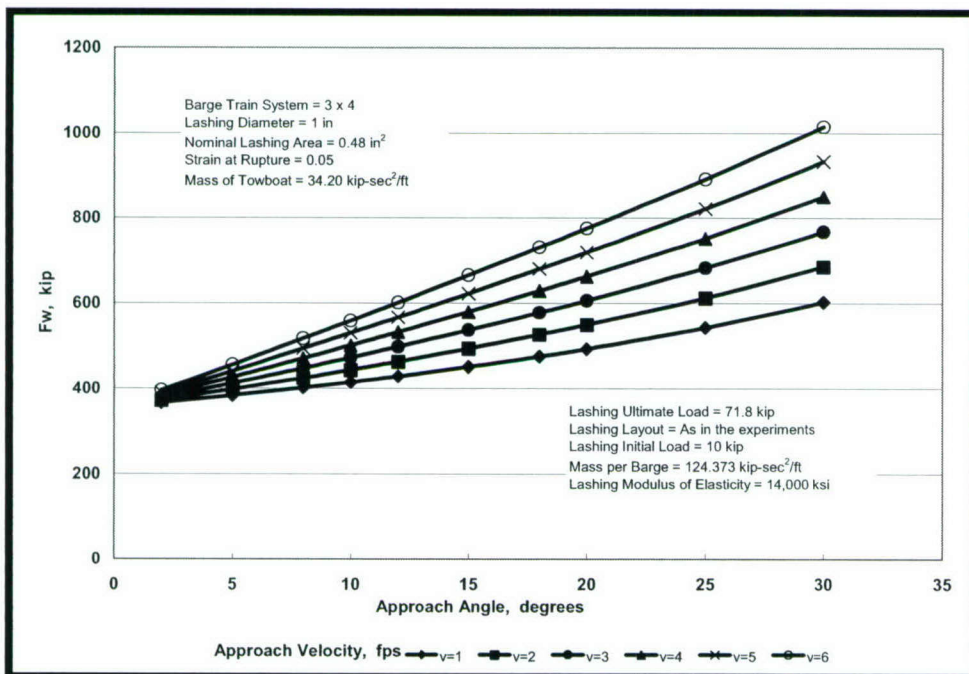


Figure 2-35. Maximum  $F_w$  for a 3x4 Barge Train System – Case D

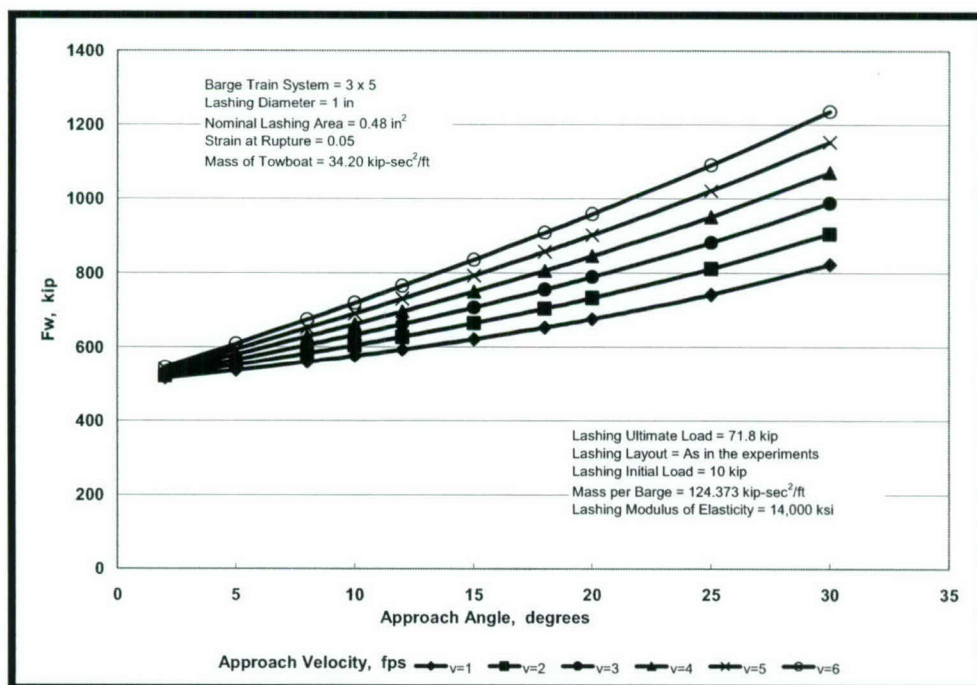


Figure 2-36. Maximum  $F_W$  for a 3x5 Barge Train System – Case D

## 2.4 Standard Lashing Layout With an Additional Wrap

This section presents the results obtained with the same parameters and conditions as those presented in the last section with the exception of the number of wraps used to join the barges. In this section one additional wrap is included in the lashing layout. In this way, the lashing layout used during the 1998 Experiments are modified to produce a stiffer system, which needs higher impact force to breaks the lashings. This condition will be reflected in the magnitude of the calculated forces.

### 2.4.1 Limiting Impact Forces Computed for 7/8-in. Diameter New Wire Rope

The results of the limiting impact forces computed for the 7/8-in. diameter new wire rope are presented next. Table 2.7 lists the parameters used. The case identification is now “AWA” (Additional Wrap case A). The results of this case can be compared with the set of results obtained with Case A presented in the last section.

Figures 2.37 through 2.42 present the variation of the maximum force normal to the wall for barge train systems 2x2, 2x3, 3x2, 3x3, 3x4, and 3x5, respectively. Additional input data are the mass of the barge train, mass of the towboat, and the lashing initial load. Each figure shows the values used in this set of calculations.

### 2.4.2 Limiting Impact Forces Computed for 7/8-in. Diameter Used Wire Rope

The results of the limiting impact forces computed for the 7/8-in. diameter used wire rope are presented next. Table 2.8 lists the parameters used. The case identification is



now “AWB” (Additional Wrap case B). The results of this case can be compared with the set of results obtained with Case B presented in the last section.

Figures 2.43 through 2.48 present the variation of the maximum force normal to the wall for barge train systems 2x2, 2x3, 3x2, 3x3, 3x4, and 3x5, respectively. Additional input data are the mass of the barge train, mass of the towboat, and the lashing initial load. Each figure shows the values used in this set of calculations.

### 2.4.3 Limiting Impact Forces Computed for 1-in. Diameter New Wire Rope

The results of the limiting impact forces computed for the 1-in. diameter new wire rope are presented next. Table 2.9 lists the parameters used. The case identification is now “AWC” (Additional Wrap case C). The results of this case can be compared with the set of results obtained with Case C presented in the last section.

Figures 2.49 through 2.54 present the variation of the maximum force normal to the wall for barge train systems 2x2, 2x3, 3x2, 3x3, 3x4, and 3x5, respectively. Additional input data are the mass of the barge train, mass of the towboat, and the lashing initial load. Each figure shows the values used in this set of calculations.

Table 2-7. Mechanical Properties of Lashing – Case AWA

Lashing Layouts	One Additional Wrap to the 1998 Experiments Layout	
Lashing Diameter	7/8	in.
Breaking Strength	69.2	kip
Nominal Area	0.37	sq in.
Rupture Strain	6	%

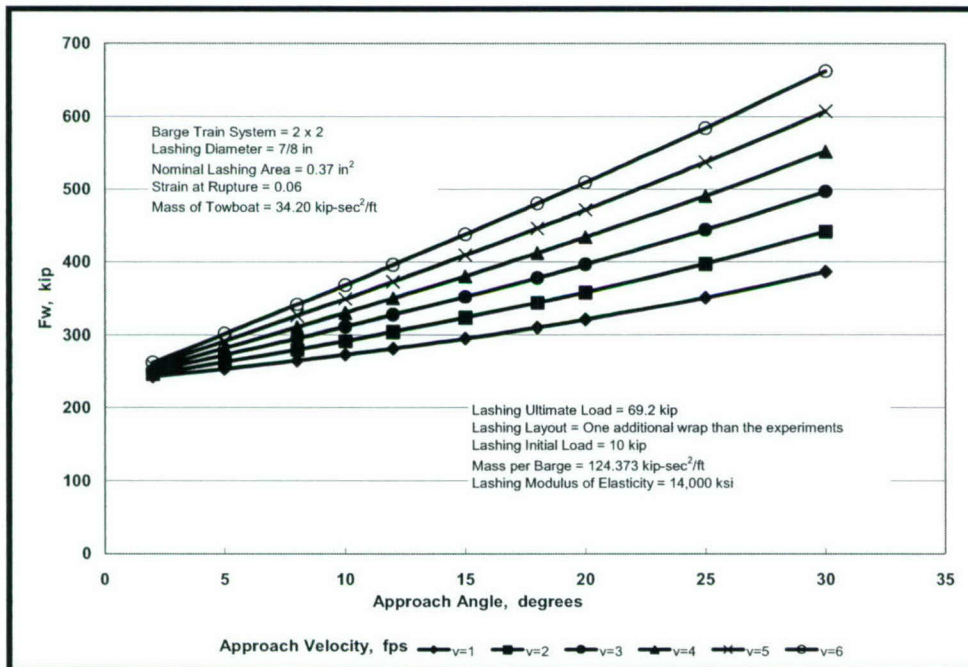


Figure 2-37. Maximum  $F_w$  for a 2x2 Barge Train System – Case AWA

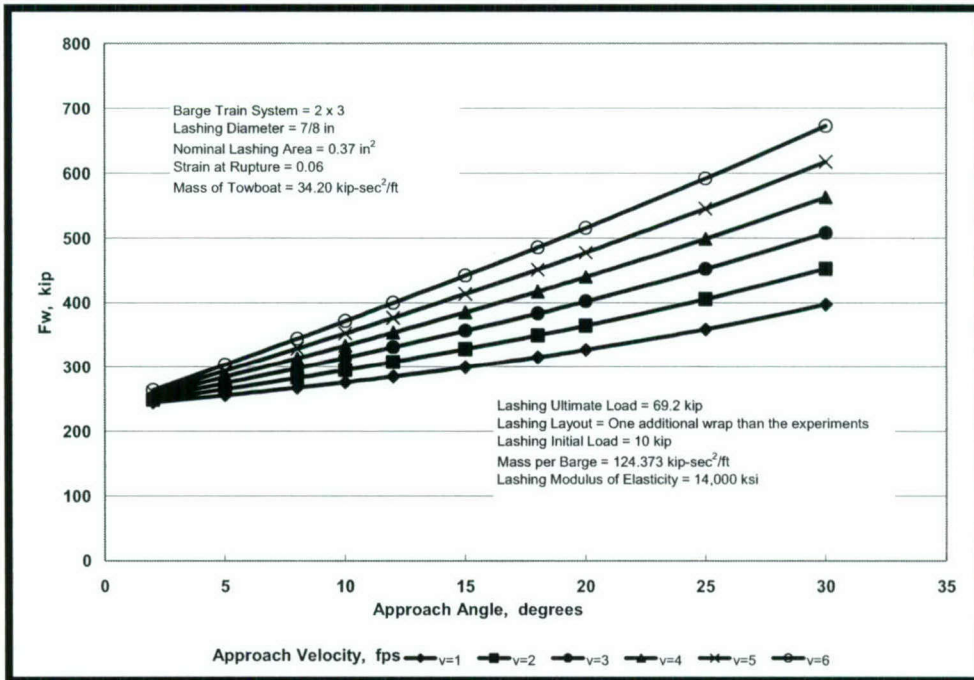


Figure 2-38. Maximum  $F_w$  for a 2x3 Barge Train System – Case AWA

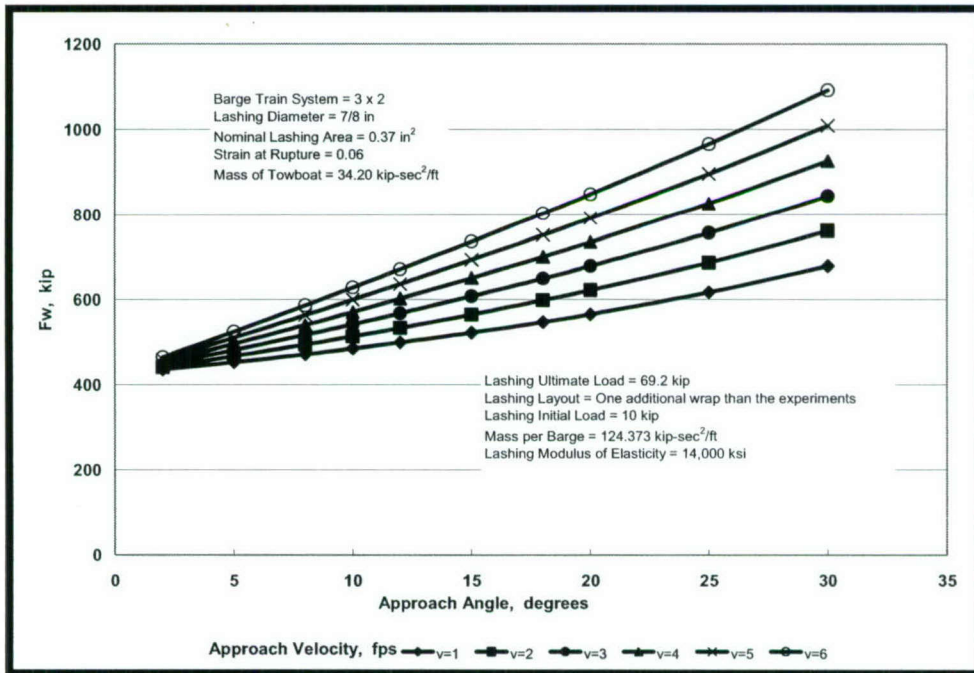


Figure 2-39. Maximum  $F_w$  for a 3x2 Barge Train System – Case AWA



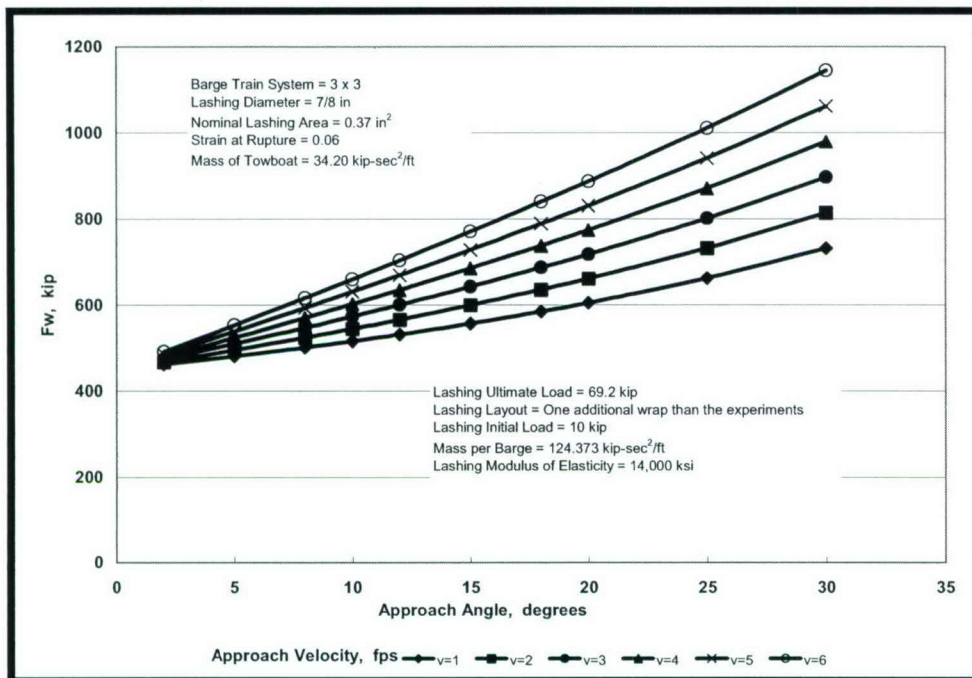


Figure 2-40. Maximum  $F_w$  for a 3x3 Barge Train System – Case AWA

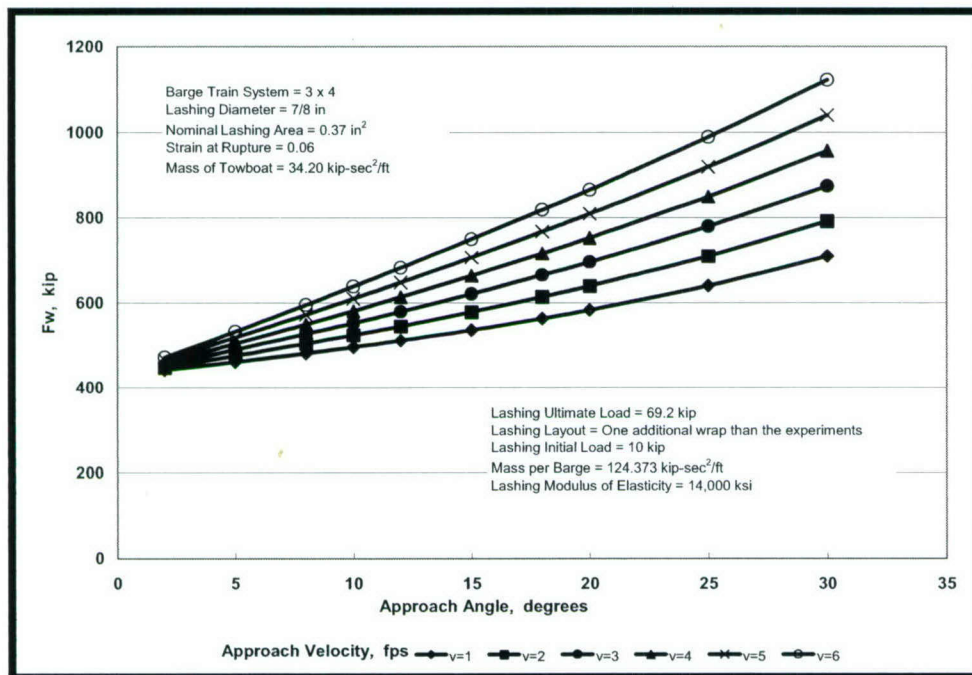


Figure 2-41. Maximum  $F_w$  for a 3x4 Barge Train System – Case AWA

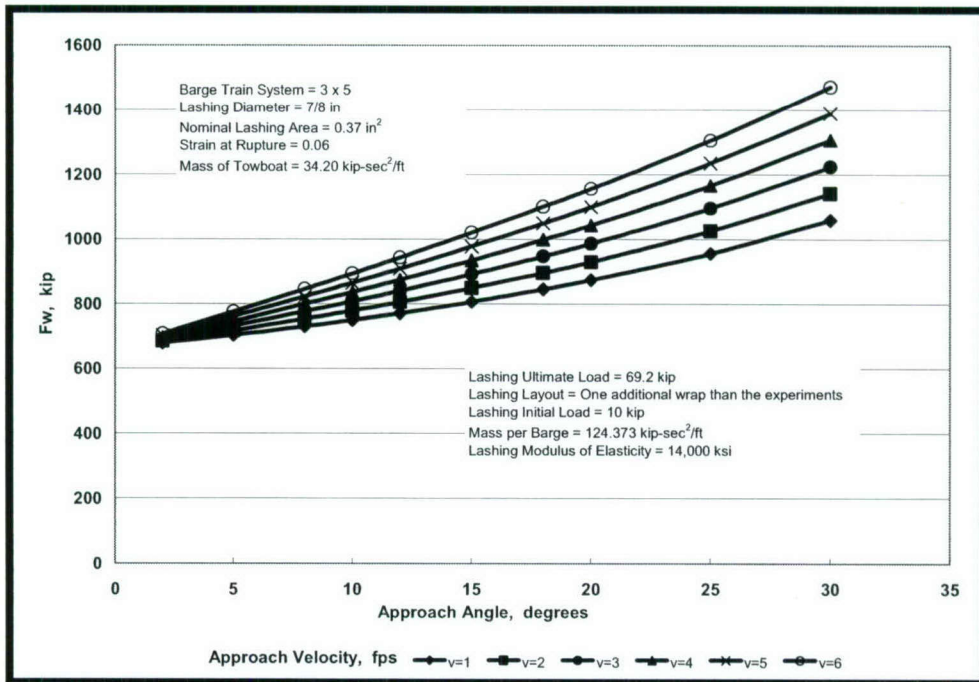


Figure 2-42. Maximum  $F_w$  for a 3x5 Barge Train System – Case AWA

Table 2-8. Mechanical Properties of Lashing – Case AWB

Lashing Layouts	One Additional Wrap to the 1998 Experiments Layout	
Lashing Diameter	7/8	in.
Breaking Strength	55.4	kip
Nominal Area	0.37	sq in.
Rupture Strain	5	%

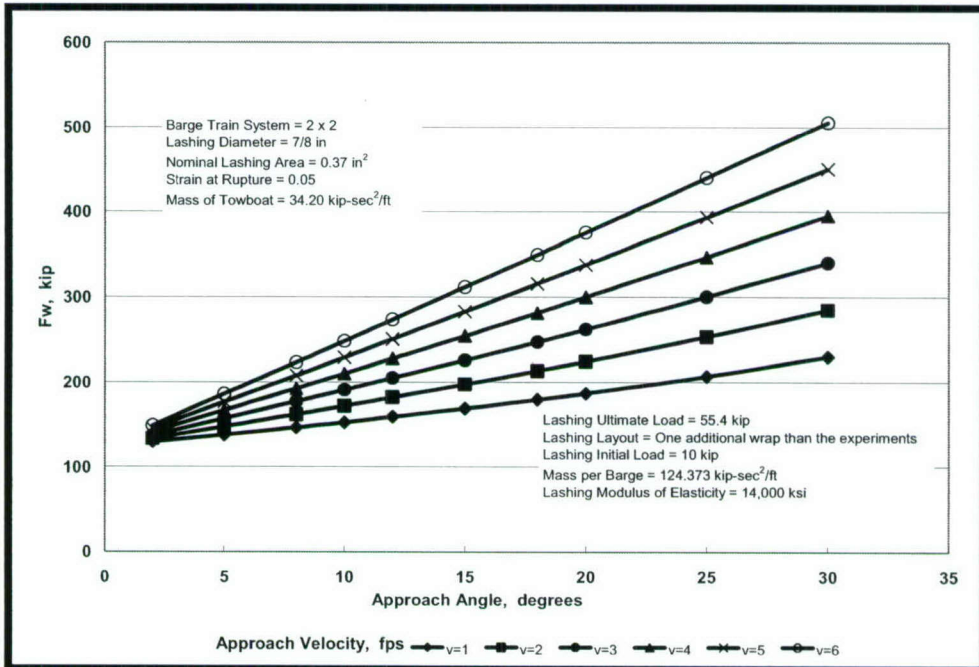


Figure 2-43. Maximum  $F_w$  for a 2x2 Barge Train System – Case AWB



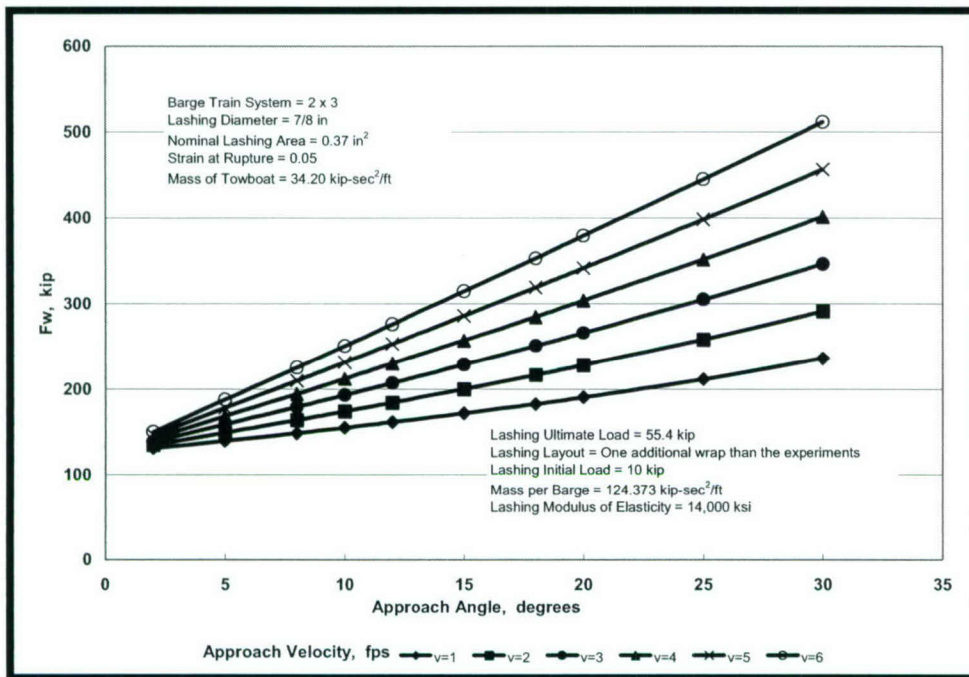


Figure 2-44. Maximum  $F_w$  for a 2x3 Barge Train System – Case AWB

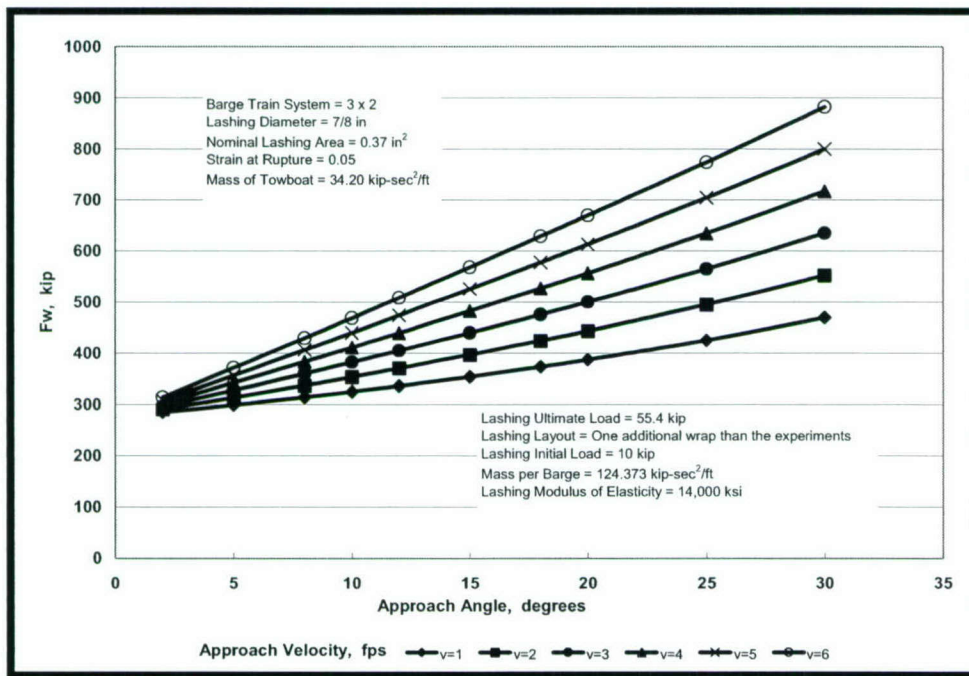


Figure 2-45. Maximum  $F_w$  for a 3x2 Barge Train System – Case AWB

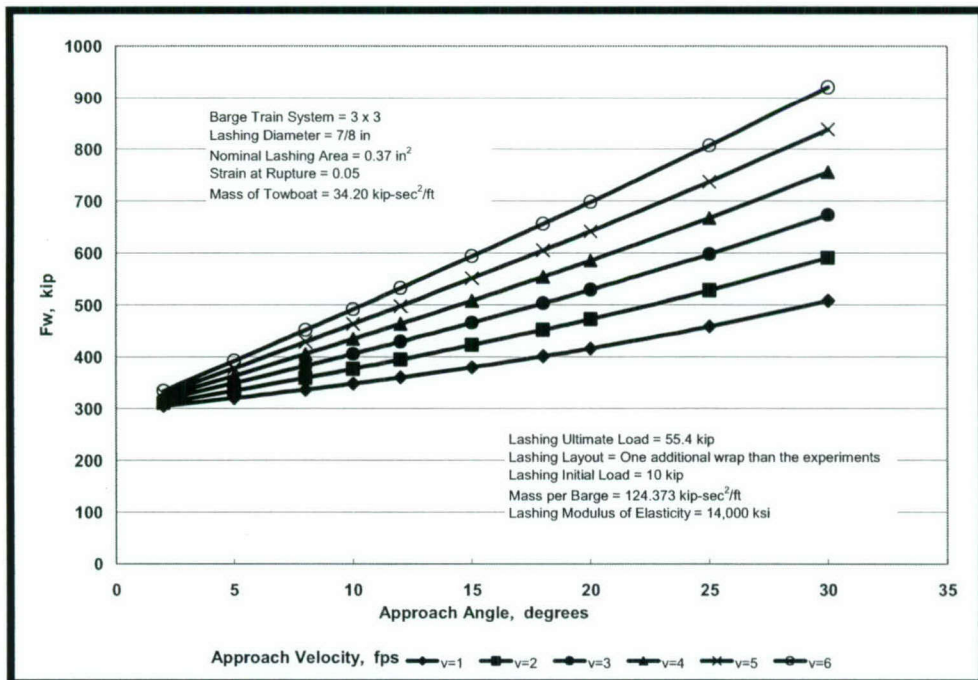


Figure 2-46. Maximum  $F_w$  for a 3x3 Barge Train System – Case AWB

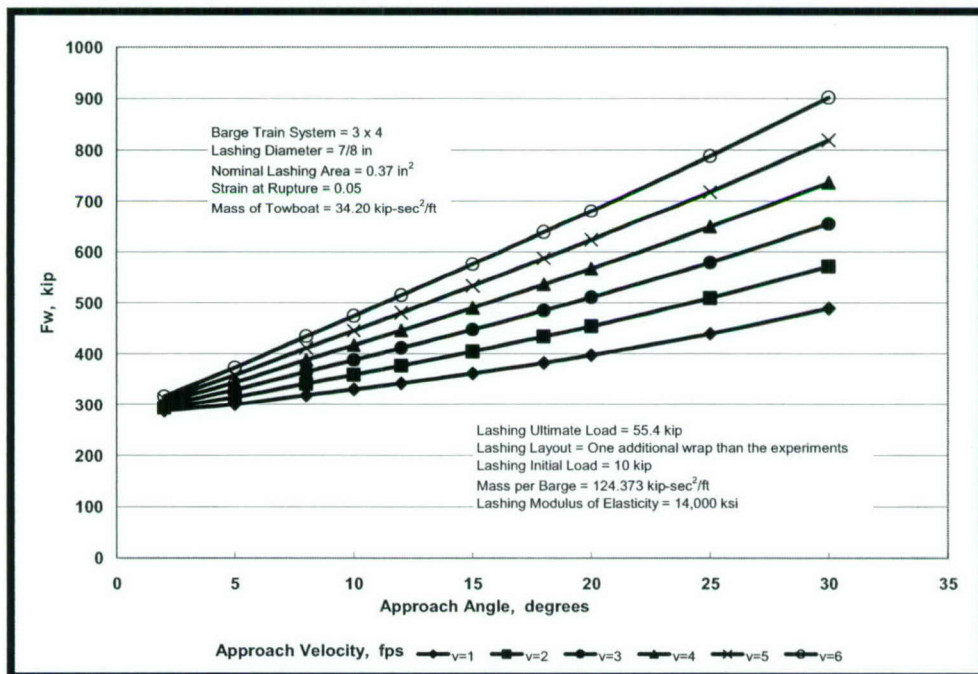


Figure 2-47. Maximum  $F_w$  for a 3x4 Barge Train System – Case AWB



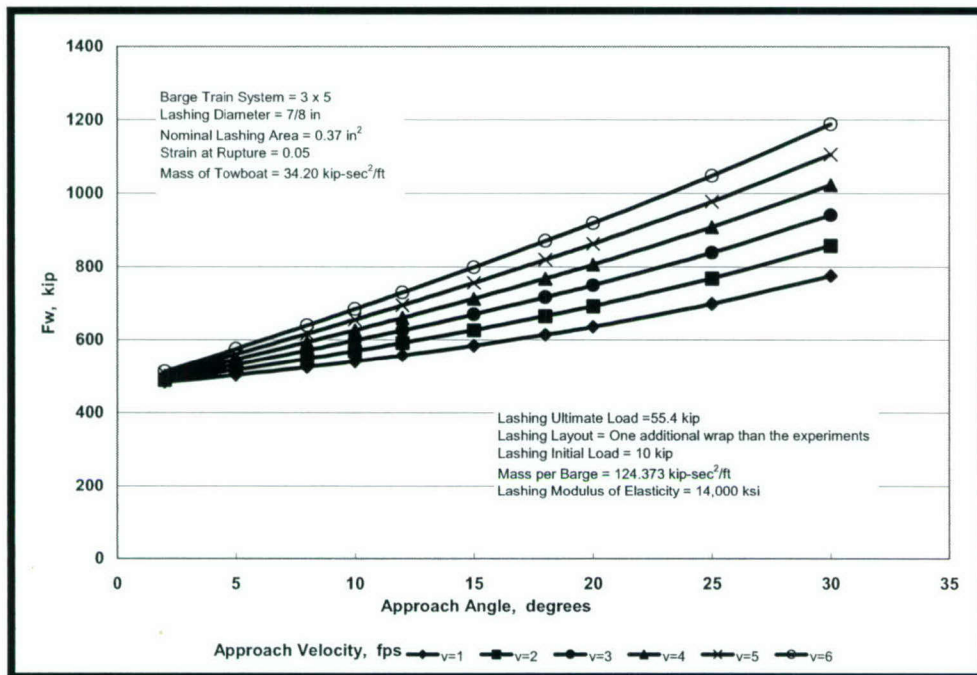


Figure 2-48. Maximum  $F_w$  for a 3x5 Barge Train System – Case AWB

Table 2-9. Mechanical Properties of Lashing – Case AWC

Lashing Layouts	One Additional Wrap to the 1998 Experiments Layout	
Lashing Diameter	1	in.
Breaking Strength	89.8	kip
Nominal Area	0.48	sq in.
Rupture Strain	6	%

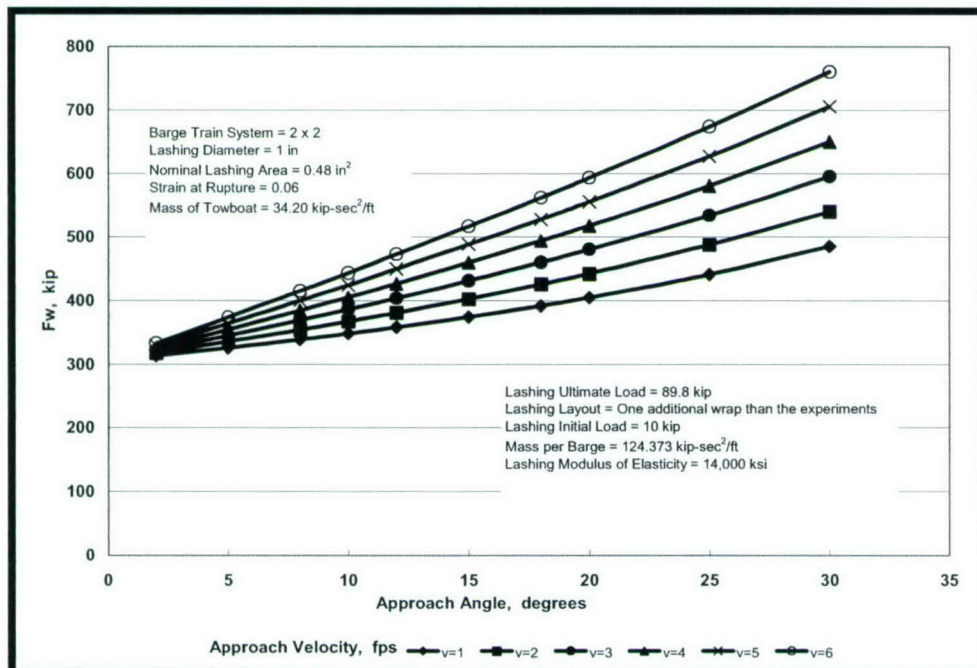


Figure 2-49. Maximum  $F_w$  for a 2x2 Barge Train System – Case AWC

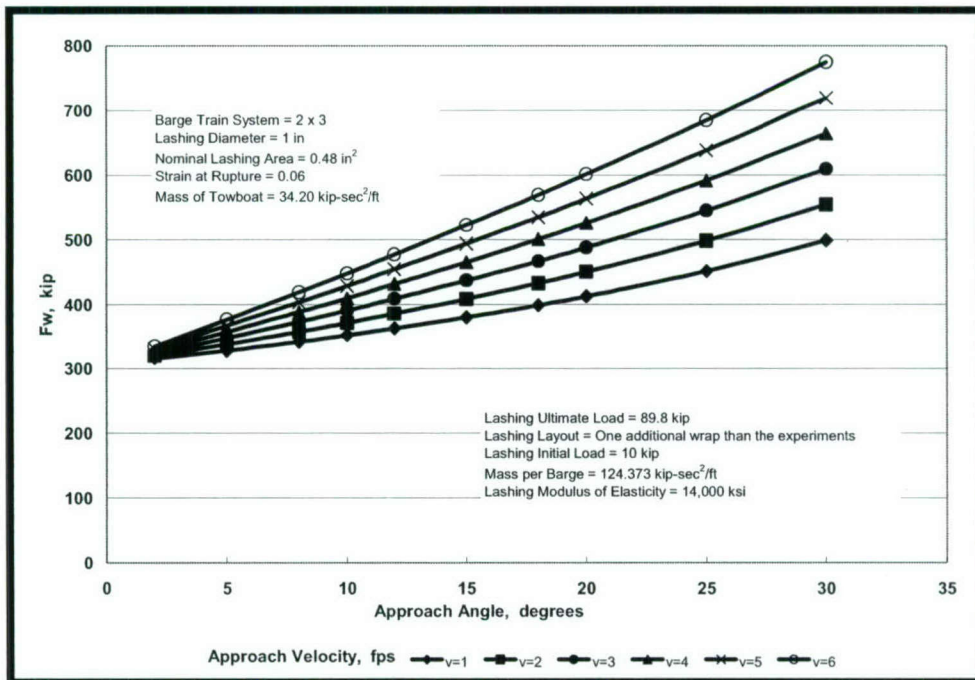


Figure 2-50. Maximum  $F_w$  for a 2x3 Barge Train System – Case AWC

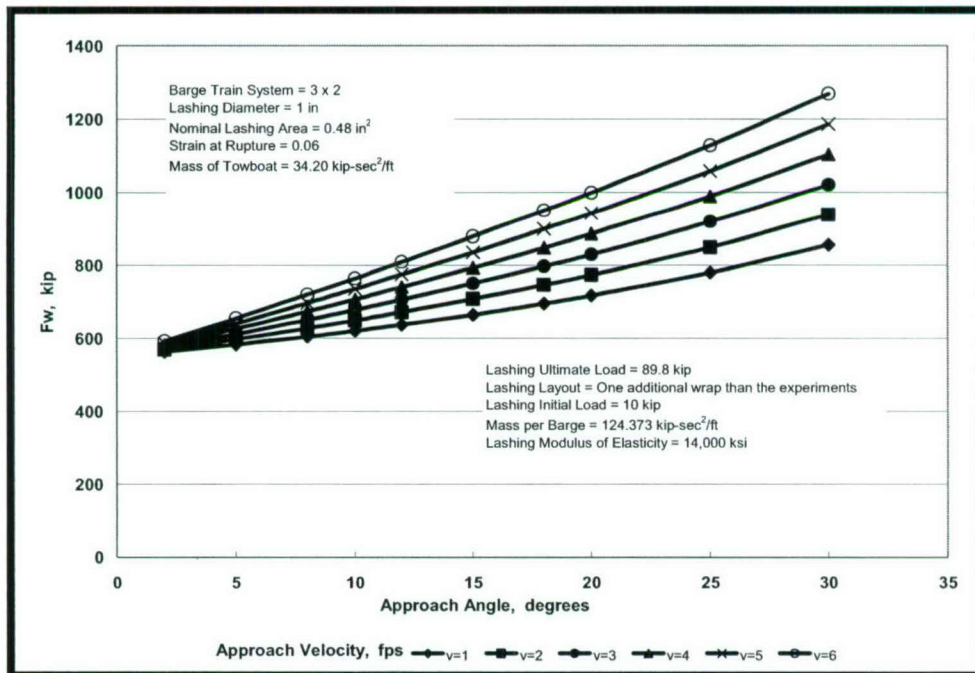


Figure 2-51. Maximum  $F_w$  for a 3x2 Barge Train System – Case AWC



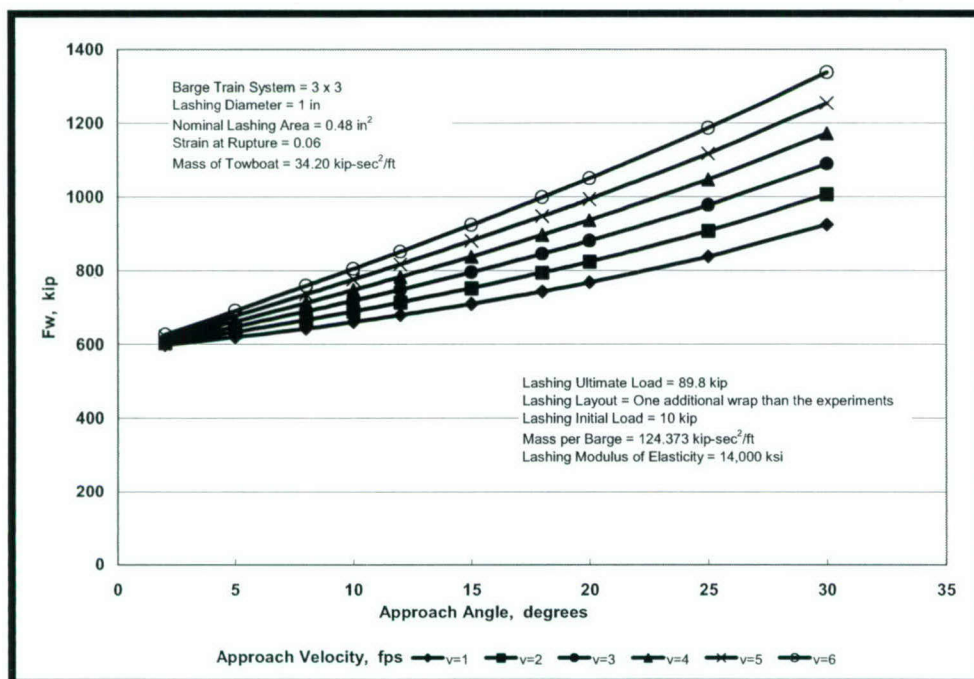


Figure 2-52. Maximum  $F_w$  for a 3x3 Barge Train System – Case AWC

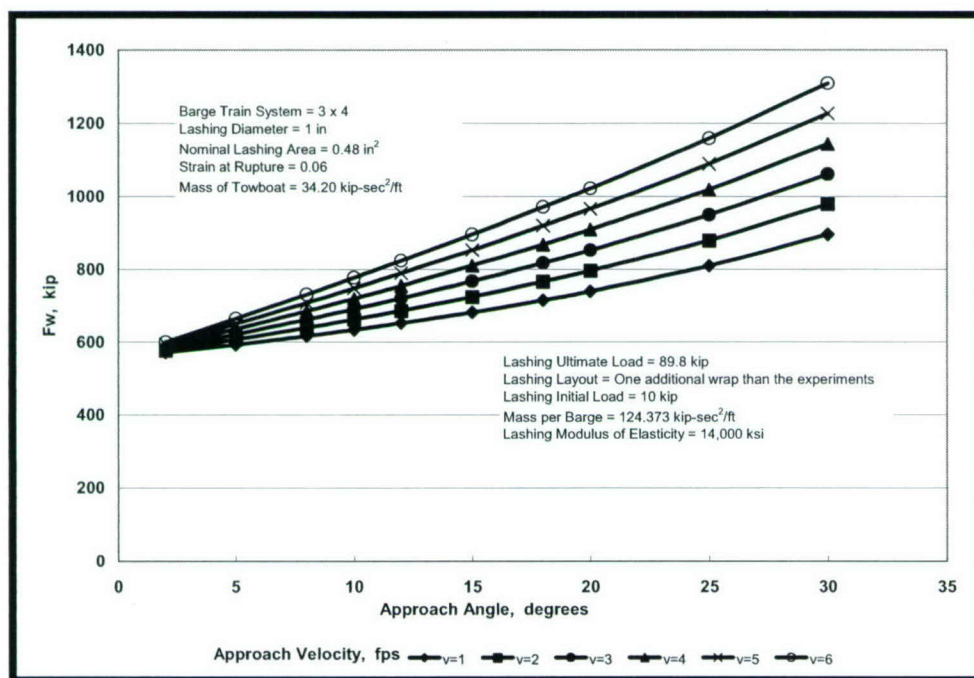


Figure 2-53. Maximum  $F_w$  for a 3x4 Barge Train System – Case AWC

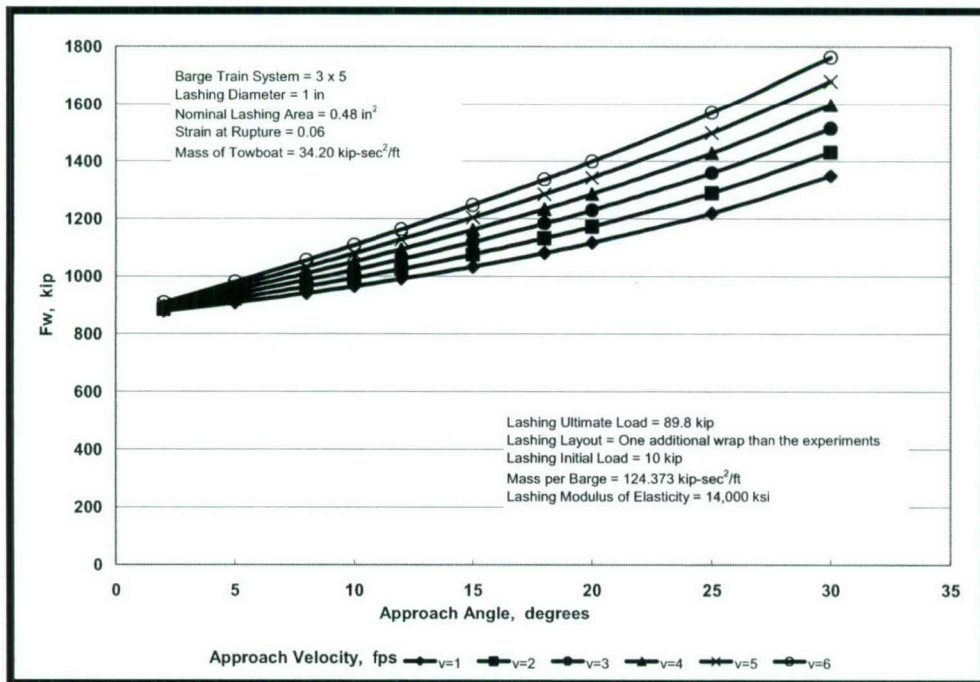


Figure 2-54. Maximum  $F_w$  for a 3x5 Barge Train System – Case AWC

#### 2.4.4 Limiting Impact Forces Computed for 1-in. Diameter Used Wire Rope

The results of the limiting impact forces computed for the 1-in. diameter used wire rope are presented next. Table 2.10 lists the parameters used. The case identification is now “AWD” (Additional Wrap case D). The results of this case can be compared with the set of results obtained with Case D presented in the last section.

Figures 2.55 through 2.60 present the variation of the maximum force normal to the wall for barge train systems 2x2, 2x3, 3x2, 3x3, 3x4, and 3x5, respectively. Additional input data are the mass of the barge train, mass of the towboat, and the lashing initial load. Each figure shows the values used in this set of calculations.

### 2.5 Standard Lashing Layout Less One Wrap

This section presents the results obtained with the same parameters and conditions as those presented in Section 2.3 with the exception of the number of wraps used to join the barges. This section uses the standard lashing layout presented in Section 2.3 *less one wrap* to join the barges in the barge train. In this way, the lashing layout used during the Experiments 1998 was modified to produce a more flexible system, which needs lower impact force to break the lashings. This condition will be reflected in the magnitude of the calculated forces.

#### 2.5.1 Limiting Impact Forces Computed for 7/8-in. Diameter New Wire Rope

The results of the limiting impact forces computed for the 7/8-in. diameter new wire rope are presented next. Table 2.11 lists the parameters used. The case identification is



now “LWA” (Less Wrap case A). The results of this case can be compared with the set of results obtained with Case A presented in Section 2.3.

Figures 2.61 through 2.66 show the variation of the maximum force normal to the wall for barge train systems 2x2, 2x3, 3x2, 3x3, 3x4, and 3x5, respectively. Additional input data are the mass of the barge train, mass of the towboat, and the lashing initial load. Each figure shows the values used in this set of calculations.

## 2.5.2 Limiting Impact Forces Computed for 7/8-in. Diameter Used Wire Rope

The results of the limiting impact forces computed for the 7/8-in. diameter used wire rope are presented next. Table 2.12 lists the parameters used. The case identification is now “LWB” (Less Wrap case B). The results of this case can be compared with the set of results obtained with Case B presented in Section 2.3.

Figures 2.67 through 2.72 present the variation of the maximum force normal to the wall for barge train systems 2x2, 2x3, 3x2, 3x3, 3x4, and 3x5, respectively. Additional input data are the mass of the barge train, mass of the towboat, and the lashing initial load. Each figure shows the values used in this set of calculations.

Table 2-10. Mechanical Properties of Lashing – Case AWD

Lashing Layouts	One Additional Wrap to the 1998 Experiments Layout	
Lashing Diameter	1	in.
Breaking Strength	71.8	kip
Nominal Area	0.48	sq in.
Rupture Strain	5	%

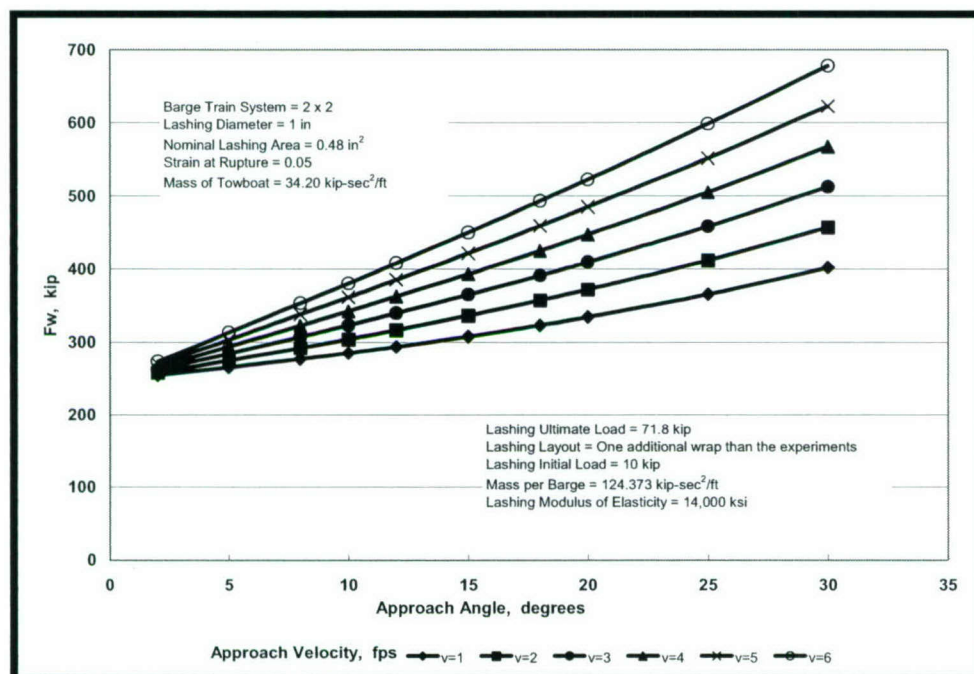


Figure 2-55. Maximum  $F_w$  for a 2x2 Barge Train System – Case AWD

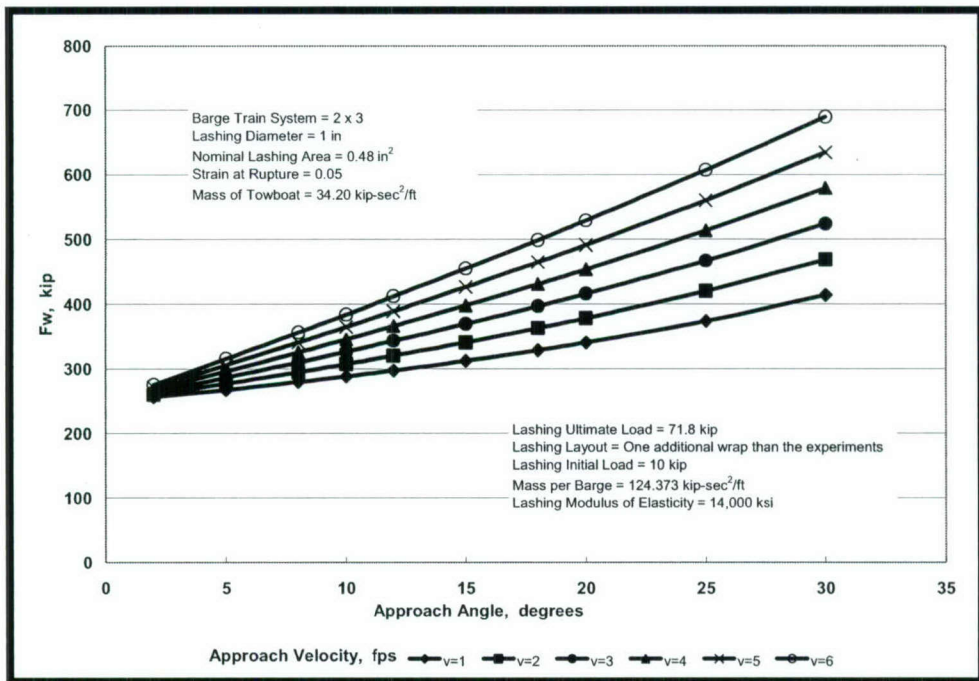


Figure 2-56. Maximum  $F_w$  for a 2x3 Barge Train System – Case AWD

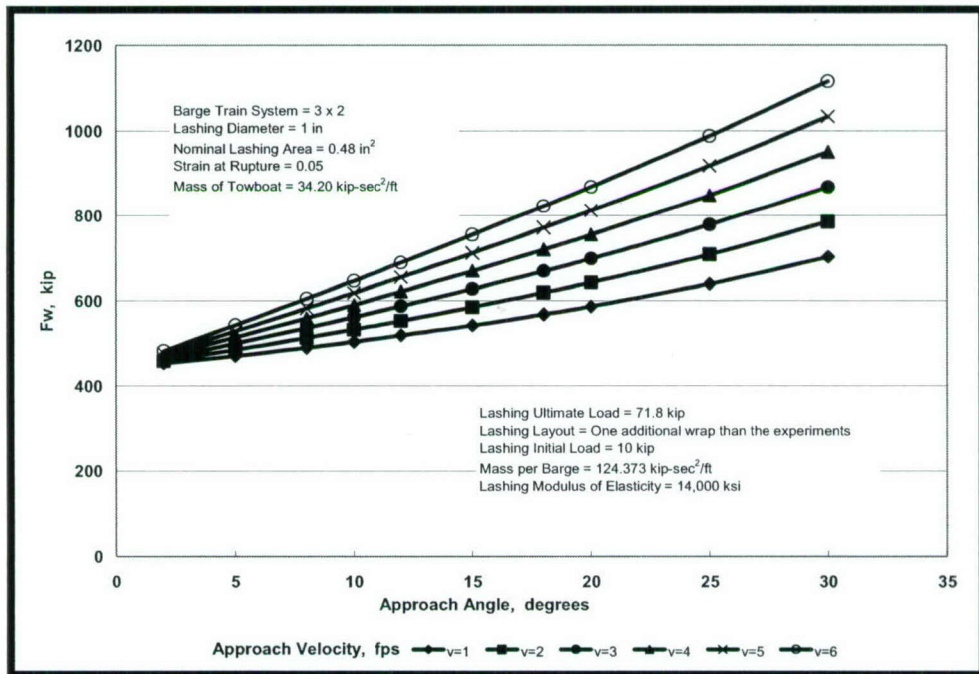


Figure 2-57. Maximum  $F_w$  for a 3x2 Barge Train System – Case AWD



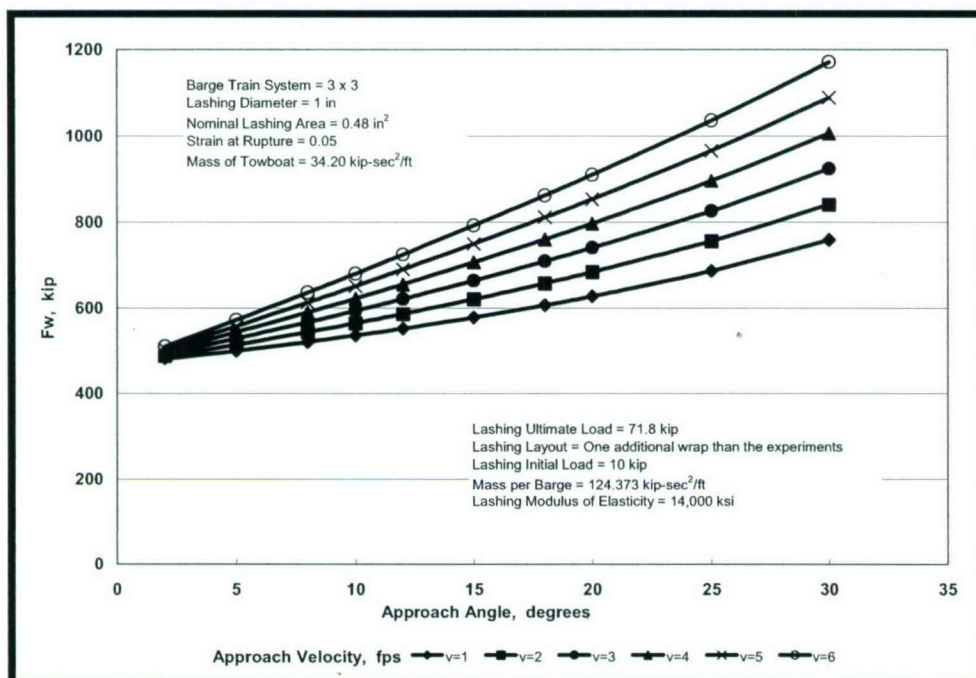


Figure 2-58. Maximum  $F_w$  for a 3x3 Barge Train System – Case AWD

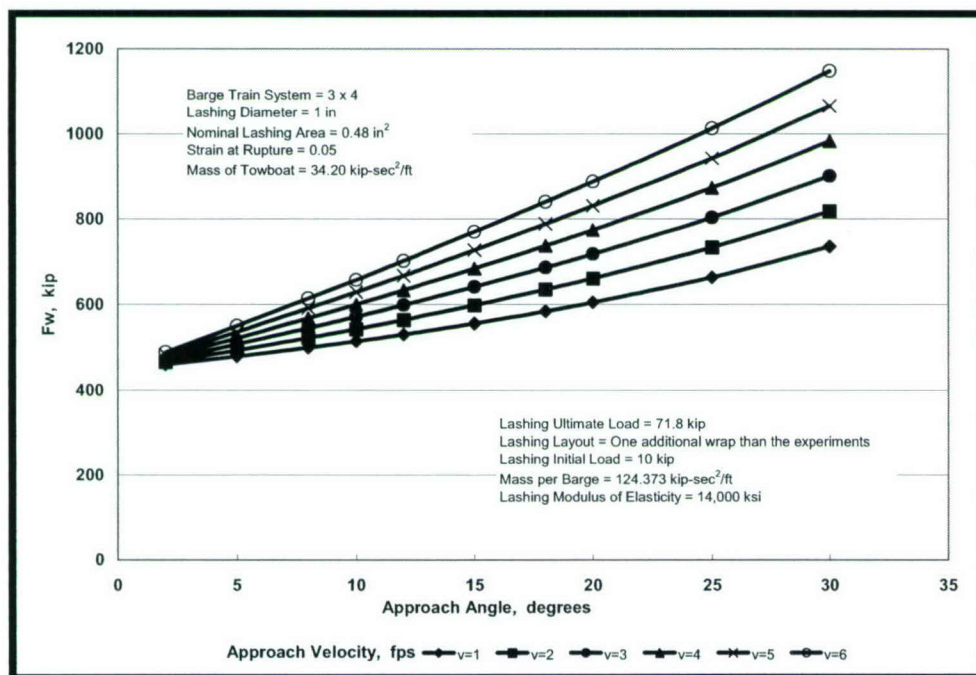


Figure 2-59. Maximum  $F_w$  for a 3x4 Barge Train System – Case AWD

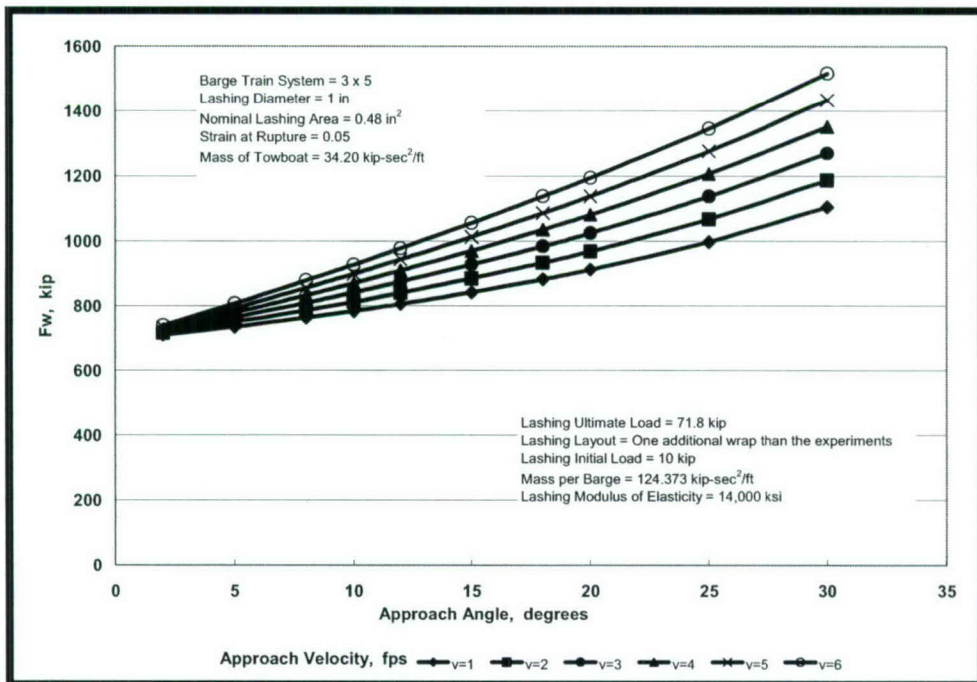


Figure 2-60. Maximum  $F_w$  for a 3x5 Barge Train System – Case AWD

Table 2-11. Mechanical Properties of Lashing – Case LWA

Lashing Layouts	One Wrap Less Than the 1998 Experiments Layout	
Lashing Diameter	7/8	in.
Breaking Strength	69.2	kip
Nominal Area	0.37	sq in.
Rupture Strain	6	%

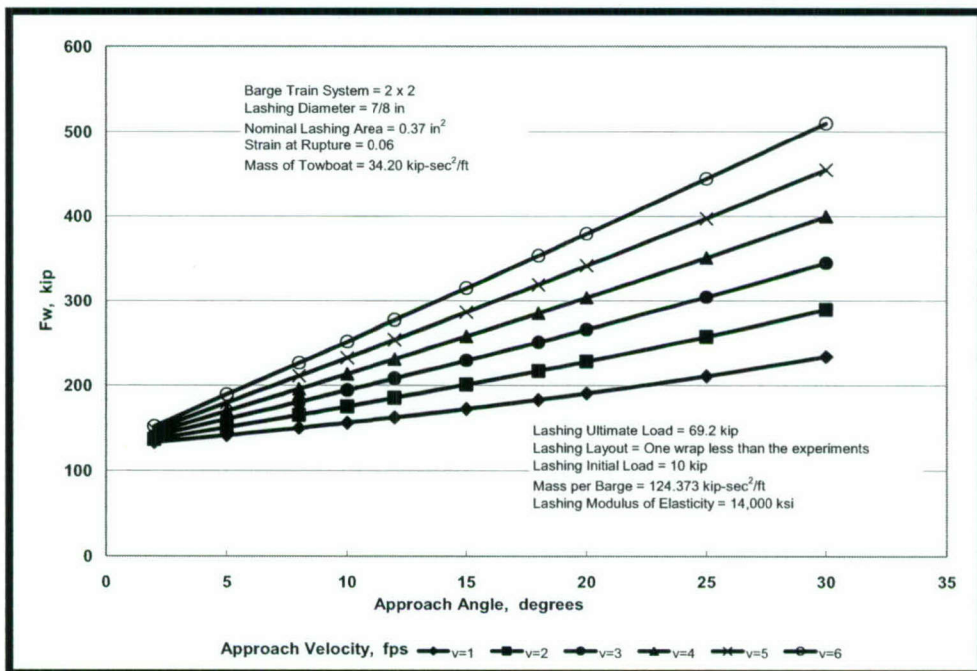


Figure 2-61. Maximum  $F_w$  for a 2x2 Barge Train System – Case LWA



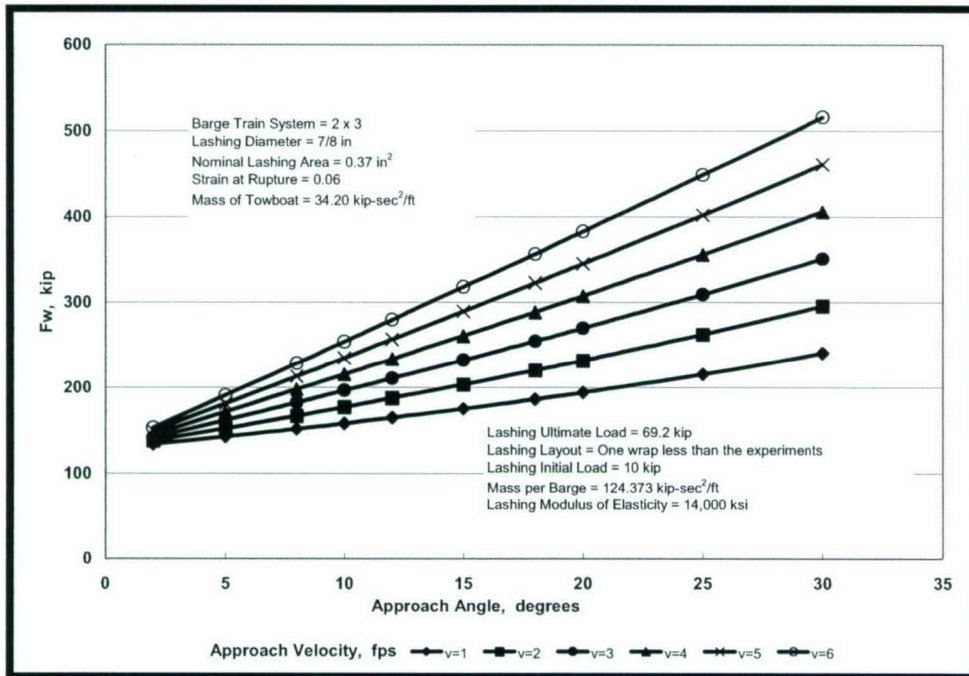


Figure 2-62. Maximum  $F_w$  for a 2x3 Barge Train System – Case LWA

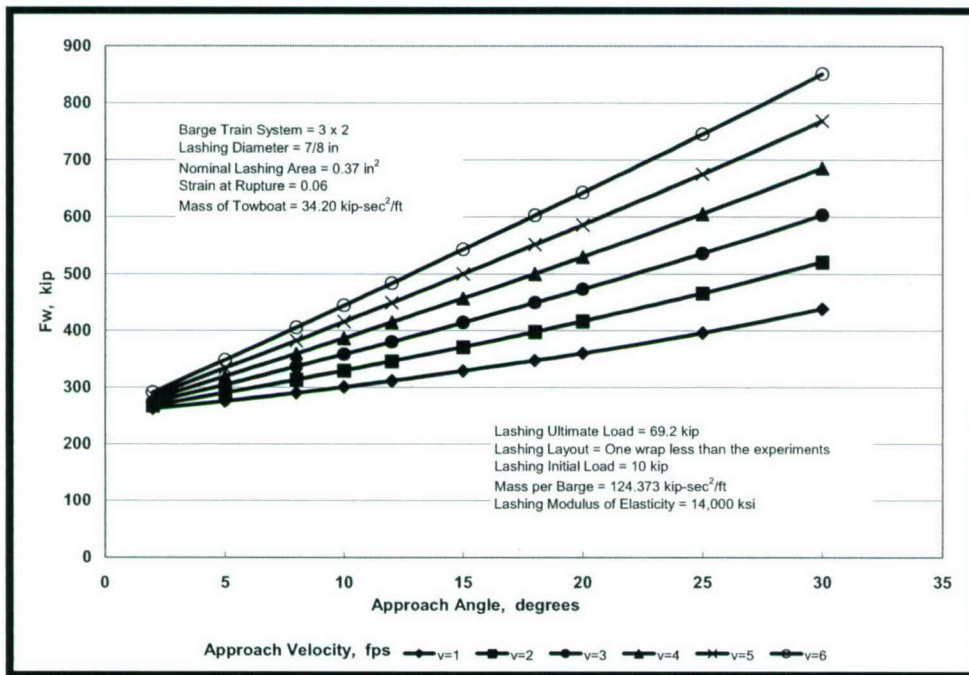


Figure 2-63. Maximum  $F_w$  for a 3x2 Barge Train System – Case LWA

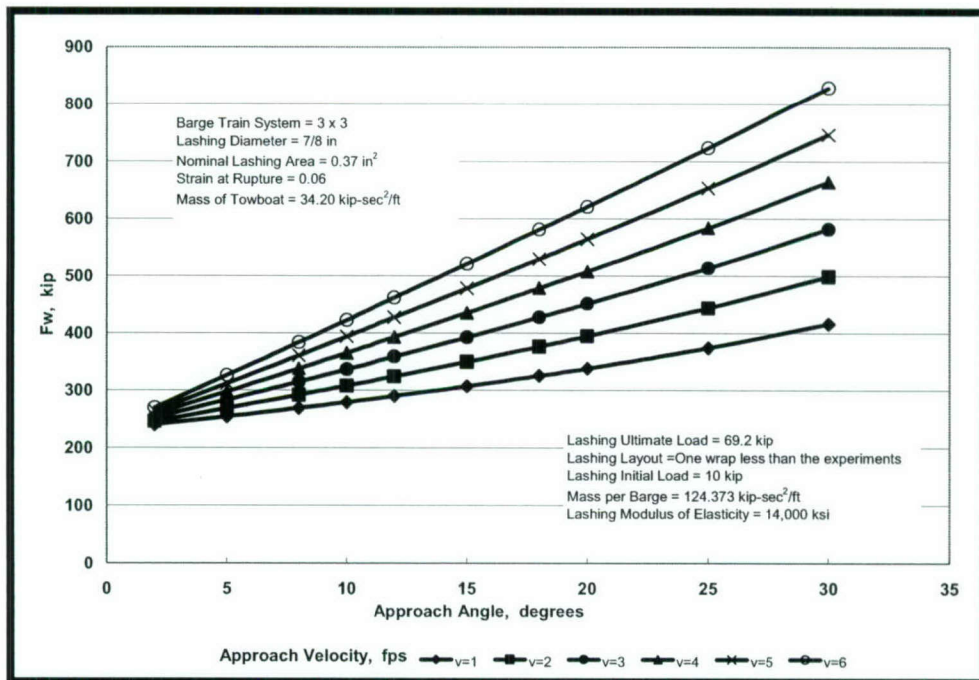


Figure 2-64. Maximum  $F_w$  for a 3x3 Barge Train System – Case LWA

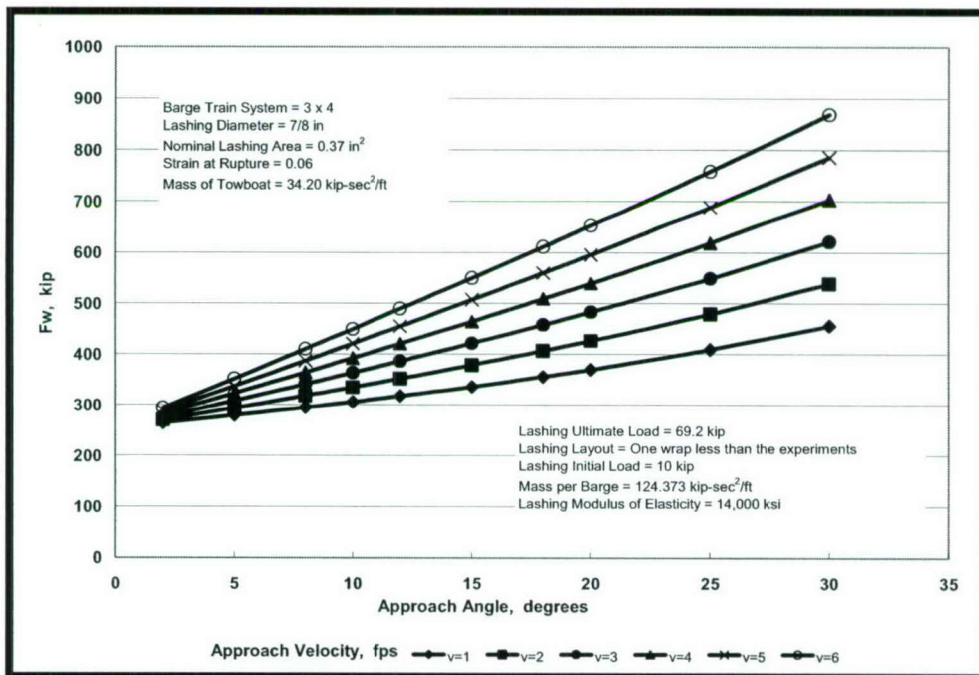


Figure 2-65. Maximum  $F_w$  for a 3x4 Barge Train System – Case LWA



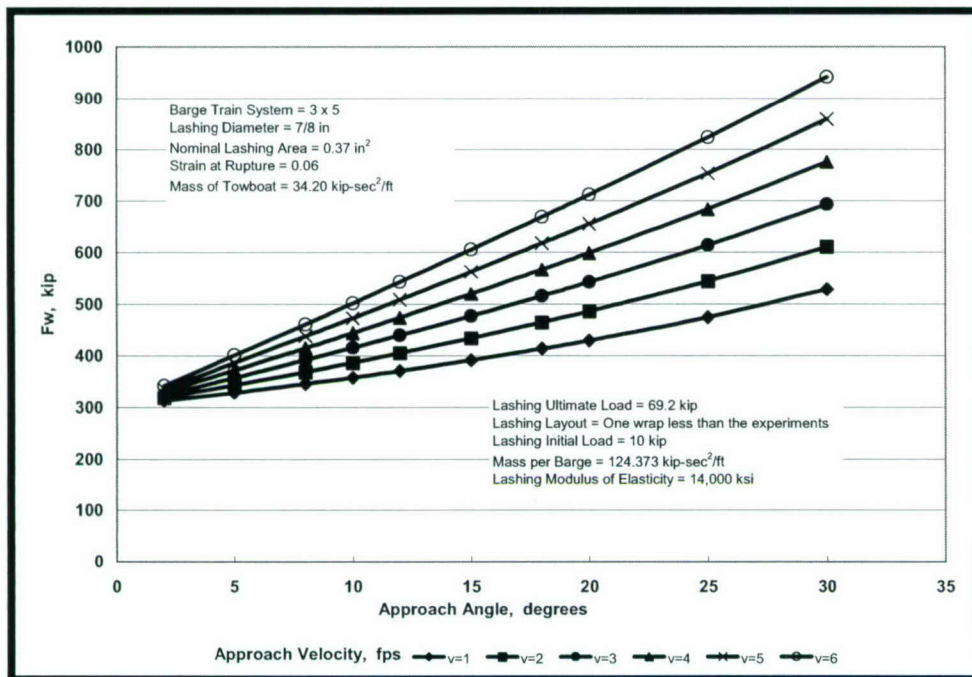


Figure 2-66. Maximum F<sub>w</sub> for a 3x5 Barge Train System – Case LWA

Table 2-12. Mechanical Properties of Lashing – Case LWB.

Lashing Layouts	One Wrap Less Than the 1998 Experiments Layout	
Lashing Diameter	7/8	in.
Breaking Strength	55.4	kip
Nominal Area	0.37	sq in.
Rupture Strain	5	%

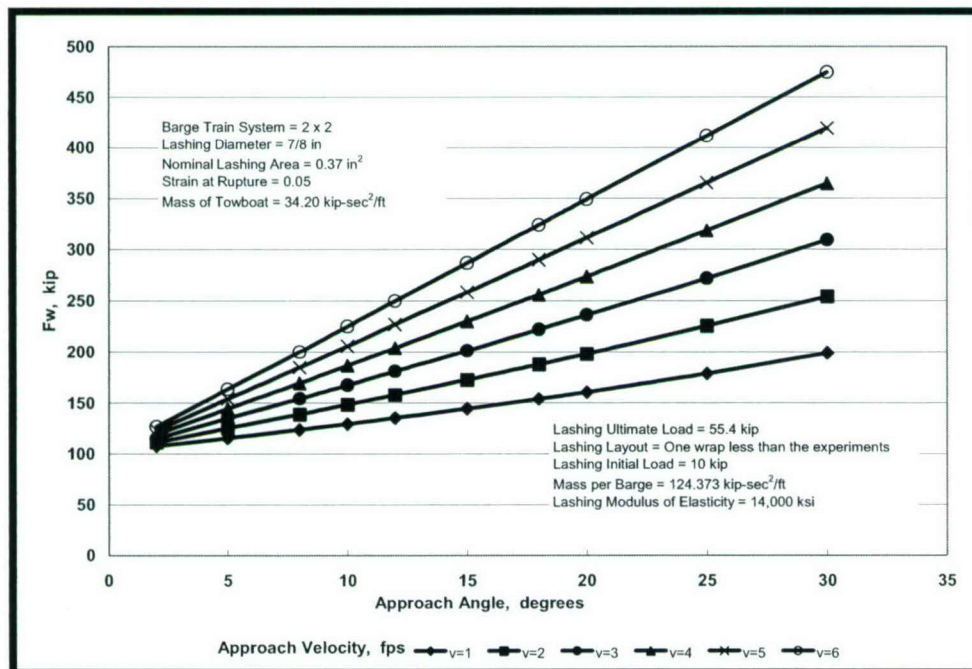


Figure 2-67. Maximum F<sub>w</sub> for a 2x2 Barge Train System – Case LWB

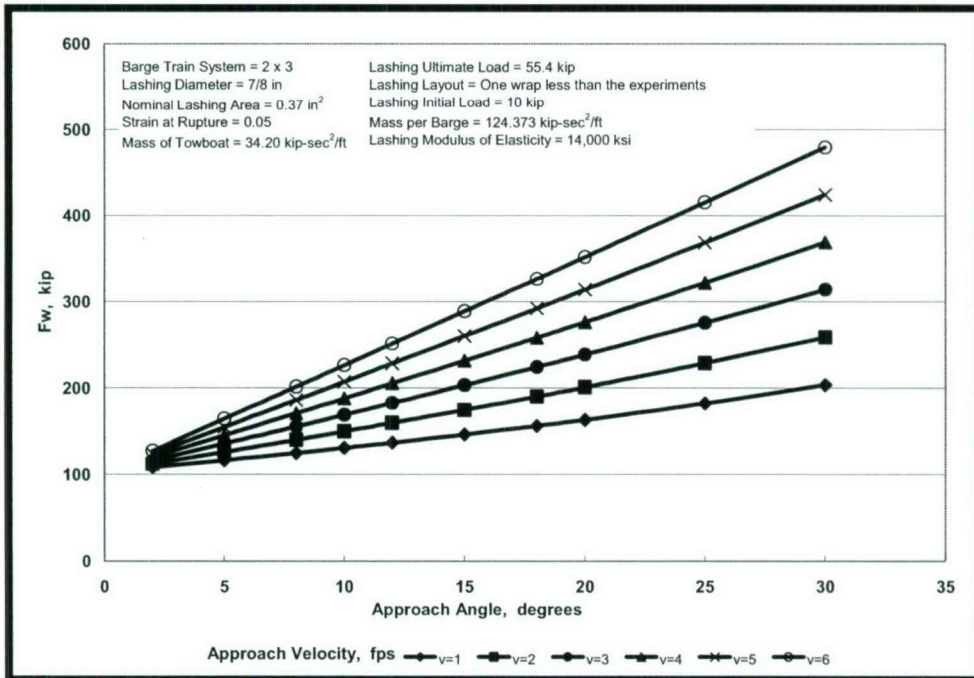


Figure 2-68. Maximum  $F_w$  for a 2x3 Barge Train System – Case LWB

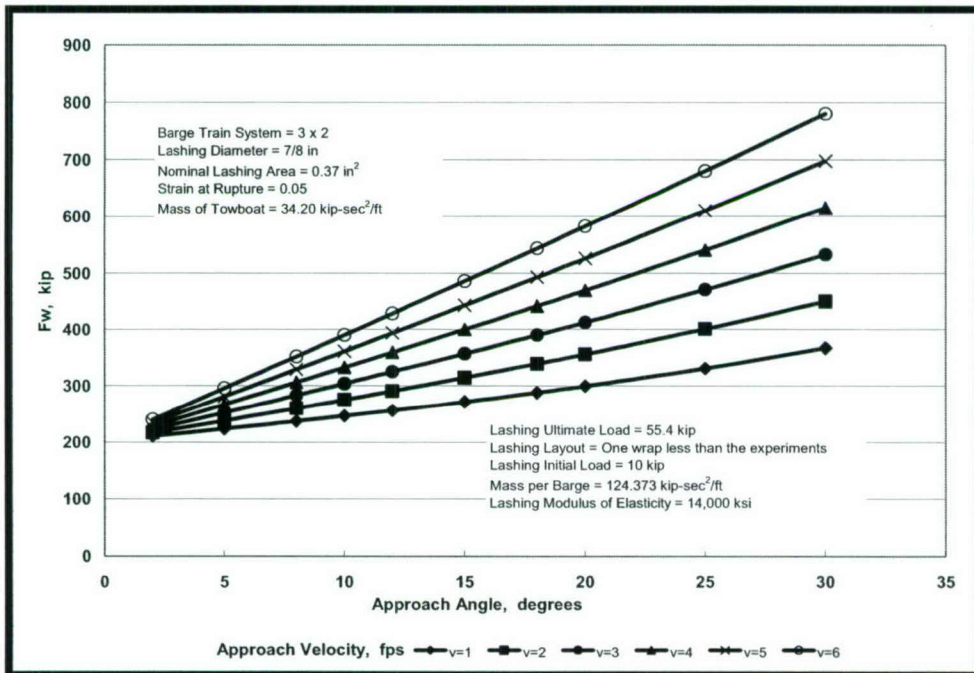


Figure 2-69. Maximum  $F_w$  for a 3x2 Barge Train System – Case LWB



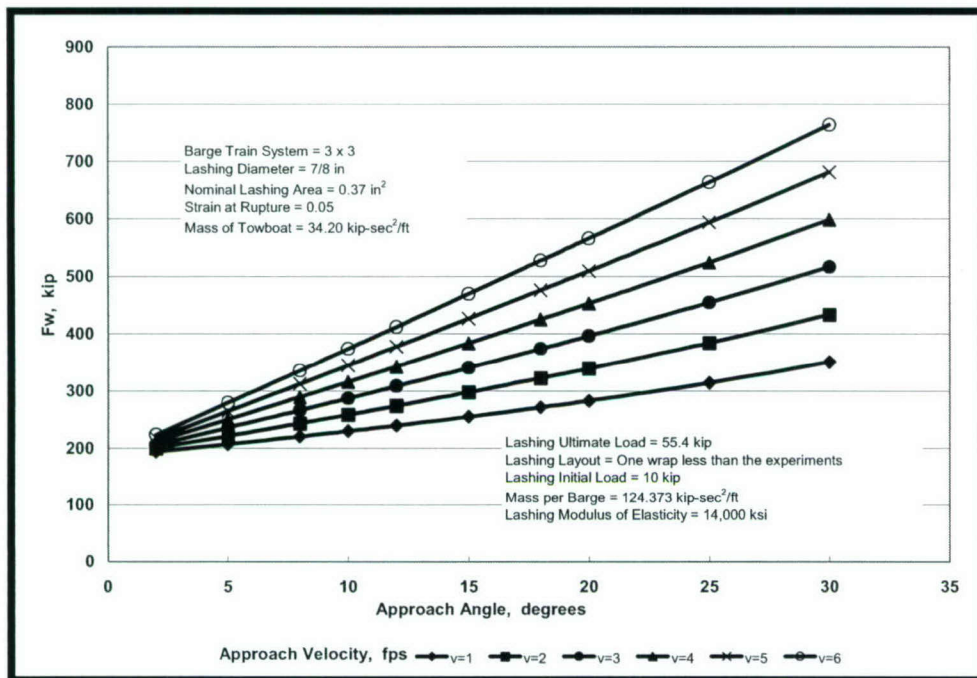


Figure 2-70. Maximum  $F_w$  for a 3x3 Barge Train System – Case LWB

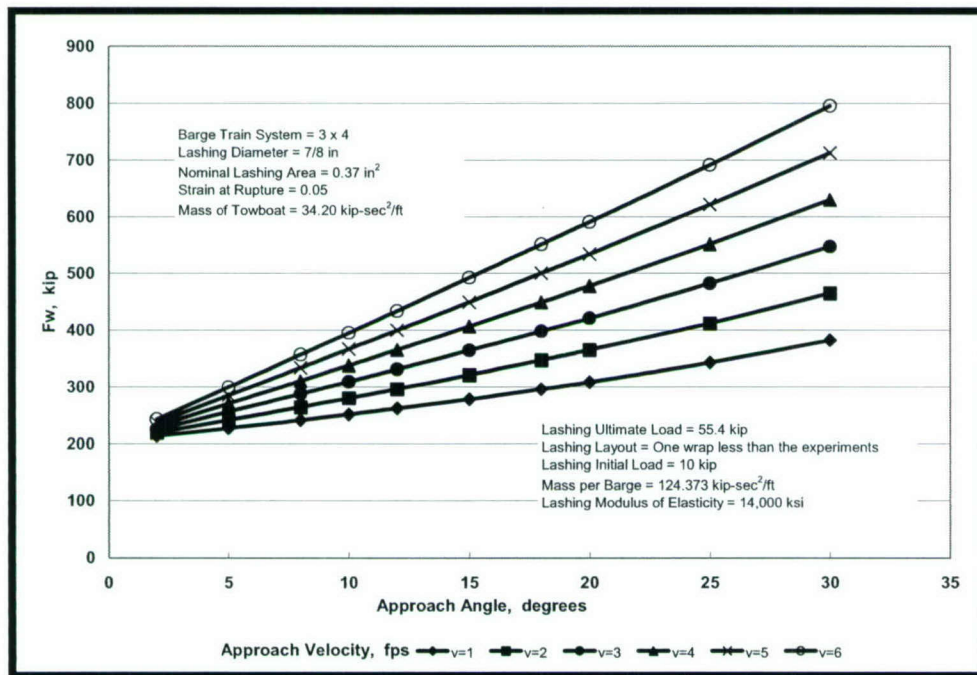


Figure 2-71. Maximum  $F_w$  for a 3x4 Barge Train System – Case LWB

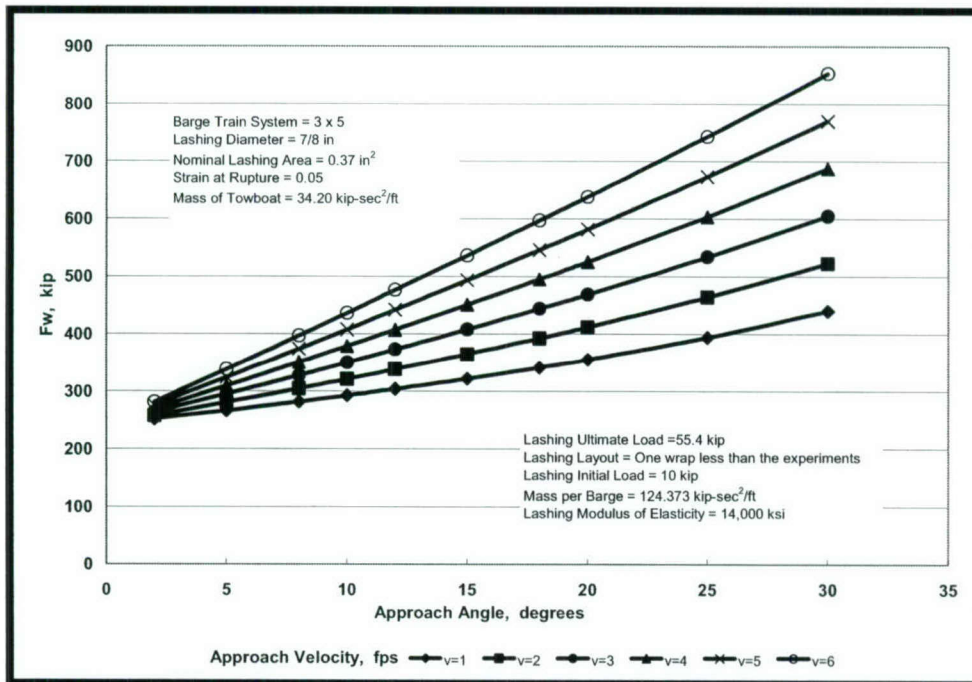


Figure 2-72. Maximum  $F_w$  for a 3x5 Barge Train System – Case LWB

### 2.5.3 Limiting Impact Forces Computed for 1-in. Diameter New Wire Rope

The results of the limiting impact forces computed for the 1-in. diameter new wire rope are presented next. Table 2.13 lists the parameters used. The case identification is now “LWC” (Less Wrap case C). The results of this case can be compared with the set of results obtained with Case C presented in Section 2.3.

Figures 2.73 through 2.78 present the variation of the maximum force normal to the wall for barge train systems 2x2, 2x3, 3x2, 3x3, 3x4, and 3x5, respectively. Additional input data are the mass of the barge train, mass of the towboat, and the lashing initial load. Each figure shows the values used in this set of calculations.

### 2.5.4 Limiting Impact Forces Computed for 1-in. Diameter Used Wire Rope

The results of the limiting impact forces computed for the 1-in. diameter used wire rope are presented next. Table 2.14 lists the parameters used. The case identification is now “LWD” (Less Wrap case D). The results of this case can be compared with the set of results obtained with Case D presented in Section 2.3. Figures 2.79 through 2.84 present the variation of the maximum force normal to the wall for barge train systems 2x2, 2x3, 3x2, 3x3, 3x4, and 3x5, respectively. Additional input data are the mass of the barge train, mass of the towboat, and the lashing initial load. Each figure shows the values used in this set of calculations.

Table 2-13. Mechanical Properties of Lashing – Case LWC.

Lashing Layouts	One Wrap Less Than the 1998 Experiments Layout	
Lashing Diameter	1	in.
Breaking Strength	89.8	kip
Nominal Area	0.48	sq in.
Rupture Strain	6	%



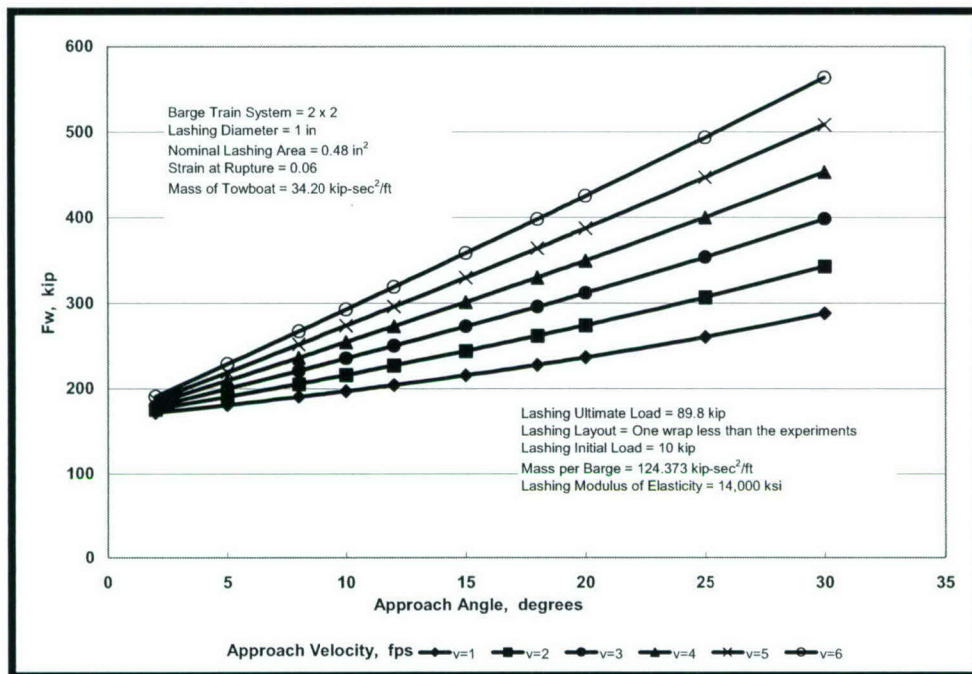


Figure 2-73. Maximum  $F_w$  for a 2x2 Barge Train System – Case LWC

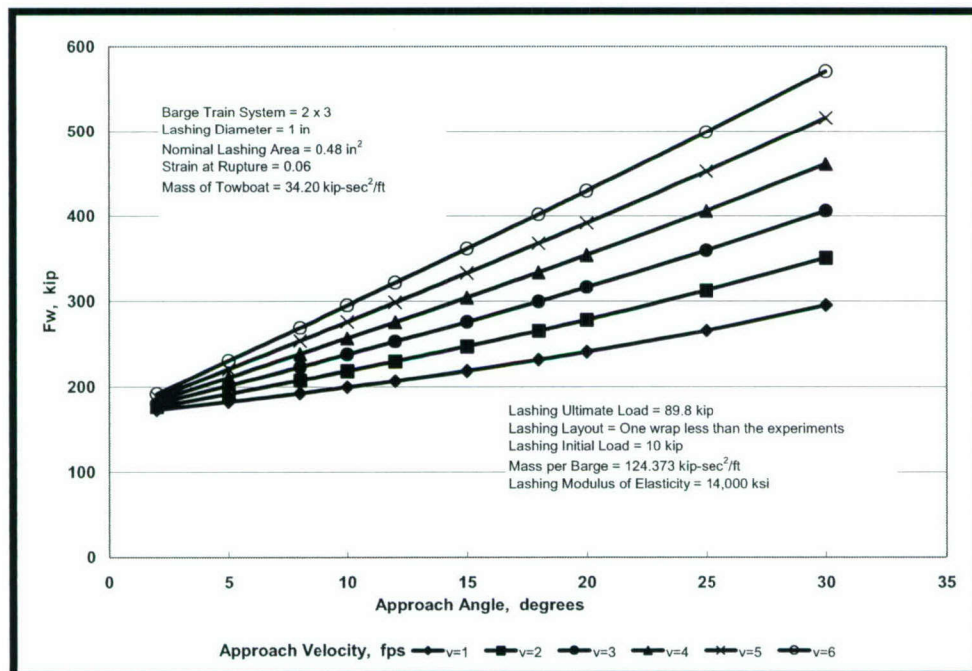


Figure 2-74. Maximum  $F_w$  for a 2x3 Barge Train System – Case LWC

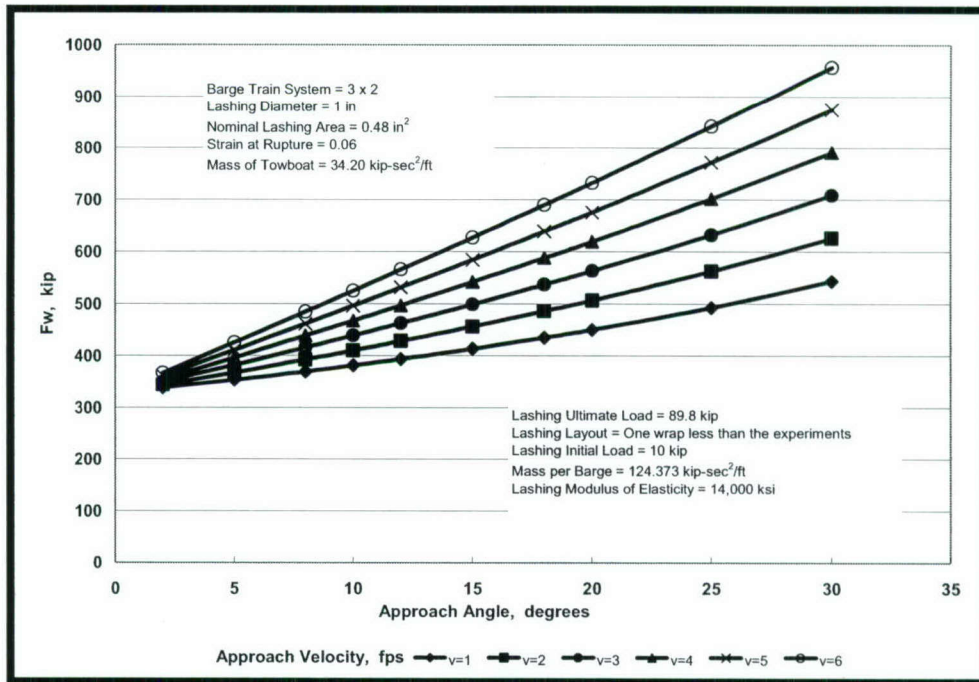


Figure 2-75. Maximum  $F_w$  for a 3x2 Barge Train System – Case LWC

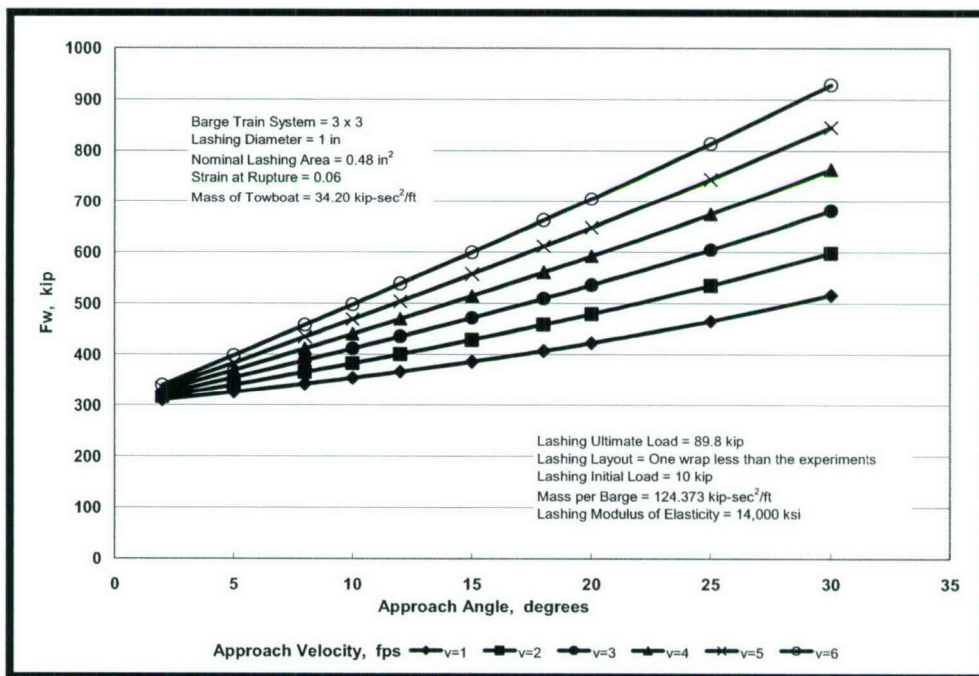


Figure 2-76. Maximum  $F_w$  for a 3x3 Barge Train System – Case LWC



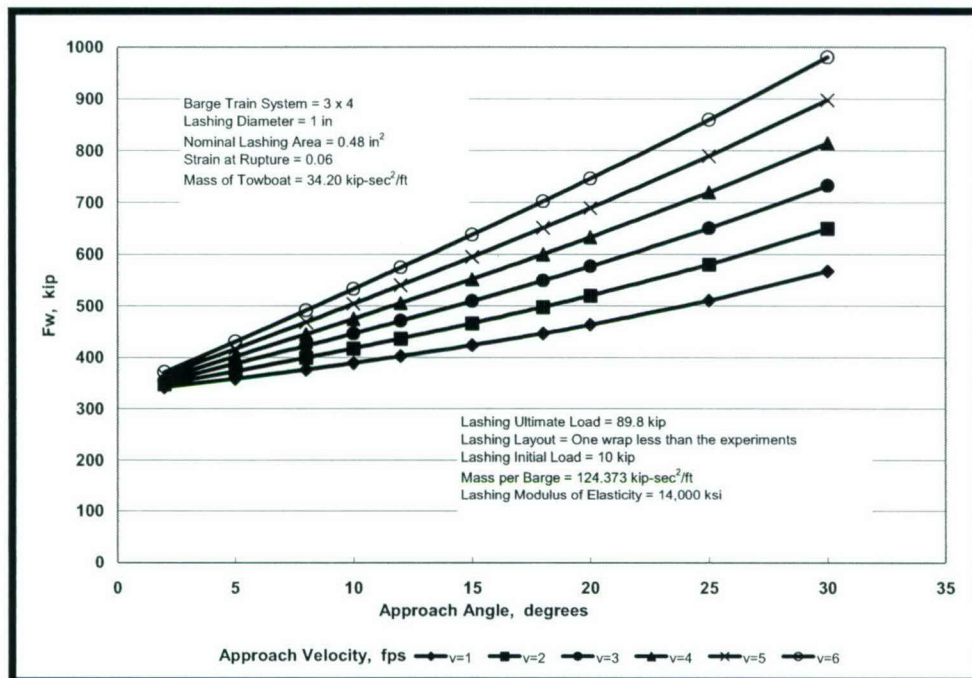


Figure 2-77. Maximum  $F_w$  for a 3x4 Barge Train System – Case LWC

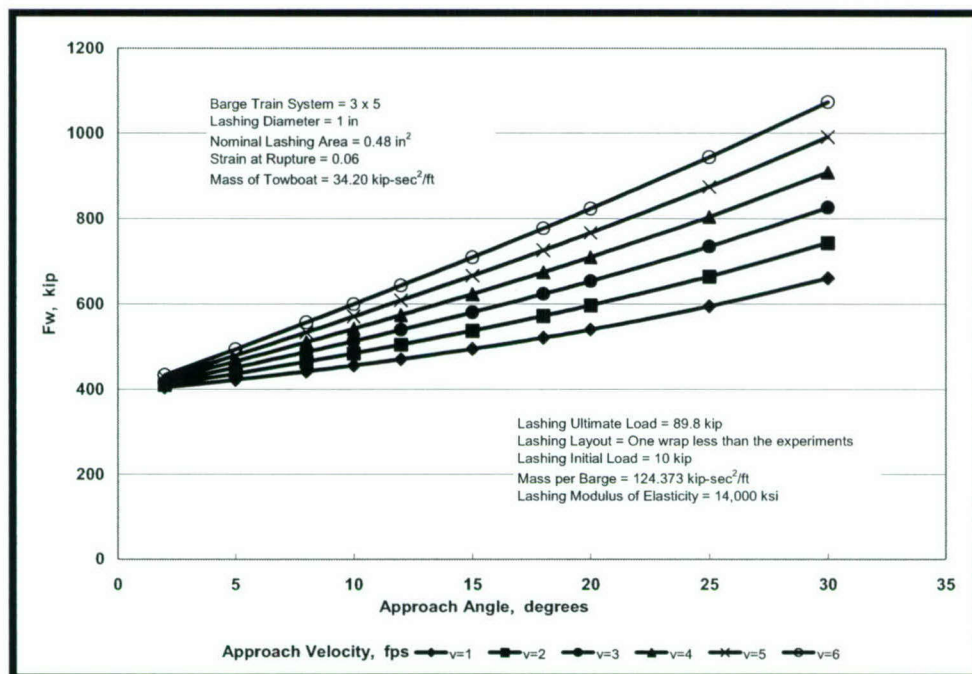


Figure 2-78. Maximum  $F_w$  for a 3x5 Barge Train System – Case LWC

Table 2-14. Mechanical Properties of Lashing – Case LWD

Lashing Layouts	One Wrap Less Than the 1998 Experiments Layout	
Lashing Diameter	1	in.
Breaking Strength	71.8	kip
Nominal Area	0.48	sq in.
Rupture Strain	5	%

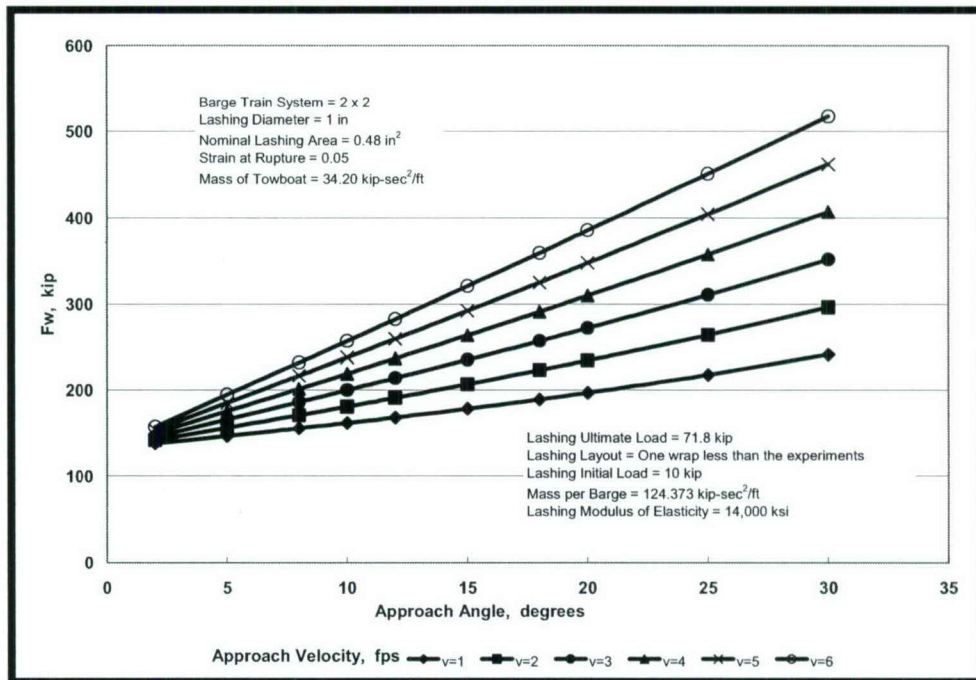


Figure 2-79. Maximum  $F_w$  for a 2x2 Barge Train System – Case LWD

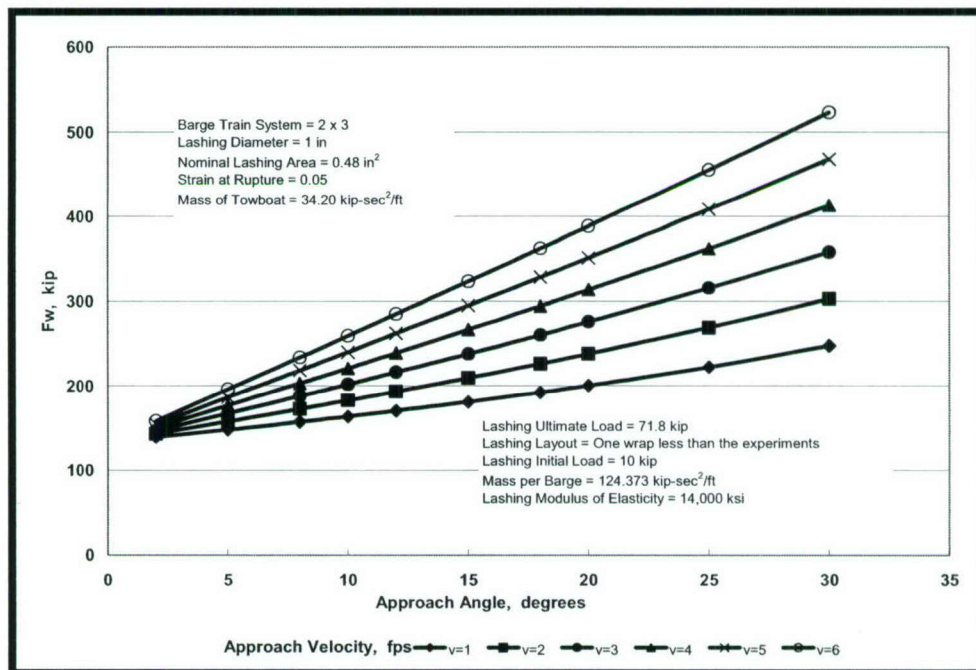


Figure 2-80. Maximum  $F_w$  for a 2x3 Barge Train System – Case LWD



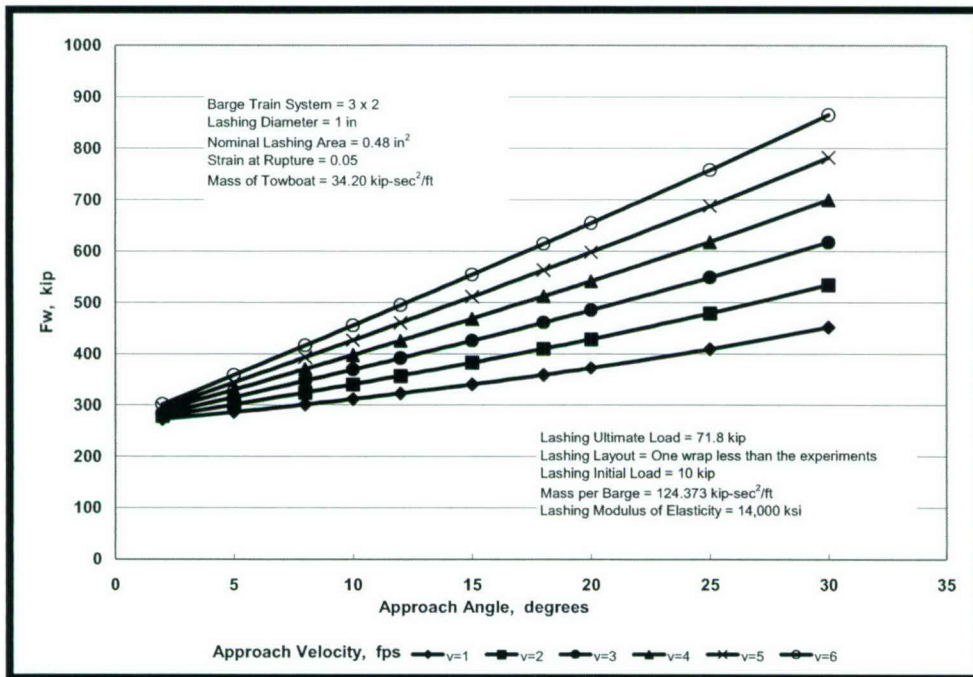


Figure 2-81. Maximum  $F_w$  for a 3x2 Barge Train System – Case LWD

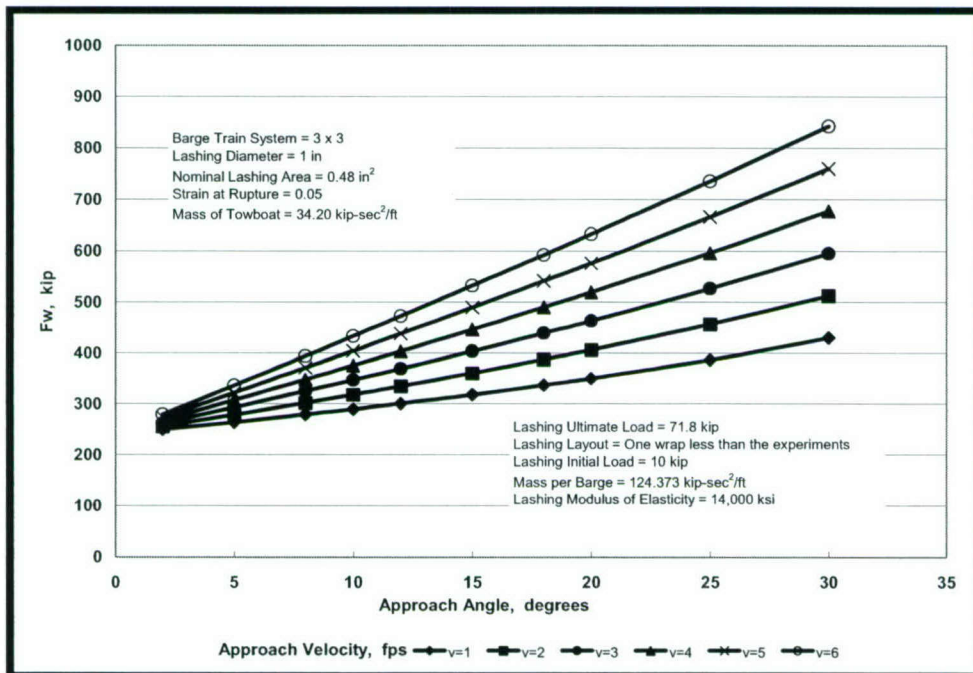


Figure 2-82. Maximum  $F_w$  for a 3x3 Barge Train System – Case LWD

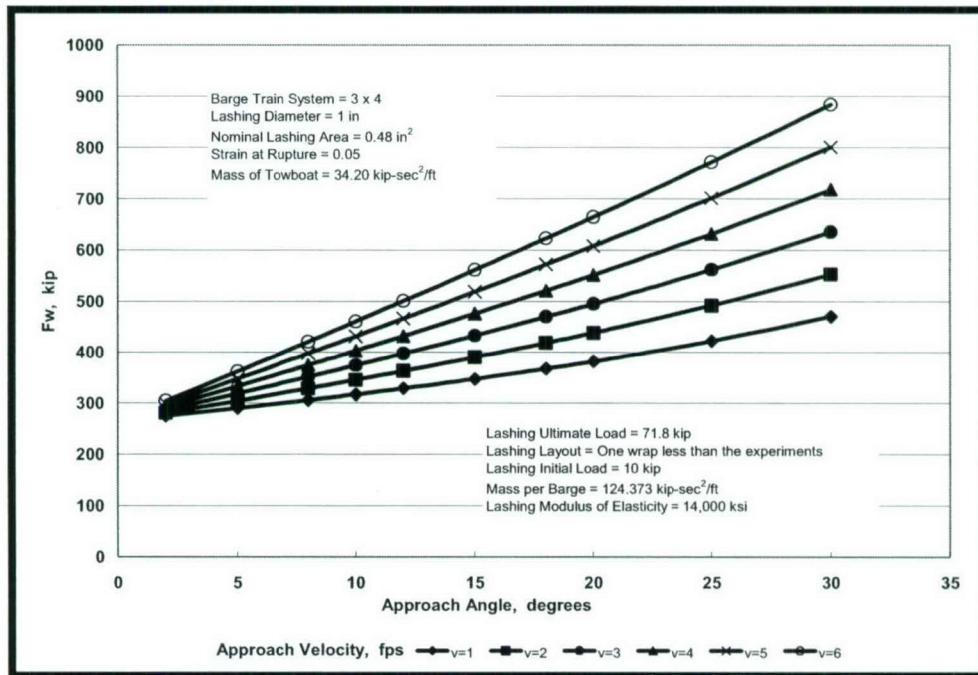


Figure 2-83. Maximum  $F_w$  for a 3x4 Barge Train System – Case LWD

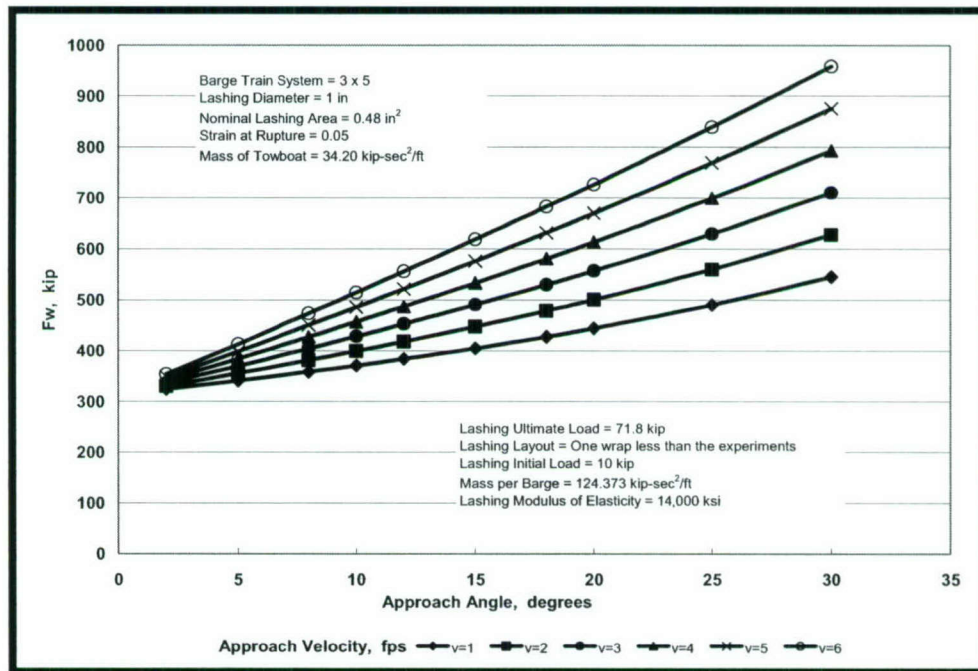


Figure 2-84. Maximum  $F_w$  for a 3x5 Barge Train System – Case LWD

## 2.6 “Glancing Blow” Results Summary

This chapter presented the results of the parametric study for the “glancing blow” impact event. The results showed the following tendencies:



1. The impact force normal to the wall increases with an increase in the approach angle.
2. The impact force normal to the wall increases with an increase in the approach velocity.
3. Increasing the number of wraps increases the impact force.
4. Increasing the number of barges in the barge train, also increases the impact force.
5. The larger lashing diameter produces a higher impact force.
6. A higher ultimate lashing load produces a higher impact force.
7. A higher ultimate strain produces a higher impact load.
8. New lashings result in a greater impact load than used lashings.

These observations are expected from the logical point of view. However, the magnitude of the impact force is now described based on the variations of the fundamental parameters that involved the impact process of a barge train and rigid wall based on the lashing limit states.

## 3 Head-On Impact Forces

---

### 3.1 Longitudinal Failure Mechanism

A barge train system consists of a group of barges joined together with steel cables, referred to as lashings. These lashings define a system of potentially weak zones at each barge connection. The motion of each barge relative to the other has direct bearing on how the barge train system distributes the impact forces among the barges during the impact process. As has been observed during barge train impact events, an almost direct impact of a barge train system on an end cell or nose pier can produce a failure of lashings in the longitudinal axis of the barge system. This failure extends from the bow to the aft of the barge train system. This is comparable to a shear failure mechanism in which the barge train separates into two columns of barges with one system of barges moving relative to the other system of barges. Figure 3.1 shows an idealized example of this failure mechanism for a barge train that impacts a concrete lock wall at an approach angle of  $\theta = 90$  degrees to the impacted structure. This potential failure mechanism is designated as the Longitudinal Failure Mechanism. This failure mechanism is based on the relative motion of two systems of barges (System one and System two) as shown in Figure 3.1.

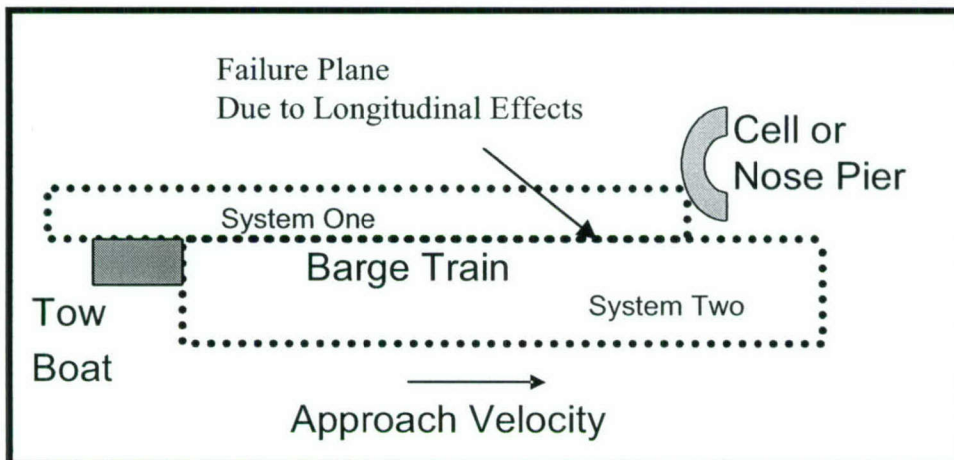


Figure 3-1. Longitudinal Failure Mechanism for a Head-On Impact ( $\theta = 90$  deg)



Figure 3.1 shows an idealized image of a barge train impacting an end cell or nose pier and the development of a failure plane along the longitudinal axis of the system. Based on this figure, two systems of barges can be identified. The system that is in a direct contact with the wall is referred to as System one and the remaining barges form System two. If the impact is head-on with the corner barge of the barge train, then the row of lashings between the first and second row of barges along the longitudinal axis will deform more than the other lashings in the barge train. In this idealized failure mechanism both systems of barges are assumed to be rigid and no transverse relative motion is allowed.

In this simplified model, each of the barge systems is idealized as a rigid body and the wall is assumed rigid. When barge System one impacts the *rigid* wall head-on (as depicted in Figure 3.1), it is subject to a boundary condition of no further forward movement. The tendency for barge System two would be for it to continue its forward motion if it were not subject to “constraints.” Note that System two is not subject to the same severe constraint that System one is (i.e., forward movement being prevented by the presence of a rigid wall). Instead, System two is subject to a “constraint” that is imposed by its lashings connection to System one. It is reasoned that barge System two rigid body will have to decelerate only because it is “lashed” to barge System one with a finite number of cables (i.e., lashings), each with a finite tensile strength.

Note that in the extreme, should the lashings between System two and System one be of zero or only a nominal tensile strength; System two would continue its forward motion without decelerating. It is further reasoned that when System one stops its forward motion upon impact with a rigid wall, barge System one will decelerate at a more rapid rate than will System two (Figure 3.2). Consequently, it is envisioned for this simplified model that the deceleration of barge System two will be at far different and a lower deceleration rate than occurs for System one. The magnitude of the deceleration for System two is a function of the number and orientation of the lashings as well as their size, ultimate capacity and condition (e.g., new, used but in good condition, used and in poor condition, etc.).

In this model, the Longitudinal failure mechanism, allows the relative displacement between barges in the local (barge) “x” direction. In this way, all the lashings along the longitudinal failure plane will break by means of the relative displacement between barges of System one and System two, as shown in Figure 3.1. The relative displacement can be obtained by assuming different linear accelerations in the global “Y” direction for System one and System two. A zero linear global acceleration in the “Y” direction of System one is assumed in this simplified model because the impact with a *rigid* wall occurs with this system in the global “Y” direction. System two motion continues and the lashings that connect System one to System two will try to stop (or decelerate) System two. Thus, the deceleration of System two is nonzero.

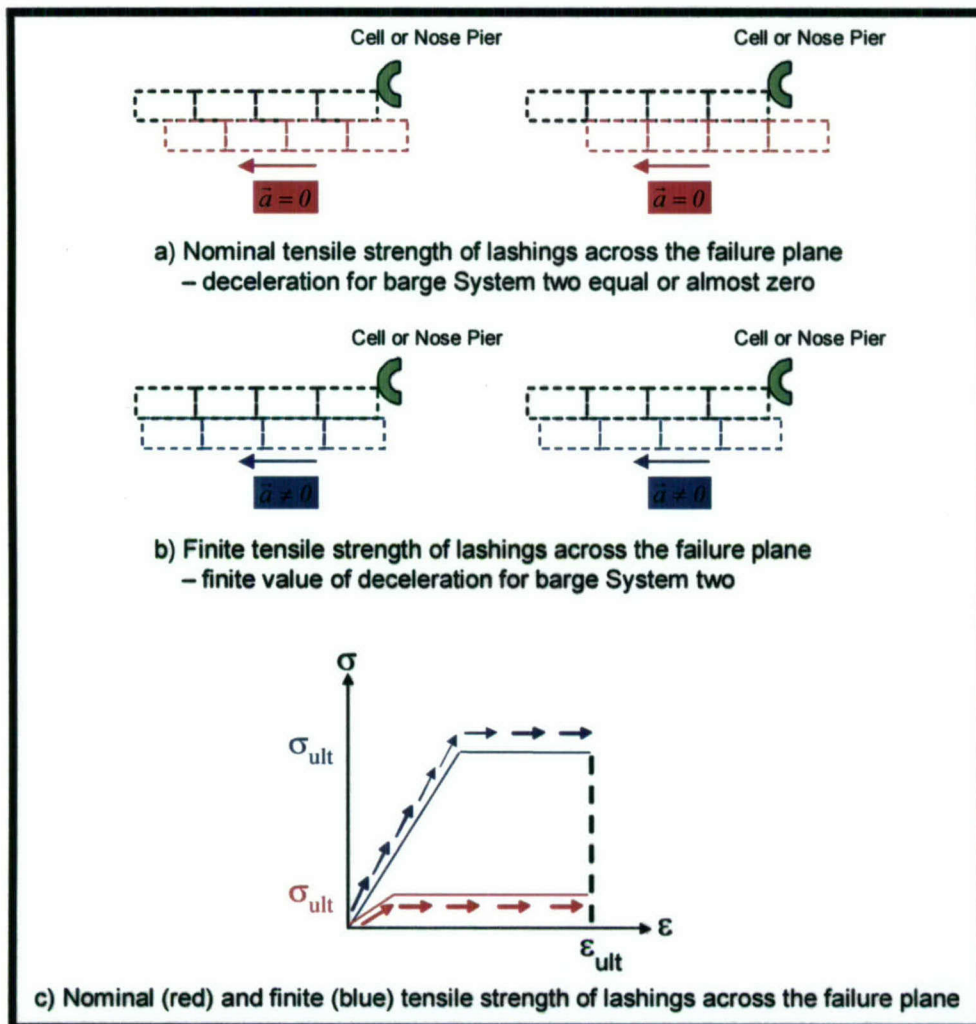


Figure 3-2. Nominal and Finite Tensile Strength of Lashing

In summary, as discussed in Arroyo and Ebeling (2004), the longitudinal failure mechanism is based on the following general assumptions:

1. The linear acceleration in the global "Y" direction in barge System one is assumed to be zero. This means that in the global "Y" direction the barge stops instantly at the moment of impact. This condition ensures the relative motion between the two barge systems.
2. The linear acceleration in the global "X" direction for barge System one is assumed to be equal to the global "X" linear acceleration for barge System two.
3. The angular acceleration for barge System one is assumed to be equal to the angular acceleration for barge System two.
4. Barge System one, which is in contact with the struck wall, abruptly/instantaneously stops motion while barge System two continues motion. The lashings across the longitudinal failure plane provide resistance to the motion of barge System two.



Two special cases exist for the longitudinal failure mechanism when a direct impact occurs (i.e., with an approach angle of 90 degrees): For a 90-degree impact, a central impact or an oblique impact can occur. Considering that the central impact represents an extreme impact event, the next section will present this special case.

### 3.2 Longitudinal Failure Mechanism – Impact at 90 Degrees Without Eccentricity

Central impact occurs when a barge train impacts a cell or nose pier at 90 degrees and the line of action of the impact normal force is align with the center of mass of the entire barge train system. This case can occur when a barge train impacts a bridge pier, a nose pier, or end cells. The lack of loading eccentricity is present because the center of mass of the barge train is aligned with the line of action of the impact force normal to the cell or nose pier. (It is assumed that the mass distribution among the barges is uniform.) Because it is a direct impact, no shear force between the corner barge and the wall is assumed to develop during the impact. In this case, we have also two failure planes because the central barge System stops its motion at impact while the two side systems continue their motion until the lashings fails. Figure 3.3 generally shows this case.

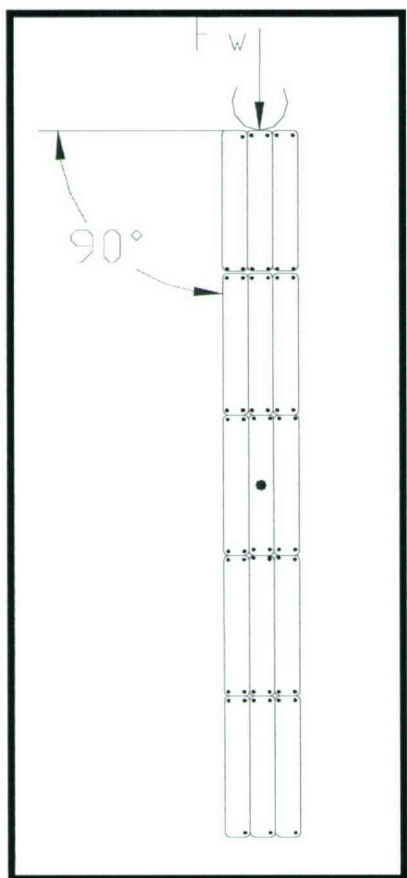


Figure 3-3. Scheme of Barge Train with a Direct Impact without Eccentricity

In this model, the Longitudinal failure mechanism in a direct impact without eccentricity allows the relative displacement between barges in the local (barge) "x" direction, which, for  $\theta = 90$  degrees, corresponds to the global "Y" axis. In this way, all the lashings along the failure planes will break by means of the relative displacements between the barges of System one with those of Systems two and three. System one is defined by the column of center barges that impact the rigid wall and Systems two and three are defined by the side column of barges. The relative displacement between barge systems is obtained by assuming independent linear accelerations in the global "Y" direction for System one, System two, and System three. This simplified impact model assumes zero linear global acceleration in the "Y" direction of System one because impact with a rigid wall occurs for this particular system. Systems two and three continue their motion; and the lashings that connect System one to System two and System one to System three will try to stop or decelerate Systems two and three. Thus, deceleration of Systems two and three are nonzero.

### 3.3 Process of Lashing Failure for the Longitudinal Failure Mechanism

In this simplified impact model, the value computed for the resultant  $F_W$  is dependent on the magnitude of the lashing forces. The relative motion between the barges of System one and System two is produced by a different linear acceleration in the local "x" axis for the two systems. This can be achieved by means of an elongation of the lashing in the forward direction, as shown in Figure 3.4. This incremental relative displacement translates into incremental changes in the lashing forces across the longitudinal failure plane between barge systems. The sequential process to calculate the  $F_W$  is:

1. The initial length of the lashing is calculated using the initial internal force in the lashing. (Lashings usually have a tensile force that is introduced when the barges are initially assembled into a barge train.) If the initial force is known, then the initial elongation produced by the initial force can be calculated.
2. Using the initial length of the lashing, an increment of length is added to the lashing, which then elongates in the longitudinal failure plane. Note that some of the lashings might reduce their internal load should they be oriented opposite to the direction of the relative motion. For example, it is observed in Figure 3.4.a that the green lashings are oriented in a direction such that an increment of relative displacement according to the simplified Longitudinal failure mechanism reduces their internal lashing force.
3. A continuous increment of the relative displacement between the barge systems (and along the longitudinal failure plane) produces an incremental stretch in the red and blue lashings in Figure 3.4.a.



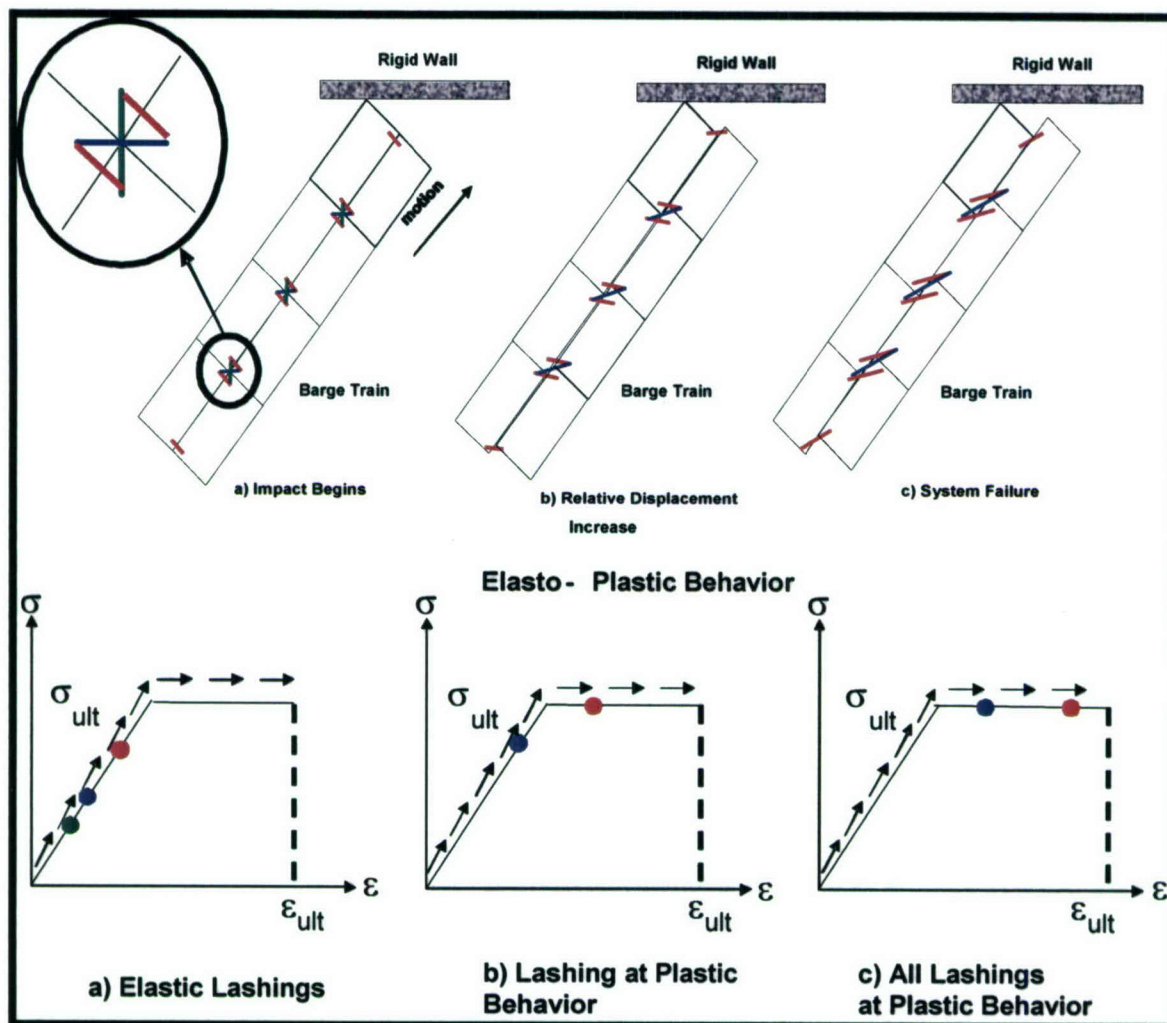


Figure 3-4. Progressive Longitudinal Failure of Lashings Across a Longitudinal Failure Plane Within the Barge Train

4. As the incremental displacements increase, the green lashings ultimately reach a value of zero internal force. This lashing is then deleted from the analysis because it is unstretched.
5. As the idealized image in Figure 3.4.b shows, as the relative motion between barge systems increases, the lashing can reach the horizontal plateau of the elasto-plastic stress-strain model.
6. With sufficient relative deformation between the barge systems, all lashings can break, as shown in the idealized image in Figure 3.4.c.
7. Each of the lashings is likely to reach its ultimate stress value at a different instant during the relative motion process.
8. Should a lashing accrue a strain equal to the ultimate strain, the lashing is assumed to rupture and is removed from the connection system across the Longitudinal failure plane.

It is important to mention that the lashing failure occurs in a sequence; it is not assumed that all lashings reach their ultimate stress at once. As explained in Arroyo and

Ebeling (2004), actual impact response among the barges and the lashings during impact is quite complex. The difference in bit locations and lashing configurations between bits as well as the different initial forces set in the lashings provide the system with an uneven distribution of forces at the connections (lashing locations). In addition, as soon as the corner barge impacts the *rigid* wall, the internal impact wave generated in the barge train reaches all points throughout the barge train at different instants of time, producing different stresses and strains among the lashings. This *simplified model* considers these conditions when the relative motion between barge systems is adopted. This relative motion produces different relative decelerations for the two components in the model of the barge systems in the local “x” axis of the barge train. These different decelerations for System one and System two are responsible for the stress and strain in the lashings across the failure plane.

### 3.4 Additional Information of the Longitudinal Failure Mechanism

In this simplified model, each of the barge systems is idealized as a rigid body and the wall is assumed rigid. When barge System one impacts the *rigid* wall head-on, it is subject to a boundary condition of no further forward movement. The tendency for barge System two would be for it to continue its forward motion if it were not subject to “constraints.” Note that System two is not subject to the same severe constraint that System one is (i.e., forward movement being prevented by the presence of a rigid wall). Instead, System two is subject to a “constraint” that is imposed by its lashings connection to System one. It is reasoned that barge System two rigid body will have to decelerate only because it is “lashed” to barge System one with a finite number of cables (i.e., lashings), each with a finite tensile strength. Note that in the extreme, should the lashings between System two and System one be of zero or only a nominal tensile strength; System two would continue its forward motion without decelerating.

It is further reasoned that, when System one stops its forward movement upon impact with a rigid wall, barge System one will decelerate at a more rapid rate than System two, as shown in Figure 3.2. Consequently, it is envisioned for this simplified model that the deceleration of barge System two will be at far different and a lower deceleration rate than occurs for System one. The magnitude of the deceleration for System two is a function of the number and orientation of the lashings as well as their size, ultimate capacity and condition (e.g., new, used but in good condition, used and in poor condition, etc.). It is important to note that the time of maximum normal force against the rigid wall produced by System one may not coincide with the time of maximum normal force during deceleration of System two. The maximum impact force of System two will depend on the number and orientation of the lashings as well as on their size, ultimate capacity, and condition (e.g., new, used but in good condition, used and in poor condition, etc.). That is, immediately after impact of System one, the force normal to the wall increases and the lashings that keep together System one and System two do not develop the strength until System two begins to move relative to System one. When system two begins to move and the lashings reach their ultimate strength, System one is at rest in the



global “Y” direction. This procedure produces different maximum values of the force normal to the wall.

### 3.5 Parametric Study

This section presents the variation of the force normal to the wall during the impact event. The parametric study was done by modifying the following parameters: (1) approach velocity, (2) wire rope diameter, (3) wire rope nominal breaking strength, (4) wire rope rupture strain, (5) size of barge train, and (6) lashing layouts. Each one of these variables will be discussed next.

The approach velocity is the velocity of the barge train system measured in the (local barge) longitudinal axis of the barge train system. The Limit\_LASHING computer program can accept two kind of approach velocity, the approach velocity of the barge train system in each local “x” and “y” axes. In the parametric study, the approach velocity refers to the velocity in the local “x” axis of the barge train. The velocity in the local “y” axis is assumed to be zero because a head-on impact is analyzed in this parametric study. The approach velocity in the local “x” axis used for the parametric study for the head-on impact events 1, 2, 3, 4, 5, and 6 fps.

One kind of wire rope (lashings) was used in the parametric study, 6x19 Independent Wire Rope Cores (6x19 IWRC). The parametric study considers two diameters, 7/8 in. and 1 in. (the two most used dimensions in the towing industry). It is important to mention that the nominal area for each of these lashings are 0.37 sq in. and 0.48 sq in. for the lashings with diameters of 7/8 in. and 1 in., respectively. The Young’s modulus of elasticity for this kind of wire rope is estimated at 14,000 ksi.

The breaking strength of this lashing is another important parameter in the parametric analysis. The breaking strength is estimated based on the condition of the lashing. If the wire rope is new, the breaking strength is estimated as 69.2 kip and 89.8 kip for the lashings with diameters of 7/8 in. and 1 in. respectively. However, if a used lashing is assumed, the breaking strength is reduced. In the parametric study, the breaking strength for the used wire rope was estimated as 55.4 kip and 71.8 kip for the lashings with diameters of 7/8 in. and 1 in., respectively. The rupture strain is a property of the wire rope that is related to the nominal breaking strength. This is the maximum strain the lashing can reach before the lashing breaks. Also, the condition of the wire rope affects the value of this property. For a new wire rope and a used wire rope, the rupture strain is estimated as 6 percent and 5 percent, respectively. Table 3.1 lists the mechanical properties of the wire rope used in the parametric study.

Finally, the following sections present the results of the parametric study performed to a series of typical barge train configurations. Among the configurations used are the 2x2, 2x3, 3x2, 3x3, 3x4, and 3x5 barge train. The first number indicates the number of barges in the local “y” axis and the second number indicates the amount of barges in the local “x” axis. That is, a 3x5 barge train consists on three rows and five columns of

barges. Figure 3.5 shows the barge train configuration used in the parametric analysis. In the parametric study, three lashing layouts were used.

Table 3-1. Mechanical Properties of Wire Rope Used in the Parametric Study.

Wire Rope	Diameter (in.)	New Wire Rope Nominal Breaking Strength, $P_{ult}$ (kip)	E (ksi)	Nominal Area (in. <sup>2</sup> )	New Wire Rope Rupture Strain, $\epsilon_{Rupture}$ (%)	Used Wire Rope Nominal Breaking Strength, $P_{ult}$ (kip)	Used Wire Rope Rupture Strain, $\epsilon_{Rupture}$ (%)
6 x 19 with IWRC	7/8	69.2	$14 \times 10^3$	0.37	6	55.4	5
	1	89.8		0.48		71.8	

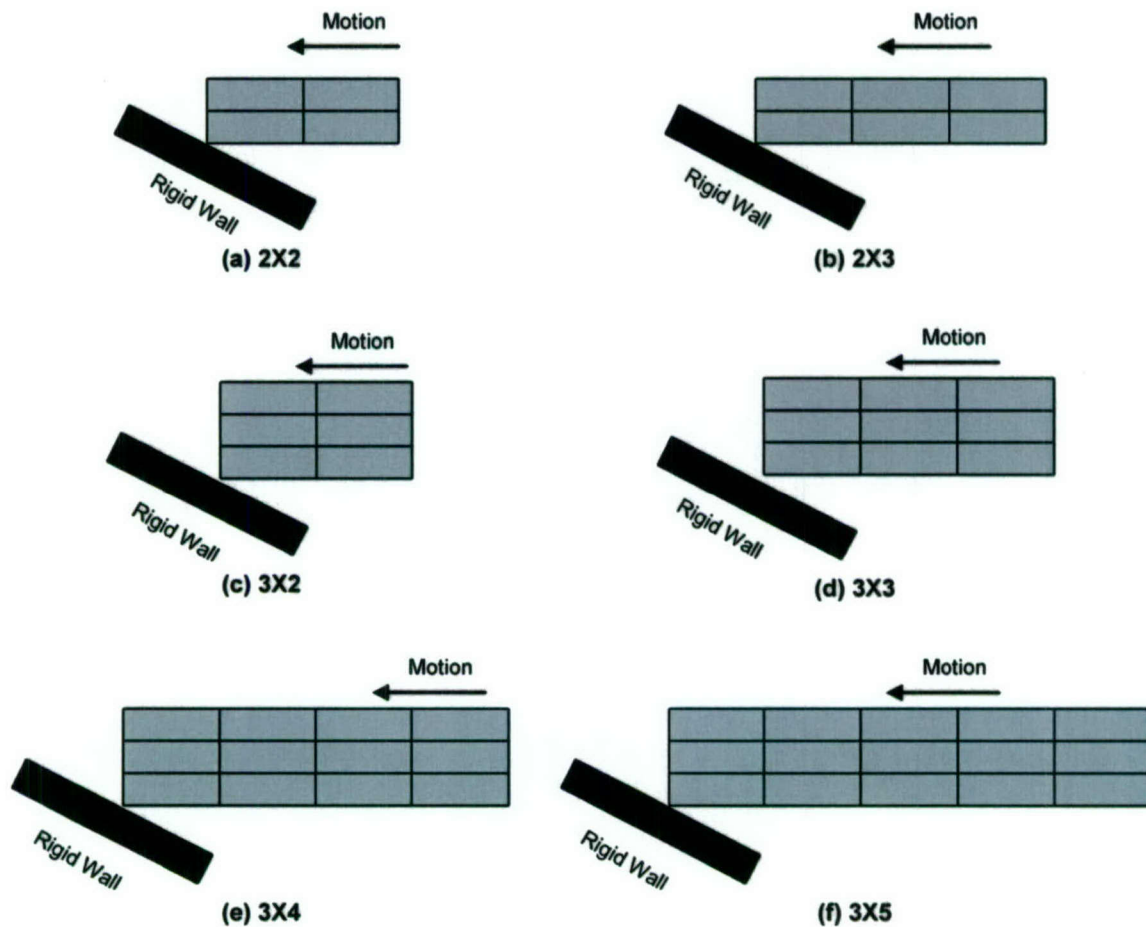


Figure 3-5. Barge Train Configuration Used in the Parametric Study



The principal layout was the one used in the full-scale experiments performed in 1998 and reported in Patev, Barker and Koestler (2003), and Arroyo and Ebeling (2004). Figures 3.6 through 3.9 show these lashing configurations. These configurations were taken as the baseline of the parametric study in terms of the parametric study.

Configuration one (Figure 3.6) was the arrangement used in the 1998 full-scale experiments to join a pair of barges along the outside edge of the barge train. It is also the configuration used on the bow, port, aft, and starboard sides. It consists of three turns of the bits along the edge of the two joined barges. Figure 3.6 also shows the generic sequence of the bits connected. The name “generic sequence” means that the assigned numbers can change in each model configuration. However, the lashing configuration must follow the sequence shown in Figure 3.6.

Three configuration levels were available at the center joints where four barges come together. In the 1998 experiments, there were eight of these connections because 15 barges were joined together. Figures 3.6 through 3.9 show the top, middle, and bottom configurations. The bottom layer (configuration two) is similar to configuration one.

This configuration is considered to be a separate configuration because it is associated with the center connections between barges. The middle configuration at the inner connections, designated configuration three, is like a “scissor” passing each lashing over the edge of the joined barges three times. Finally, configuration four, or the top layer in the inner connection, has two turns for each lashing over the edge of the joined barges. Note that the configurations shown in these figures are not the only configurations available for use in Limit\_LASHING computer program.

The user specifies the coordinates of each bit on the barges to determine the angle that each force (within the lashing) makes with the local axis of the system. Using these coordinates, Limit\_LASHING calculates the necessary angles to determine the components of the internal force for the lashings in the local axis. It is important to note that these arrangements are prepared for both a forward and backward motion of the lashings.

Two additional lashing configurations were used to describe the barge train impact process. The lashing properties and configurations are the most important parameters in the limit states based on the lashing ultimate strength. One additional wrap and one less wrap for each lashing of the baseline layout used on the 1998 experiments are the two additional layouts used on the parametric study. These two conditions cover the cases where the barge train is well connected and weakly connected.

Finally, it is important to mention that the approach angle, which is the angle that orients the longitudinal axis of the barge train with respect to the longitudinal axis of the rigid wall, is equal to 90 degrees for the head-on impacts.

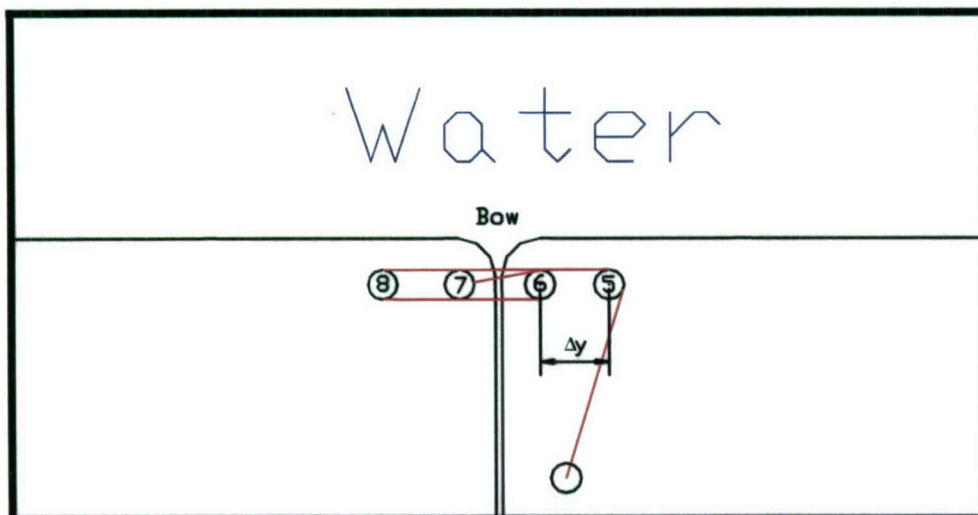


Figure 3-6. Configuration 1 Located at Bow, Port, Aft, and Starboard Sides: Generic Sequence - 7,6,8,5

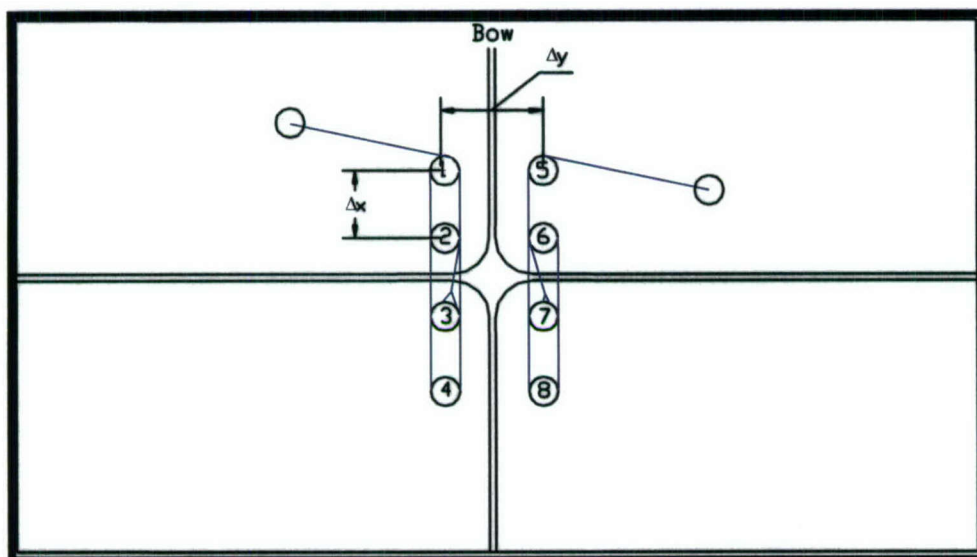


Figure 3-7. Configuration 2 Located at the Bottom Layer in the Inside Connection: Generic Sequence - 7, 6, 8, 5 and 3, 2, 4, 1



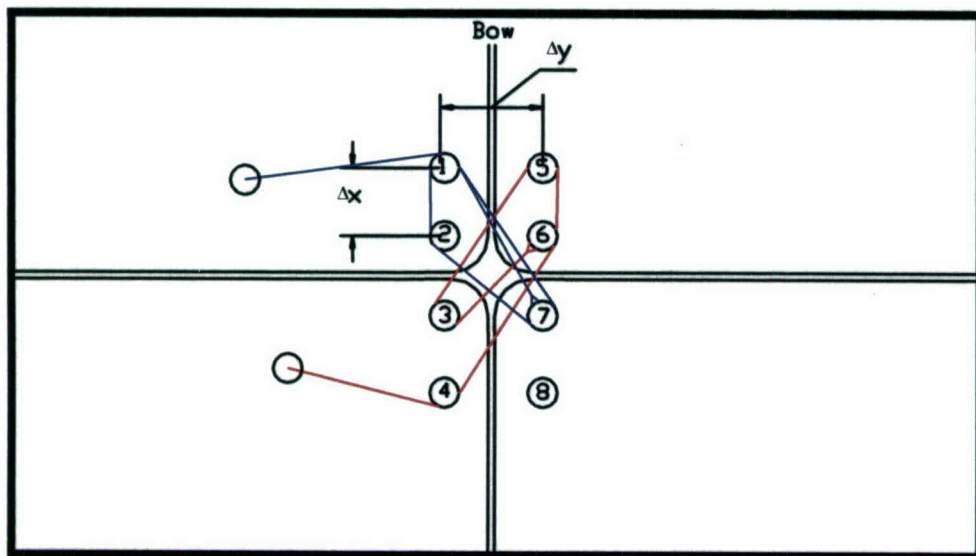


Figure 3-8. Configuration 3 Located at the Middle Layer in the Inside Connection: Generic Sequence – 6, 3, 5, 6, 4 and 7, 1, 2, 7, 1

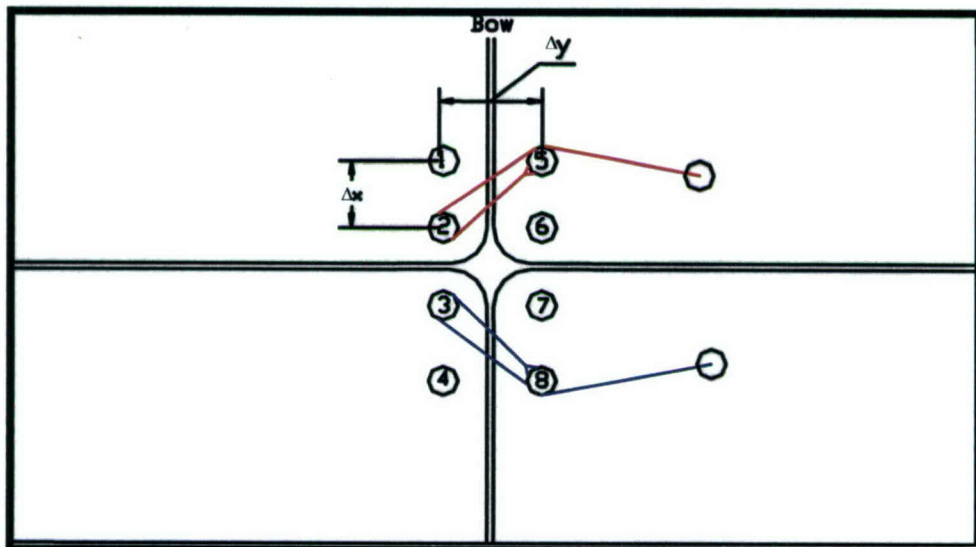


Figure 3-9. Configuration 4 Located at the Top Layer in the Inside Connection: Generic Sequence – 5, 2, 5 and 8, 3, 8

### 3.5.1 Limiting Impact Forces Computed for 7/8-in. Diameter New Wire Rope

The results of the limiting impact forces computed for the 7/8-in. diameter new wire rope are presented next. Table 3.2 lists the parameters used.

Table 3-2. Mechanical Properties of Lashing – Case A.

Lashing Layouts	As in the 1998 Experiments	
Lashing Diameter	7/8	in.
Breaking Strength	69.2	kip
Nominal Area	0.37	sq in.
Rupture Strain	6	%

Figure 3.10 shows the variation of the maximum force normal to the wall for barge train systems 3x2, 3x3, 3x4, and 3x5 in a head-on impact. Additional input data are the mass of the barge train, mass of the towboat, and the lashing initial load. Figure 3.10 also shows the values used in this set of calculations.

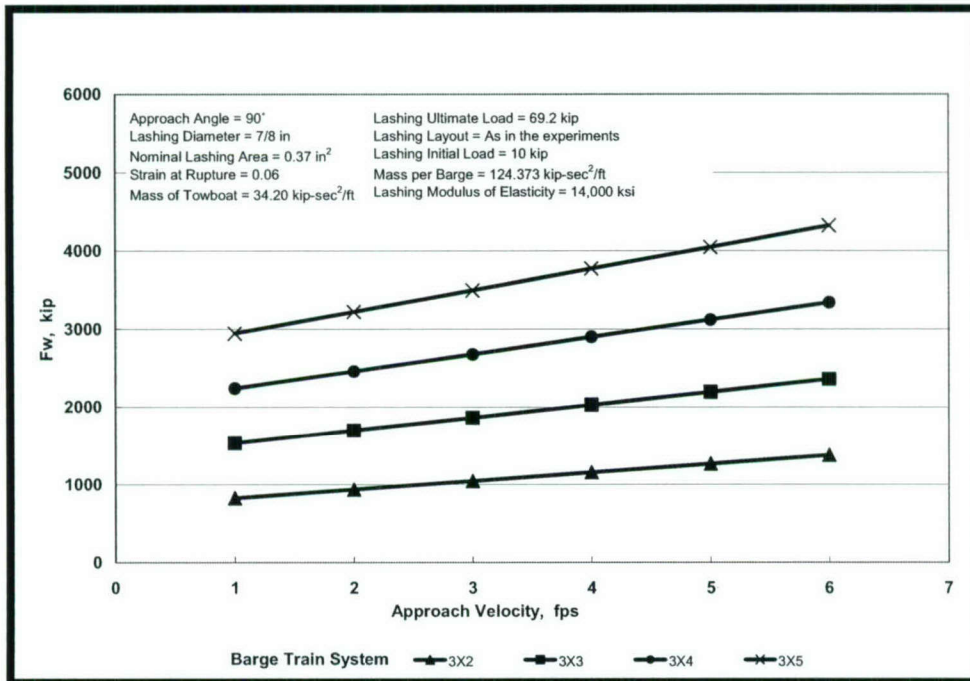


Figure 3-10. Maximum Head-On Impact  $F_w$  – Case A

### 3.5.2 Limiting Impact Forces Computed for 7/8-in. Diameter Used Wire Rope

The results of the limiting impact forces computed for the 7/8-in. diameter used wire rope are presented next. Table 3.3 lists the parameters used.

Figure 3.11 shows the variation of the maximum force normal to the wall for barge train systems 3x2, 3x3, 3x4, and 3x5 in a head-on impact. Additional input data are the mass of the barge train, mass of the towboat, and the lashing initial load. Figure 3.11 shows the values used in this set of calculations.

### 3.5.3 Limiting Impact Forces Computed for 1-in. Diameter New Wire Rope

The results of the limiting impact forces computed for the 1-in. diameter new wire rope are presented next. Table 3.4 lists the parameters used.

Figure 3.12 presents the variation of the maximum force normal to the wall for barge train systems 3x2, 3x3, 3x4, and 3x5 in a head-on impact. Additional input data are the mass of the barge train, mass of the towboat, and the lashing initial load. Figure 3.12 shows the values used in this set of calculations.



Table 3-3. Mechanical Properties of Lashing – Case B.

Lashing Layouts	As in the 1998 Experiments	
Lashing Diameter	7/8	in.
Breaking Strength	55.4	kip
Nominal Area	0.37	sq in.
Rupture Strain	5	%

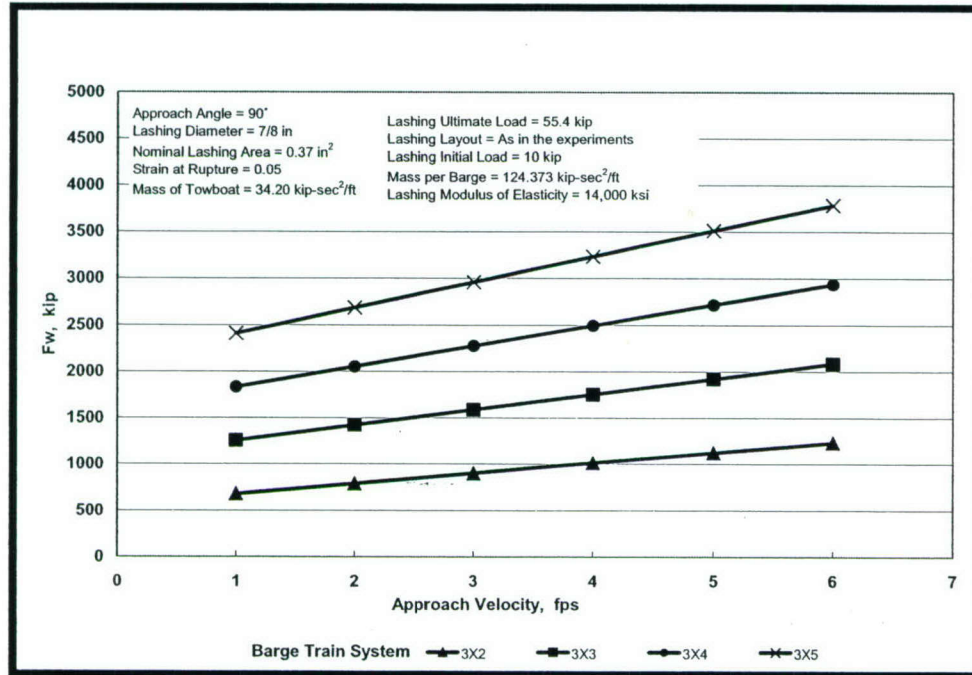


Figure 3-11. Maximum Head-On Impact  $F_w$  – Case B

Table 3-4. Mechanical Properties of Lashing – Case C.

Lashing Layouts	As in the 1998 Experiments	
Lashing Diameter	1	in.
Breaking Strength	89.8	kip
Nominal Area	0.48	sq in.
Rupture Strain	6	%

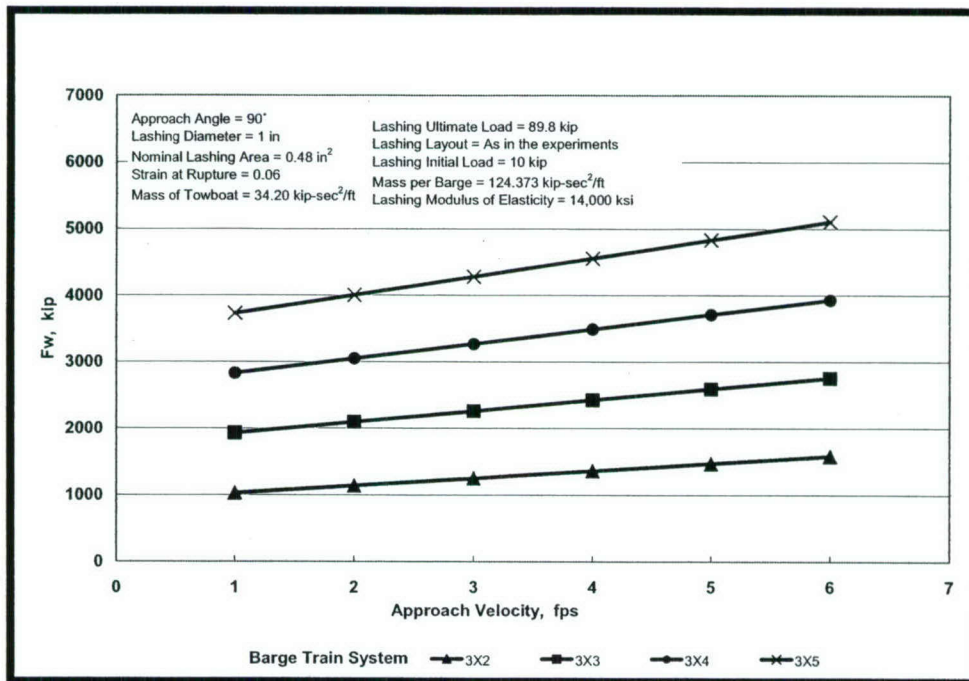


Figure 3-12. Maximum Head-On Impact  $F_w$  – Case C

### 3.5.4 Limiting Impact Forces Computed for 1-in. Diameter Used Wire Rope

The results of the limiting impact forces computed for the 1-in. diameter used wire rope are presented next. Table 3.5 lists the parameters used.

Figure 3.13 presents the variation of the maximum force normal to the wall for barge train systems 3x2, 3x3, 3x4, and 3x5 in a head-on impact. Additional input data are the mass of the barge train, mass of the towboat, and the lashing initial load. Figure 3.13 shows the values used in this set of calculations.

## 3.6 Standard Lashing Layout With an Additional Wrap

This section presents the results obtained with the same parameters and conditions as those presented in the last section with the exception of the number of wraps used to join the barges. In this section one additional wrap is included in the lashing layout. In this way the lashing layout used during the 1998 Experiments are modified to produce a stiffer system, which needs higher impact force to break the lashings. This condition will be reflected in the magnitude of the calculated forces.

Table 3-5. Mechanical Properties of Lashing – Case D.

Lashing Layouts	As in the 1998 Experiments	
Lashing Diameter	1	in.
Breaking Strength	71.8	kip
Nominal Area	0.48	sq in.
Rupture Strain	5	%



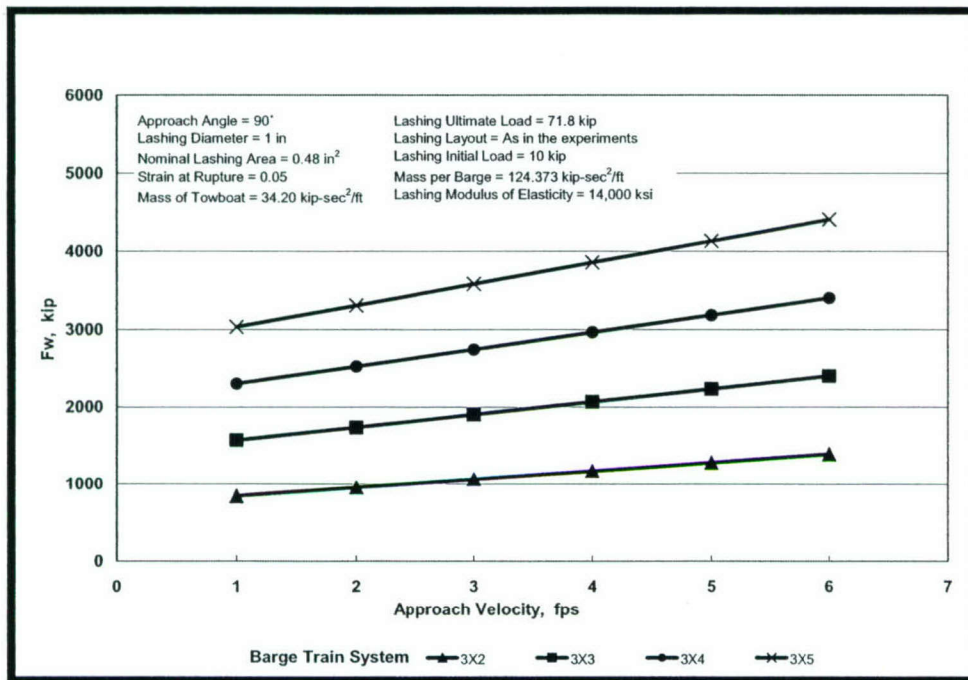


Figure 3-13. Maximum Head-On Impact  $F_w$  – Case D

### 3.6.1 Limiting Impact Forces Computed for 7/8-in. Diameter New Wire Rope

The results of the limiting impact forces computed for the 7/8-in. diameter new wire rope are presented next. Table 3.6 lists the parameters used. The case is now identified as “AWA” (Additional Wrap case A). The results of this case can be compared with the set of results obtained with Case A presented in the last section.

Figure 3.14 presents the variation of the maximum force normal to the wall for barge train systems 3x2, 3x3, 3x4, and 3x5 in a head-on impact event. Additional input data are the mass of the barge train, mass of the towboat, and the lashing initial load. Figure 3.14 shows the values used in this set of calculations.

Table 3-6. Mechanical Properties of Lashing – Case AWA

Lashing Layouts	One Additional Wrap to the 1998 Experiments Layout	
Lashing Diameter	7/8	in.
Breaking Strength	69.2	kip
Nominal Area	0.37	sq in.
Rupture Strain	6	%

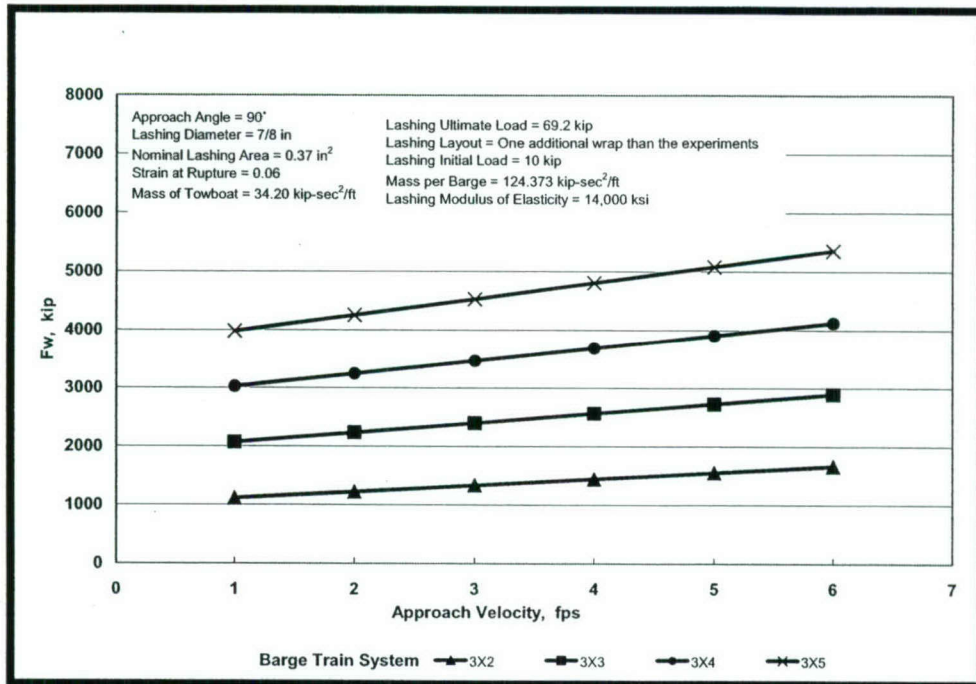


Figure 3-14. Maximum Head-On Impact  $F_w$  – Case AWA

### 3.6.2 Limiting Impact Forces Computed for 7/8-in. Diameter Used Wire Rope

The results of the limiting impact forces computed for the 7/8-in. diameter used wire rope are presented next. Table 3.7 lists the parameters used. The case is now identified as “AWB” (Additional Wrap case B). The results of this case can be compared with the set of results obtained with Case B presented in the last section.

Figure 3.15 presents the variation of the maximum force normal to the wall for barge train systems 3x2, 3x3, 3x4, and 3x5 in a head-on impact event. Additional input data are the mass of the barge train, mass of the towboat, and the lashing initial load. Figure 3.15 shows the values used in this set of calculations.

Table 3-7. Mechanical Properties of Lashing – Case AWB

Lashing Layouts	One Additional Wrap to the 1998 Experiments Layout	
Lashing Diameter	7/8	in.
Breaking Strength	55.4	kip
Nominal Area	0.37	sq in.
Rupture Strain	5	%



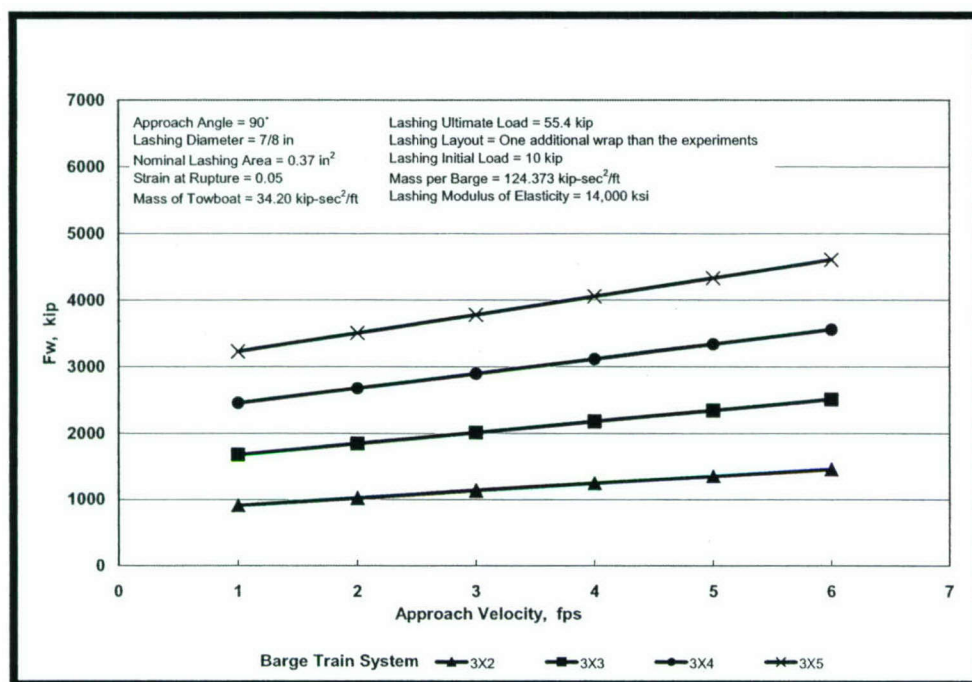


Figure 3-15. Maximum Head-On Impact  $F_w$  – Case AWB

### 3.6.3 Limiting Impact Forces Computed for 1-in. Diameter New Wire Rope

The results of the limiting impact forces computed for the 1-in. diameter new wire rope are presented next. Table 3.8 lists the parameters used. The case is now identified as “AWC” (Additional Wrap case C). The results of this case can be compared with the set of results obtained with Case C presented in the last section.

Figure 3.16 presents the variation of the maximum force normal to the wall for barge train systems 3x2, 3x3, 3x4, and 3x5 in a head-on impact event. Additional input data are the mass of the barge train, mass of the towboat, and the lashing initial load. Figure 3.16 shows the values used in this set of calculations.

Table 3-8. Mechanical Properties of Lashing – Case AWC

Lashing Layouts	One Additional Wrap to the 1998 Experiments Layout	
Lashing Diameter	1	in.
Breaking Strength	89.8	kip
Nominal Area	0.48	sq in.
Rupture Strain	6	%

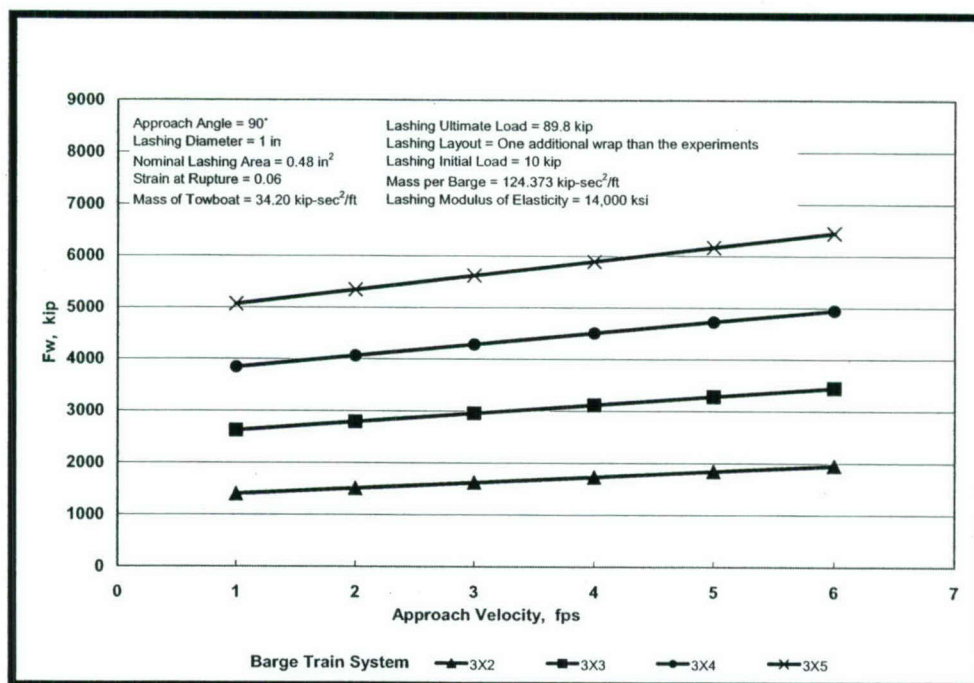


Figure 3-16. Maximum Head-On Impact  $F_w$  – Case AWC

### 3.6.4 Limiting Impact Forces Computed for 1-in. Diameter Used Wire Rope

The results of the limiting impact forces computed for the 1-in. diameter used wire rope are presented next. Table 3.9 lists the parameters used. The case is now identified as “AWD” (Additional Wrap case D). The results of this case can be compared with the set of results obtained with Case D presented in the last section.

Figure 3.17 presents the variation of the maximum force normal to the wall for barge train systems 3x2, 3x3, 3x4, and 3x5 in a head-on impact event. Additional input data are the mass of the barge train, mass of the towboat, and the lashing initial load. Figure 3.17 shows the values used in this set of calculations.

Table 3-9. Mechanical Properties of Lashing – Case AWD.

Lashing Layouts	One Additional Wrap to the 1998 Experiments Layout	
Lashing Diameter	1	in.
Breaking Strength	71.8	kip
Nominal Area	0.48	sq in.
Rupture Strain	5	%



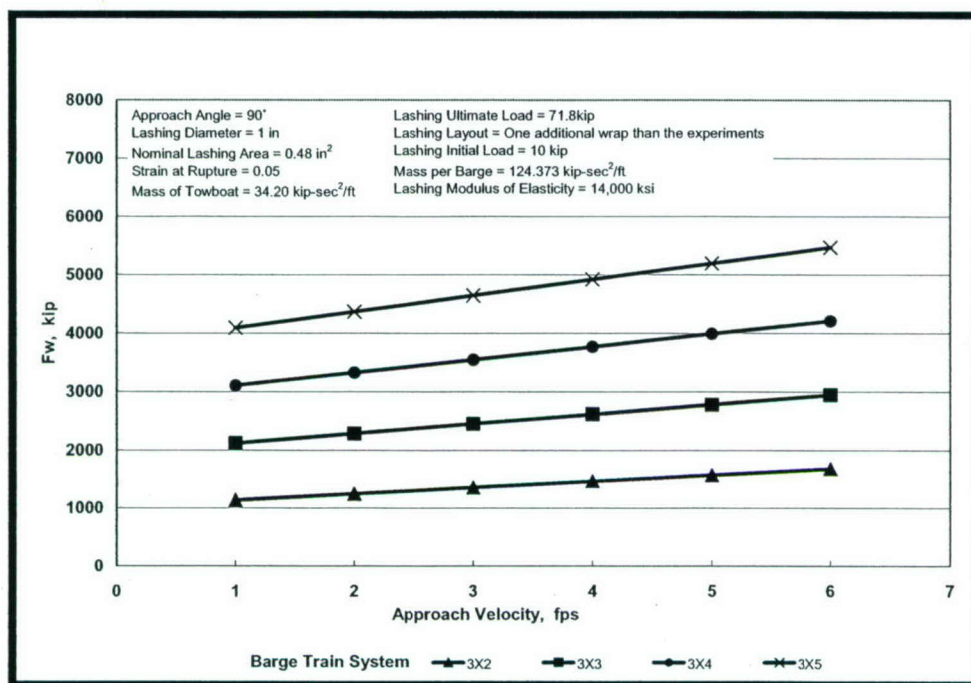


Figure 3-17. Maximum Head-On Impact  $F_w$  – Case AWD

### 3.7 Standard Lashing Layout Less One Wrap

This section presents the results obtained with the same parameters and conditions as those presented in Section 3.5 with the exception of the number of wraps used to join the barges. In this section, the standard lashing layout presented in Section 3.5 less one wrap is used to join the barges in the barge train. In this way, the lashing layout used during the Experiments 1998 are modified to produce a more flexible system, which needs lower impact force to breaks the lashings. This condition will be reflected in the magnitude of the calculated forces.

#### 3.7.1 Limiting Impact Forces Computed for 7/8-in. Diameter New Wire Rope

The results of the limiting impact forces computed for the 7/8-in. diameter new wire rope are presented next. Table 3.10 lists the parameters used. The case identification is now “LWA” (Less Wrap case A). The results of this case can be compared with the set of results obtained with Case A presented in Section 3.5.

Figure 3.18 presents the variation of the maximum force normal to the wall for barge train systems 3x2, 3x3, 3x4, and 3x5 in a head-on impact event. Additional input data are the mass of the barge train, mass of the towboat, and the lashing initial load. Figure 3.18 shows the values used in this set of calculations.

Table 3-10. Mechanical Properties of Lashing – Case LWA.

Lashing Layouts	One Wrap Less Than the 1998 Experiments Layout	
Lashing Diameter	7/8	in.
Breaking Strength	69.2	kip
Nominal Area	0.37	sq in.
Rupture Strain	6	%

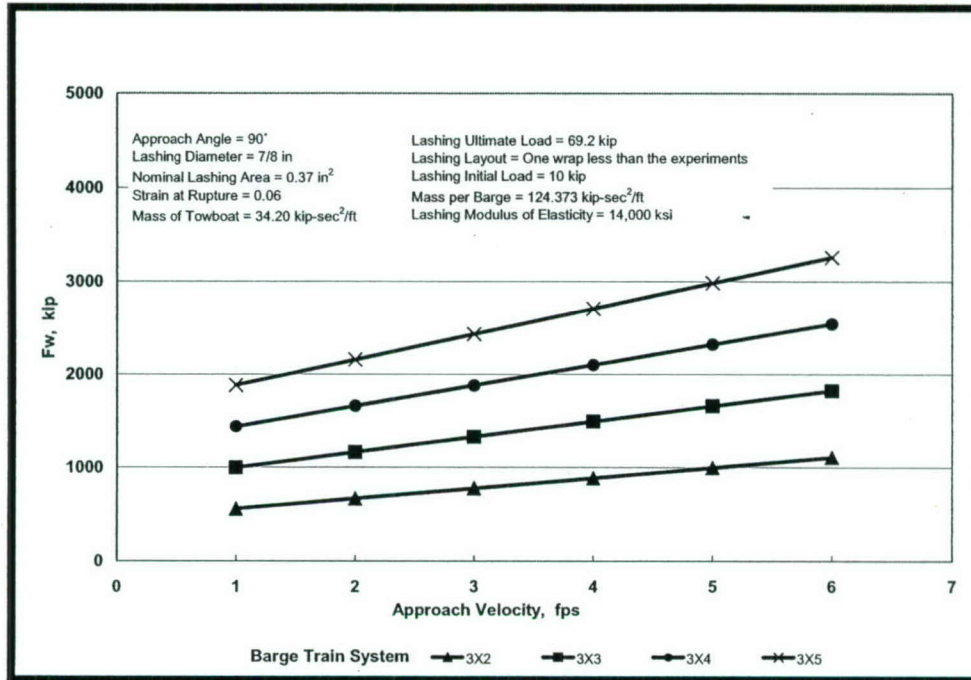


Figure 3-18. Maximum Head-On Impact  $F_w$  – Case LWA

### 3.7.2 Limiting Impact Forces Computed for 7/8-in. Diameter Used Wire Rope

The results of the limiting impact forces computed for the 7/8-in. diameter used wire rope are presented next. Table 3.11 lists the parameters used. The case identification is now “LWB” (Less Wrap case B). The results of this case can be compared with the set of results obtained with Case B presented in Section 3.5.

Figure 3.19 presents the variation of the maximum force normal to the wall for barge train systems 3x2, 3x3, 3x4, and 3x5 in a head-on impact event. Additional input data are the mass of the barge train, mass of the towboat, and the lashing initial load. Figure 3.19 shows the values used in this set of calculations.



Table 3-11. Mechanical Properties of Lashing – Case LWB.

Lashing Layouts	One Wrap Less Than the 1998 Experiments Layout	
Lashing Diameter	7/8	in.
Breaking Strength	55.4	kip
Nominal Area	0.37	sq in.
Rupture Strain	5	%

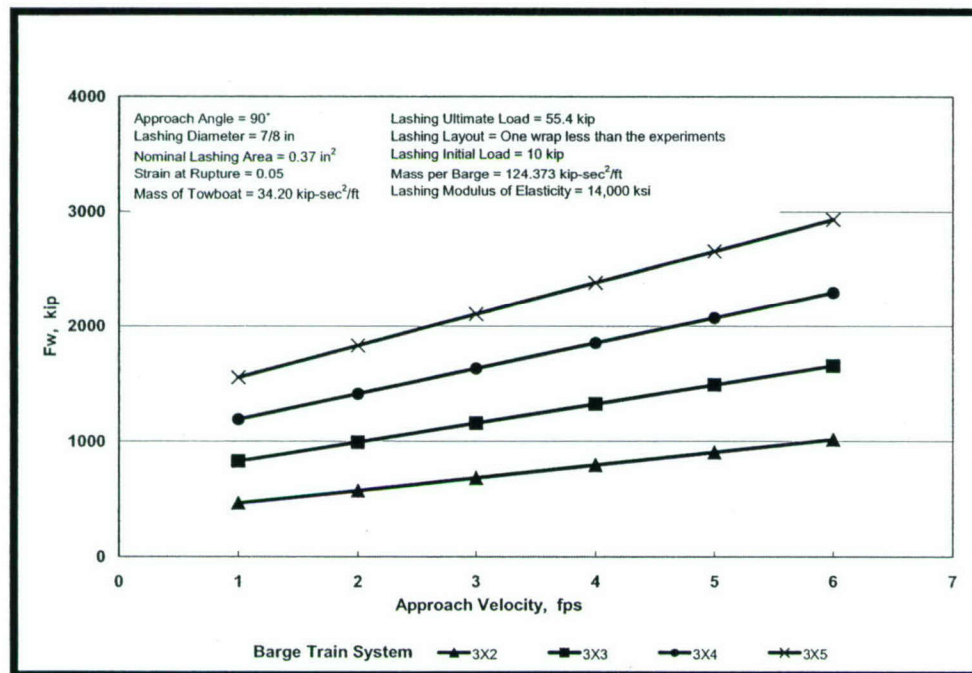


Figure 3-19. Maximum Head-On Impact  $F_w$  – Case LWB

### 3.7.3 Limiting Impact Forces Computed for 1-in. Diameter New Wire Rope

The results of the limiting impact forces computed for the 1-in. diameter new wire rope are presented next. Table 3.12 lists the parameters used. The case identification is now “LWC” (Less Wrap case C). The results of this case can be compared with the set of results obtained with Case C presented in Section 3.5.

Figure 3.20 presents the variation of the maximum force normal to the wall for barge train systems 3x2, 3x3, 3x4, and 3x5 in a head-on impact event. Additional input data are the mass of the barge train, mass of the towboat, and the lashing initial load. Figure 3.20 shows the values used in this set of calculations.

Table 3-12. Mechanical Properties of Lashing – Case LWC

Lashing Layouts	One Wrap Less Than the 1998 Experiments Layout	
Lashing Diameter	1	in.
Breaking Strength	89.8	kip
Nominal Area	0.48	sq in.
Rupture Strain	6	%

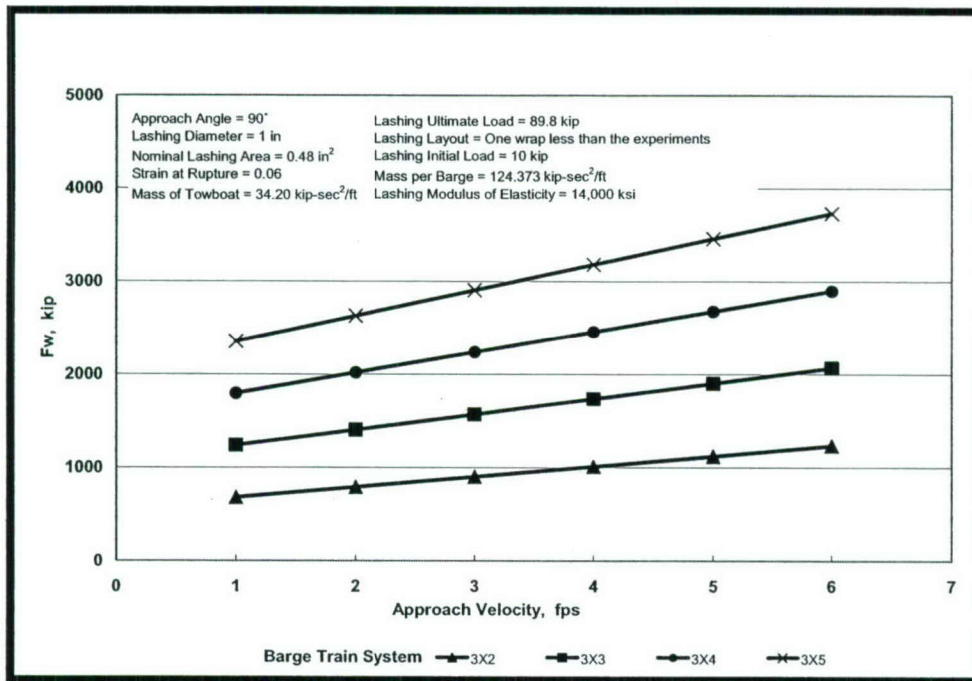


Figure 3-20. Maximum Head-On Impact  $F_w$  – Case LWC

### 3.7.4 Limiting Impact Forces Computed for 1-in. Diameter Used Wire Rope

The results of the limiting impact forces computed for the 1-in. diameter used wire rope are presented next. Table 3.13 lists the parameters used. The case identification is now “LWD” (Less Wrap case D). The results of this case can be compared with the set of results obtained with Case D presented in Section 3.5.

Figure 3.21 presents the variation of the maximum force normal to the wall for barge train systems 3x2, 3x3, 3x4, and 3x5 in a head-on impact event. Additional input data are the mass of the barge train, mass of the towboat, and the lashing initial load. Figure 3.21 shows the values used in this set of calculations.

Table 3-13. Mechanical Properties of Lashing – Case LWD

Lashing Layouts	One Wrap Less Than the 1998 Experiments Layout	
Lashing Diameter	1	in.
Breaking Strength	71.8	kip
Nominal Area	0.48	sq in.
Rupture Strain	5	%



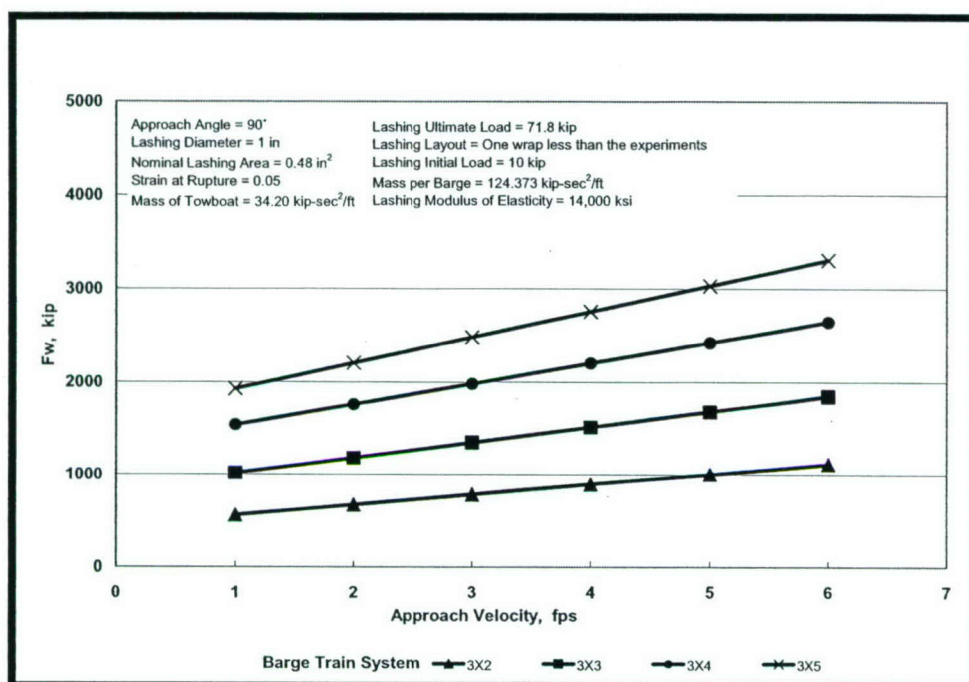


Figure 3-21. Maximum Head-On Impact  $F_w$  – Case LWD

### 3.8 Head-On Impact Results Summary

This chapter presented the results of the parametric study for the head-on impact event. The following tendencies were observed in the results:

1. The impact force normal to the wall increases with an increase in the approach velocity.
2. Increasing the number of wraps increases the impact force normal to the wall.
3. Increasing the number of barges in the barge train, also increases the impact force.
4. A larger the lashing diameter produces a higher impact force.
5. A higher ultimate lashing load produces a higher impact force.
6. A higher ultimate strain produces a higher impact load.
7. New lashings result in a greater impact load than used lashings.

From the logical point of view, these observations were expected. However, the magnitude of the impact force is now described based on the variations of the fundamental parameters that involved the impact process of a barge train and rigid wall based on the lashing limit states.

## 4 Conclusions and Recommendations

---

### 4.1 “Glancing Blow” Impact Event

This study performed a parametric study of the variables that affect the “glancing blow” impact event. The most important variables are: the approach angle, approach velocity, and the mechanical properties of the lashings. In the “glancing blow” impact event, the approach angle was varied from 2 to 30 degrees, and the approach velocity varied from 1 to 6 fps.

This work also evaluated two mechanical properties of lashings, ultimate strength and rupture strain. The values for these mechanical properties were varied depending on the assumed lashing condition; i.e., “new” and “used” lashing condition was a classification used to assign typical values to the mechanical properties to lashings.

The study also considered lashing layout. The configuration of lashings used in the full-scale experiments performed in 1998 and reported in Patev, Barker, and Koestler (2003) were used as the base lashing configuration. Two additional lashing layouts were used in the parametric study. The base lashing layout was modified by increasing by one and decreasing by one the number of wraps per lashing.

The barge train layouts used in the parametric study for the “glancing blow” impact events were 2x2, 2x3, 3x2, 3x3, 3x4, and 3x5. In general, these barge train layouts consider the small to large barge trains used in the towing industry for the portions of the river where locks are used. Other variables that affect in the maximum force normal to the wall were: the mass of the barge train, coefficient of friction between barge-barge and barge-wall, and bits location. These variables were held constant in the parametric analysis.

The corner failure mechanism was selected to describe the “glancing blow” impact event because it produces lower impact forces than the transverse failure mechanism. The explanation for this behavior can be obtained by looking at each of the failure mechanism assumptions. Basically, the corner failure mechanism has fewer lashings to break than the transverse failure mechanism. Schematically, this behavior can be



represented as shown in Figure 4.1. This figure also shows the range of applicability of the longitudinal failure mechanism.

Figure 4.1 shows the range of applicability of the numerical models developed in this study. For example, the Corner failure mechanism will dominate over the other two Limit LASHING limit state mechanisms if the approach angle is below 30 degrees. The green line in Figure 4.1 (below the purple and blue lines) shows this condition. These results were obtained using a kinetic coefficient of friction between steel-steel of 0.5 and the lashings properties and configurations presented in Appendix A. The Longitudinal failure mechanism is appropriate when the approach angle is greater than 70 degrees because produce non negative values of  $F_w$ . The other mechanism predicts negative values of  $F_w$ , which is impossible because the barge train pushes the wall, and does not pull on the wall.

The computed impact forces normal to the wall for the “glancing blow” impact event show the following trends:

1. The impact force increases with an increase in the approach angle.
2. The impact force increases with an increase in the approach velocity.
3. Increasing the number of wraps increases the impact force.
4. Increasing the number of barges in the barge train, also increases the impact force.
5. A larger lashing diameter produces a higher impact force.
6. A higher ultimate lashing load produces a higher impact force.
7. A higher ultimate strain produces a higher impact force.
8. New lashings produce greater impact load than used lashings.

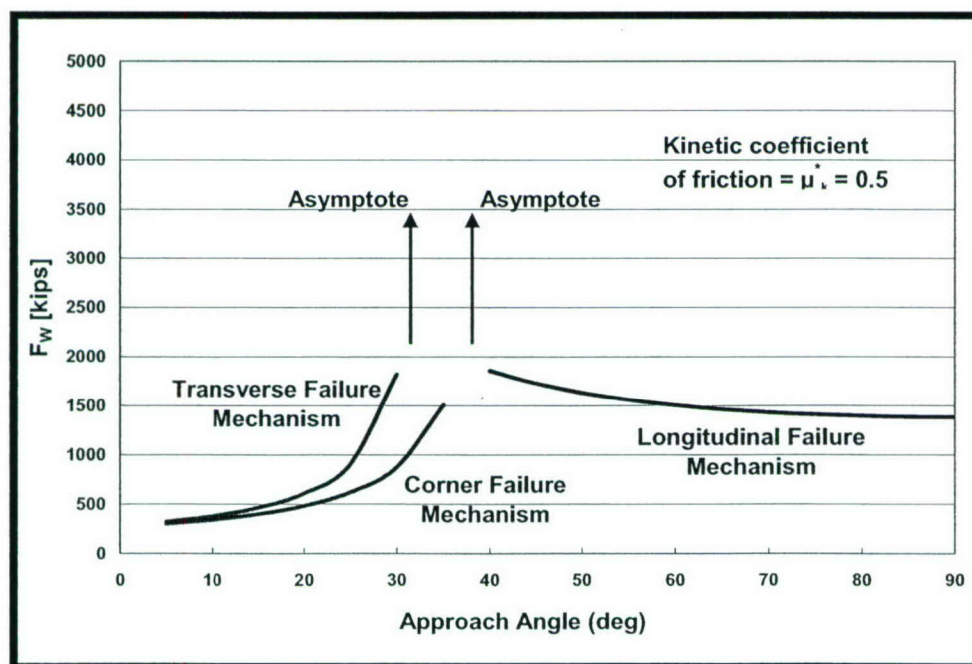


Figure 4-1. Range of Applicability of the Failure Mechanisms

From the logical point of view, these observations are expected. However, the magnitude of the impact force is now described based on the variations of the fundamental parameters involved in the impact process of a barge train and rigid wall based on the lashing limit states. Depending on the case studied, the force normal to the wall ranged between 300 and 1800 kips.

The trend of the resulting functions (as shown in Chapter 2) is not linear. However, these curves have a small curvature, which can be approximated by a linear function. It is important to mention that there are no relations between each data point because each represents a different impact event.

## 4.2 “Head-On” Impact Event

This work also conducted a parametric study of the variables that affect the head-on impact event. The most important variables are the approach velocity and the lashing mechanical properties. In the head-on impact event, the approach angle was fixed at 90 degrees, to produce a direct impact. However, the approach velocity varied from 1 to 6 fps.

Two mechanical properties of lashings, ultimate strength and rupture strain, were varied depending on the assumed lashing condition; i.e., “new” and “used” lashing condition was a classification used to assign typical values to the mechanical properties to lashings.

The study also considered lashing layout. The configuration of lashings used in the full-scale experiments performed in 1998 and reported in Patev, Barker, and Koestler (2003) were used as the base lashing configuration. Two additional lashing layouts were used in the parametric study. The base lashing layout was modified by increasing by one and decreasing by one the number of wraps per lashing.

The parametric study for the head-on impact events used the following barge train layouts: 3x2, 3x3, 3x4, and 3x5. In general, these barge train layouts consider the small to large barge train used in the towing industry. Other variables that enter in the calculations of the maximum force normal to the wall were: the mass of the barge train, coefficient of friction between barge-barge and barge-wall, and bits location. These variables were held constant in the parametric analysis.

This study concludes that head-on impact events show the same general tendencies as the “glancing blow” impact events. However, the magnitude of the force normal to the wall (impact force) ranges between 1000 and 5000 kip. This range of values indicates that the head-on impact event is an extreme impact case.



# References

---

- American Society for Testing and Materials (ASTM) Designation: A 931-96 (reapproved 2002), *Standard Test Method for Tension Testing of Wire Ropes and Strand*, West Conshohocken, PA.
- ASTM Designation: A 1023/A 1023M-02 (2003), *Standard Specification for Stranded Carbon Steel Wire Ropes for General Purposes*, West Conshohocken, PA.
- Arroyo, J.R., Ebeling, R., and Barker, B. (2003), *Analysis of Full-Scale Low Velocity, Controlled Barge Impact Experiments*, December 1998, ERDC/ITL/ Technical Report (TR) 03-3, U.S. Army Engineer Research and Development Center, Vicksburg, MS.
- Arroyo, J.R., and Ebeling, R. (2004), *A Numerical Method for Computing Barge Impact Forces Based on Ultimate Strength of the Lashings between Barges*, ERDC/ITL/ TR-04-2, U.S. Army Engineer Research and Development Center, Vicksburg, MS.
- Headquarters, Department of the Army (1993), *Barge Impact Analysis*, Engineering Technical Letter 1110-2-338.
- McCormick, Michael. E (1973), *Ocean Engineering Wave Mechanics*, John Wiley & Sons, New York, NY.
- Patev, R.C., Barker, B.C., and Koestler, L.V. (2003), *Full-Scale Barge Impact Experiments, Robert C. Byrd Lock and Dam, Gallipolis Ferry, West Virginia*, ERDC/ITL TR-03-7, U.S. Army Engineer Research and Development Center, Vicksburg, MS.
- Pytel, A., and Kiusalaas, J. (1994), *Engineering Mechanics*, Harper Collins College Publishers, New York, NY.
- Sarpkaya, T., and Isaacson M. (1981), *Mechanics of Wave Forces on Offshore Structure*, Van Nostrand Reinhold Company, New York, NY.
- Tedesco, Joseph, McDougal, William, and Ross, Allen (1999), *Structural Dynamics, Theory and Applications*, Addison Wesley Inc., Menlo Park, CA.
- Wilson, James F. (1984), *Dynamic of Offshore Structures*, John Wiley & Sons, New York, NY.
- Wire Rope Technical Board (1993), *Wire Rope Users Manual*, 3d ed., USA.5M/2000.

# Appendix A: Lashing Configurations

---

All simplified failure mechanisms used during the course of this research were based on the assumption that the lashings joining the barges provide the strength to the barge train such that barge System 2 decelerates when barge System 1 impacts the wall. This assumption combined with the equations of equilibrium for the two-barge system allows for the calculation of the normal and shear force between the barge train and the *rigid* wall during the impact process. The configurations of the lashings between barges are allowed to differ. In this research, the configuration of lashings used in the full-scale experiments performed in 1998 and reported in Patev, Barker, and Koestler (2003)\* were used as the base lashing configuration. Two additional lashing layouts were used in the parametric study. The base lashing layout was modified by increasing by one and decreasing by one the number of wraps per lashing. Figures A-1 through A-4 show the four configurations observed in the 3x5 barge train used in the full-scale experiment. The computer program Limit\_LASHING has the capacity to analyze a barge train with lashing configurations that are typical of what is used on inland waterways.

Configuration 1 (Figure A-1) was the arrangement used in the 1998 full-scale experiments to join a pair of barges along the outside edge of the barge train. It is also the configuration used on the bow, port, aft, and starboard sides. It consists of three turns of the bits along the edge of the two joined barges. Figure A-1 also shows the generic sequence of the bits connected. The name “generic sequence” means that the assigned numbers can change in each model configuration. However, the lashing configuration must follow the sequence shown in Figure A-1.

Three configuration levels were available at the center joints where four barges come together. The 1998 experiments used eight of these connections because 15 barges were joined together. Figures A-2 through A-4 show the top, middle, and bottom configurations. The bottom layer, designated Configuration 2, is similar to Configuration 1. Configuration 2 is considered as a separate configuration because it is associated with the center connections between barges. The middle configuration at the inner

---

\* References cited in this appendix are included in the References section following the main text.



connections, designated Configuration 3, is like a scissor passing each lashing over the edge of the joined barges three times. Finally, Configuration 4, or the top layer in the inner connection, has two turns for each lashing over the edge of the joined barges. Note that the configurations shown in these figures are not the only configurations available for use in Limit\_LASHING. In Limit\_LASHING, the user can include more turns in each of these configurations, eliminate configurations, and use different lashings, etc. For that reason, the variable of lashing configuration and lashing properties is one of the primary variables in this program.

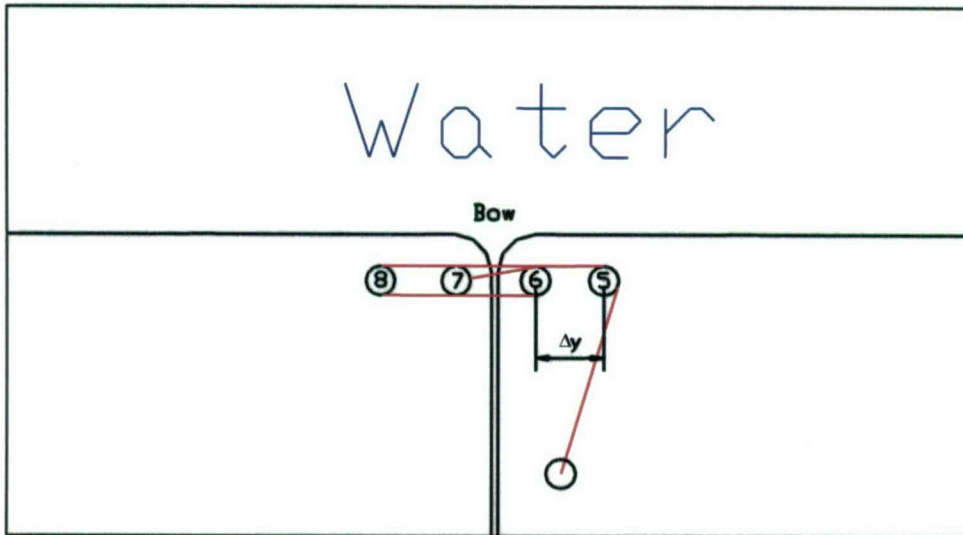


Figure A1. Configuration 1 located at bow, port, aft, and starboard sides: generic sequence - 7,6,8,5

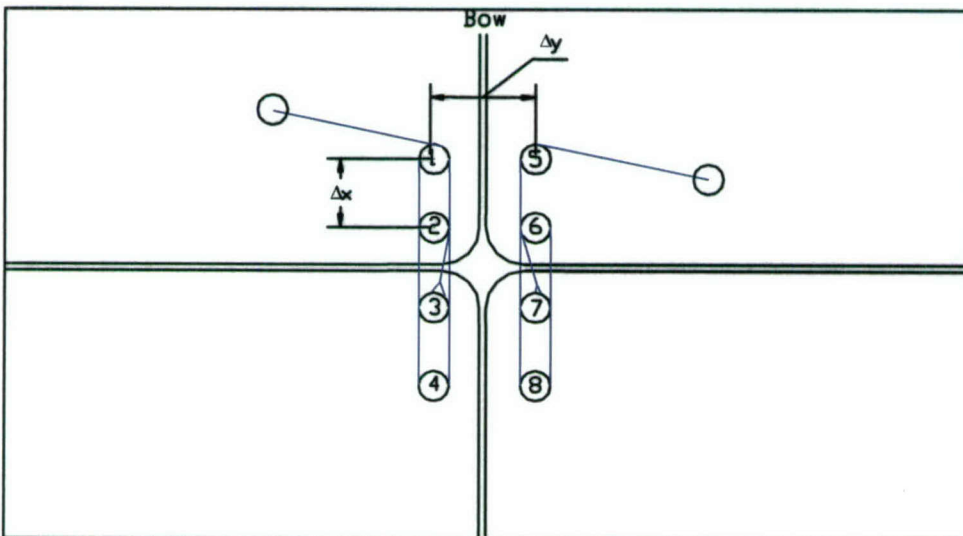


Figure A2. Configuration 2 located at the bottom layer in the inside connection: generic sequence - 7, 6, 8, 5 and 3, 2, 4, 1

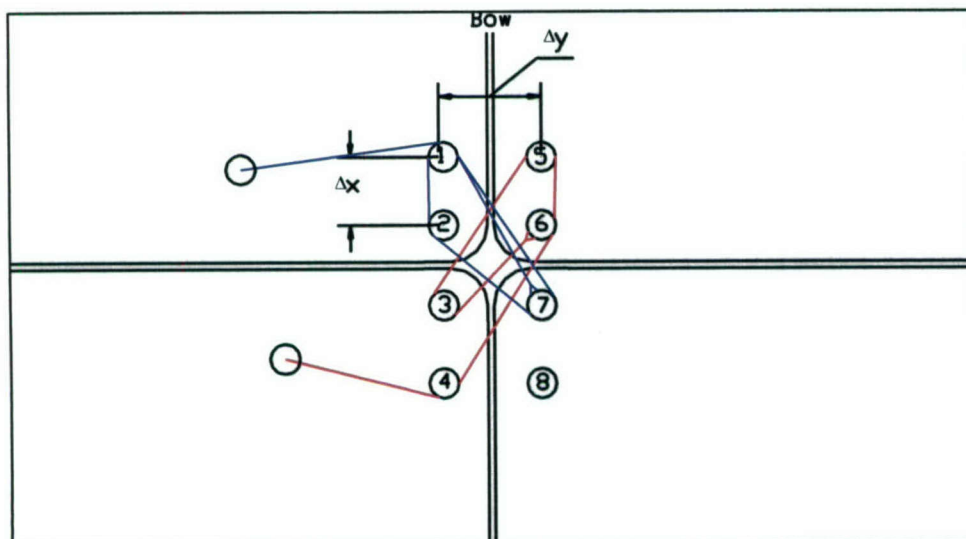


Figure A3. Configuration 3 located at the middle layer in the inside connection: generic sequence – 6, 3, 5, 6, 4 and 7, 1, 2, 7, 1

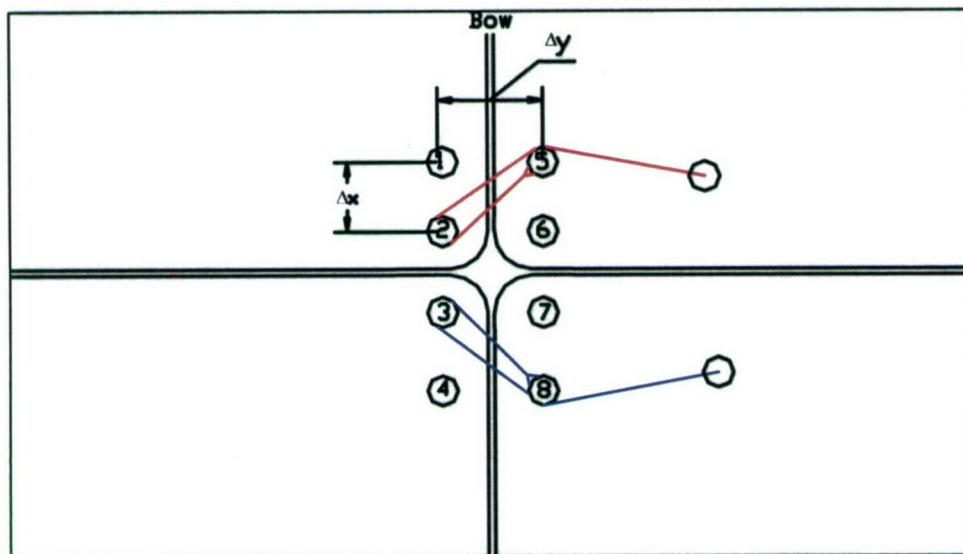


Figure A4. Configuration 4 located at the top layer in the inside connection: generic sequence – 5, 2, 5 and 8, 3, 8

The user specifies the coordinates of each bit on the barges to determine the angle that each force within the lashing makes with the local axis of the system. In this way, Limit\_LASHING can calculate the necessary angles to determine the components of the internal force for the lashings in the local axis. It is important to note that these arrangements are prepared for both a forward and backward motion of the lashings.

The lashings are made of steel. In this research, an elasto-plastic relationship that breaks when an ultimate (tensile) strain value is achieved within the lashing was used to describe the lashings' mechanical behavior. Figure A-5 shows how this behavior allows the lashing to carry load from zero up to the ultimate stress of the lashing. At this instant, the lashing remains with the ultimate stress until the ultimate strain is reached. The load



that produces the ultimate stress is the ultimate load divided by the cross-sectional area of the lashing. The initial slope of the stress-strain line is the Young's modulus of elasticity  $E$ , typically assigned a value of 29,000 ksi. Figure A-5 shows the elasto-plastic behavior adopted to model the constitutive relationship for the lashings. Table A-1 lists the typical lashings properties. The lashing diameters used in the full-scale experiments were either 1 or 1.25 in. with an ultimate load of 90 or 120 kip, respectively. Using this information combined with an ultimate load of 90 kips for a 1-in.-diameter lashing results in an ultimate stress of 114.6 ksi = 16,501.2 ksf.

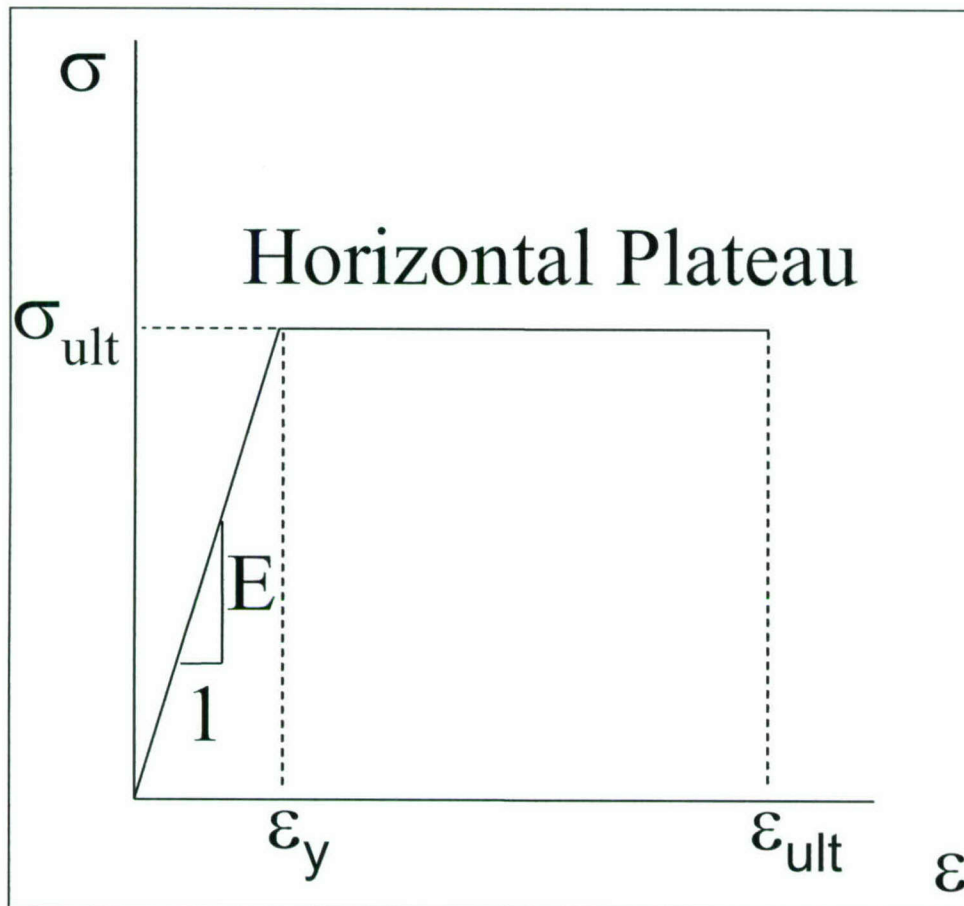


Figure A5. Constitutive relationship of the lashings

Table A1. Typical Lashing Properties (Full Scale Experiments)

Lashing Type	Diameter (in.)	Modulus Of Elasticity, (ksi)	Cross-Sectional Area (sq in.)	Ultimate Load (kip)
1	1	29,000	0.7854	90
2	1.25	29,000	1.2272	120

# REPORT DOCUMENTATION PAGE

Form Approved  
OMB No. 0704-0188

Public reporting burden for this collection of information is estimated to average 1 hour per response, including the time for reviewing instructions, searching existing data sources, gathering and maintaining the data needed, and completing and reviewing this collection of information. Send comments regarding this burden estimate or any other aspect of this collection of information, including suggestions for reducing this burden to Department of Defense, Washington Headquarters Services, Directorate for Information Operations and Reports (0704-0188), 1215 Jefferson Davis Highway, Suite 1204, Arlington, VA 22202-4302. Respondents should be aware that notwithstanding any other provision of law, no person shall be subject to any penalty for failing to comply with a collection of information if it does not display a currently valid OMB control number. PLEASE DO NOT RETURN YOUR FORM TO THE ABOVE ADDRESS.

<b>1. REPORT DATE (DD-MM-YYYY)</b> March 2005		<b>2. REPORT TYPE</b> Final		<b>3. DATES COVERED (From - To)</b>	
<b>4. TITLE AND SUBTITLE</b> Barge Train Maximum Impact Forces Using Limit States for the Lashings between Barges				<b>5a. CONTRACT NUMBER</b>	
				<b>5b. GRANT NUMBER</b>	
				<b>5c. PROGRAM ELEMENT NUMBER</b>	
<b>6. AUTHOR(S)</b> José Ramón Arroyo and Robert M. Ebeling				<b>5d. PROJECT NUMBER</b>	
				<b>5e. TASK NUMBER</b>	
				<b>5f. WORK UNIT NUMBER</b>	
<b>7. PERFORMING ORGANIZATION NAME(S) AND ADDRESS(ES)</b> U.S. Army Engineer Research and Development Center (ERDC) Information Technology Laboratory (ITL) Waterways Experiment Station, 3909 Halls Ferry Road Vicksburg, MS 39180-6199				<b>8. PERFORMING ORGANIZATION REPORT NUMBER</b> ERDC/ITL TR-05-1	
<b>9. SPONSORING / MONITORING AGENCY NAME(S) AND ADDRESS(ES)</b> Headquarters, U.S. Army Corps of Engineers (HQUSACE) 441 G St., NW Washington, DC 20314-1000				<b>10. SPONSOR/MONITOR'S ACRONYM(S)</b> CECW-CO	
				<b>11. SPONSOR/MONITOR'S REPORT NUMBER(S)</b>	
<b>12. DISTRIBUTION / AVAILABILITY STATEMENT</b> Approved for public release; distribution is unlimited.					
<b>13. SUPPLEMENTARY NOTES</b> Copies are available from the National Technical Information Service, 5285 Port Royal Road, Springfield, VA 22161.					
<b>14. ABSTRACT</b> <p>In 1993, Headquarters, U.S. Army Corps of Engineers issued Engineer Technical Letter (ETL) 1110-2-338, the first formal Corps-wide analysis procedure providing guidance for analyzing the effects of barge impact loading on navigation structures. The ETL 1110-2-338 engineering procedure calculates the magnitude of the impact forces generated by a particular collision event dependent on: the mass including hydrodynamic added mass of the barge train, the approach velocity, the approach angle, the barge train moment of inertia, damage sustained by the barge structure, and friction between the barge and the wall. This ETL 1110-2-338 Corps guidance was rescinded in 2001 due to concerns regarding the accuracy of computed results.</p> <p>Later research hypothesized that the limit value of the force normal to the wall is based on the yield of the lashing. This work presents a parametric analysis of the limit states of the lashing and an analysis of the tendencies. The models used to perform the parametric analysis are the corner (glancing blow) and longitudinal (head-on) failure mechanisms and their empirical correlations. The analyses used the Limit_LASHING computer program to estimate the maximum force normal to the wall based on the limit states of the lashing between barges.</p>					
<b>15. SUBJECT TERMS</b> Impact Lashing Limit State Rigid Wall Failure Mechanism of Barge Train					
<b>16. SECURITY CLASSIFICATION OF:</b>			<b>17. LIMITATION OF ABSTRACT</b>  SAR	<b>18. NUMBER OF PAGES</b>  124	<b>19a. NAME OF RESPONSIBLE PERSON</b> Robert M. Ebeling
<b>a. REPORT</b> Unclassified	<b>b. ABSTRACT</b> Unclassified	<b>c. THIS PAGE</b> Unclassified			<b>19b. TELEPHONE NUMBER (include area code)</b> (601) 634-3458